Unsteady Flow in the Third Navigation Channel,

Gezhouba Water Control Project, China

by

Xiaoxia Zhao

Thesis submitted to the Faculty of the

Virginia Polytechnic Institute and State University

in partial fulfillment of the requirements for the degree of

Master of Science in Civil Engineering

APPROVED:

Chin Y. Kuo, Chairman

G.V.Loganathan

T. Kuppusamy

November,1987

Blacksburg, Virginia

Unsteady Flow in the Third Navigation Channel,

Gezhouba Water Control Project, China

by

Xiaoxia Zhao

Chin Y. Kuo, Chairman

(ABSTRACT)

Based on the de St Venant Equations, the Preissmann's implicit finite difference scheme, and the double sweep algorithm, a mathematical model for one-dimensional subcritical unsteady flow in the Third Navigation Channel at the Gezhouba Water Control Project, China, has been developed. The model has been calibrated and verified using the prototype test data. All conceivable factors affecting wave propagation have been studied parametrically. The side discharge method is considered to be the best way to reduce the amplitudes of both water surface elevation and velocity variations caused by unsteady flow due to the emptying of the lock chamber. Using side discharges to distribute the discharge from the lock chamber along the channel, instead of concentrated discharge at the upstream boundary, improves greatly the navigation conditions.

Acknowledgements

I would like to express my sincere gratitude to Dr. Chin Y. Kuo, my major advisor, under whose supervision this thesis has been completed. His guidance, patience, encouragement, and his criticism have always been the source of this study.

I would also like to thank Dr. G. V. Loganathan and Dr. T. Kuppusamy for serving on my committee and for their time and effort spent in the thesis.

Additional thanks are given to my colleagues and friends in China for their support and data supplied for this study.

Thanks are also given to my fellow graduate students and friends at Virginia Tach for their help and friendship.

Table of Contents

List of Illustrations

Nomenclature

A	Cross-sectional area perpendicular to the flow direction
A_c	Flow area in the lock chamber
A_d	Flow area in the channel
a	Area of the valve opening
B	Height of the valve opening at time t
B_T	Storage width
C	A coefficient for the distribution pipe
C_D	Coefficient combining all loss coefficients
C_j	Side discharge weighting coefficients
c	Wave celerity
d	Diameter of the distribution pipe
F_f	Bed friction force acting on a control volume
F_g	Gravity force acting on a control volume
$F_{p1}, F^1_{p1}, F^2_{p1}$	Cross-sectional pressure forces acting on a control volume
$F_{p2}, F^1_{p2}, F^2_{p2}$	Lateral pressure forces acting on a control volume
f	Friction factor

g	Gravitational acceleration
H	Water head difference
ΔH	Decrease of water head difference
H_0	Initial total head difference between the lock chamber and the channel
h	Water depth; total height of the valve opening
i	Computational point index in time
I_1, I_2	Cross-sectional moment integrals
j	Computational point index in space
K	Conveyance factor of the channel
K_f	Boundary frictional head loss coefficient
K_i	Inlet head loss coefficient
K_o	Outlet head loss coefficient
K_v	Valve constrictional head loss coefficient
L	Total length of the computational domain
M	Number of computational time steps
M_f	Net momentum into a control volume
ΔM	Net increase in momentum contained in a control volume
N	Number of computational points
n	Manning's roughness coefficient; Time step index
P	Wetted perimeter of a cross-section
Q	Water discharge
ΔQ	Increase of water discharge
Q_c	Concentrated side discharge
Q_{sj}	Side discharge at cross-section j
q	Continuous lateral inflow per unit length
R	Hydraulic radius

S_0	Bed slope in the x-direction
S_f	Slope of the energy grade line in the x-direction (friction slope)
T	Time coordinate in $t - x$ plane
t	Time variable
Δt	Time step interval
u	Cross-sectional mean velocity
u_q	Longitudinal velocity component of lateral inflow
V	Velocity in the distribution pipe
w	Width of the valve opening
X	Longitudinal space coordinate in horizontal plane
x	Distance
Δx	Space step interval
Z	Water surface elevation; Vertical space coordinate above datum
ΔZ	Increase of water surface elevation
Z_b	Bed elevation above datum
α	Angle between the channel bed and the horizontal plane
η	Depth integration variable of cross-section along the Z-axis
θ	Weighting coefficient in finite difference approximation
ρ	Water density
σ	Width of cross-section
π	Constant 3.1416...

Chapter 1. Introduction

1.1. Brief Description of Gezhouba Water Control Project

The Gezhouba Water Control Project is the first dam and hydropower station ever built on the main stream of the Yangtze River which is the largest and longest river in China. Gezhouba Water Control Project, being built as a component of the proposed Three Gorges Water Control Project, will serve as a regulating reservoir to control tailwater of the Three Gorges Dam for navigation purpose [21]. It is located near the city of Yichang in Hubei Province, about 40 *km* downstream of the Three Gorges Dam site. Two small islands stand athwart the 2,000 *m* wide river at the project site, dividing the river into three channels, named as the Grand, the Second, and the Third Channels, respectively.

The project mainly comprises the dams, power stations, navigation locks, spillways, and sluiceways (see Figure 1). The main dam has a total length of 2,561 *m* with a crest elevation of 70 *m* above mean sea level, and the reservoir has a total volume of 1.58 billion m^3, controlling a catchment area of about one million km^2. The two power

stations are equipped with 21 units with a total generating capacity of 2,715 *MW*. They are scheduled to produce an average of 13,800 *GWH* of electricity annually. The 27 spillway gates and the 12 sluiceway gates, when fully opened, can discharge safely up to 110,000 m^3/s which is the maximum historical flood.

The project has three one-stage navigation locks in which the maximum water depth may reach 27 meters. Lock *No.*1 is situated along the right bank of the Grand Channel and Lock *No.*2 along the right bank of the Third Channel. Each of them has a lock chamber 280 *m* long by 34 *m* wide and a minimum draft of 5 *m*, allowing the passage of 10,000 ton ships and big flotillas of barges. Lock *No.*3 is located along the left bank of the Third Channel. It has a lock chamber 120 *m* long by 18 *m* wide and a minimum draft of 3.5 *m*. It mainly provides the passage of cargo and passenger ships less than 3,000 ton capacity and flotillas of native junks. The three navigation locks have a total annual single-direction shipping capability of 20 million tons in recent years and will be increased to 50 million tons in the future.

The Yangtze River is the most important waterway linking Southwest and East China. Navigation is as important as hydroelectric power generation for the Gezhouba Project. It has to guarantee that the locks and navigation channels are operating in a smooth condition in order to satisfy the navigation safety requirements. It is the purpose of this thesis to study the effects of unsteady flow in the Third Channel on the navigation conditions by means of a mathematical model.

1.2. Unsteady Flow in the Third Navigation Channel

As shown in Figure 2, with the Xiba island on its right hand side, the Third Channel is separated from the main stream of the Yangtze River. This channel has been made

to be the Third Navigation Channel for navigation. It is about 3.4 *km* long with a varying width of 120 *m* to 200 *m*. The design elevation for the channel bottom is 34.5 *m* above mean sea level. Its bed slope is almost horizontal and water surface profile is nearly horizontal when the lock isn't in operation. The design minimum water elevation in the channel for navigation is 39 *m* above mean sea level. It flows into the main stream of the Yangtze River further downstream [7].

When the ship moves from upstream to downstream of the dam, water is discharged from the lock chamber. The amount of discharge at a given time is proportional to the head difference between the water level in the lock chamber and that in the channel and the characteristics of the gate/valve opening. Because both the water levels and the valve opening change gradually, the discharge hydrograph resulted from the emptying of the lock chamber varies with respect to time.

When the discharge released from the lock chamber increases from 0 to a finite value in a given time period, a positive wave will then be generated at the upstream boundary (cross-section *No.*1) as shown in Figure 3a. Such a wave propagates from upstream to downstream along the channel with a wave celerity $c = (gh)^{0.5}$ on the order of 7 *m/s*. The time of wave propagation from upstream boundary to downstream boundary (cross-section *No.*14) is about 8 minutes.

When the positive wave arrives at any cross-section in the channel, the water level there will rise and cause water to flow downstream with a positive velocity. At the downstream boundary, the positive wave raises the water level there and propagates toward the Yangtze Rive in which the water level is considered to be constant during the operation of the lock. At this moment, water flows from the channel to the Yangtze River with a positive velocity.

After a certain time, the discharge released from the lock chamber will reach the maximum value and then decrease. When the discharge decreases from its maximum to

a smaller value, a negative wave will thus be generated at the upstream boundary and propagate downstream toward the downstream boundary (Fig. 3b). This negative wave causes the water level in the channel to decrease. Gradually, the water level within the channel will become lower than the water level in the Yangtze River. Naturally, water will flow into the channel from the Yangtze River. A positive wave will be generated at the downstream boundary (Fig. 3c). Such a positive wave will propagate upstream with a negative velocity. Obviously, the water level in the channel will increase even though no discharge releases from the lock chamber at this moment. When the positive wave with negative velocity arrives at the upstream boundary, it no longer propagates further upstream. Thus the water level at the upstream boundary will increase continuously and will reach its maximum value. In the meantime, water level in the channel will rise again and cause a decrease of the discharge flowing from the Yangtze River to the channel. Therefore a negative wave with a negative velocity will be generated (Figure 3d). It causes the water level gradually decrease again. Because the bed of the Third Navigation Channel is composed of fine sand, its friction coefficients are very small. The induced wave may persist for several hours, far beyond 8 minutes, propagating back and forth along the channel with little energy dissipation. For example, under design condition, based on a calibrated mathematical model (will be discussed in the subsequent chapters), simulated water surface elevation variations and velocity variations with respect to time at cross-sections *No.*2 and *No.*11 are shown in Figure 4 and Figure 5, respectively. They show that the wave propagation may last more than three hours. After three hour propagation, the amplitude of the water surface elevation variation at the cross-section *No.*2 remains to be 0.4 *m*; and the velocity variation at the cross-section *No.*11 is from -0.4 *m/s* to $+0.4$ *m/s*. Information such as these is helpful to the lock operation as related to the navigation conditions in the channel in terms of boat rocking and swinging.

1.3. Research Approach

The objective of this thesis is to study the behavior of the wave propagation and the influence of various factors, such as upstream boundary conditions, side discharge, channel roughness coefficients, and modification of channel cross-sections, etc., on the behavior of the wave propagation in the Third Navigation Channel. A mathematical model for one-dimensional unsteady open channel flow is developed. The model is based on the de St Venant Equations, using Preissmann's implicit finite difference scheme to discretize the differential equations and double sweep algorithm to solve the system of difference equations.

For application to the Third Navigation Channel, the channel is divided into 13 reaches ranging from 187 *m* to 346 *m* in length. The upstream boundary conditions are described by the function of discharge with respect to time, and the downstream boundary conditions are described by the function of water level with respect to time. The bed material of the channel is composed of fine sand. Its Manning's roughness coefficients *n* are estimated by comparing the observed and calculated water level variation at several sections in the channel. For the sake of convenience, a discharge formula to generate hydrograph for upstream boundary condition is derived and its applicability is checked by comparing its result with the measured discharge hydrograph. All conceivable factors affecting wave propagation in the channel are studied using the developed mathematical model. The mathematical model makes it possible to study the wave propagation behavior even under exceptional circumstances, such as the most 'critical' or 'unsafe' navigation conditions.

Chapter 2. Mathematical Formulation of Physical Processes

2.1. Basic Hypotheses

Mathematical modelling for open channel flow is the simulation of flow conditions based on the formulation and solution of mathematical relationships expressing known hydraulic principles. As early as the 19th century, de St Venant and Boussinesq formulated the unsteady flow equations. Massan's work published in 1889 was the earliest attempt to solve those equations [6]. But, the real engineering applications of these principles to natural situations awaited the development of computers. Now, mathematical modelling of flow in open channels is rapidly becoming an accepted engineering tool because of its reliability and economic advantage [1,2,3,5,17].

First, this chapter reviews the basic assumptions of the de St Venant Equations; Second, it develops the integral flow relations from a control volume point of view; Third, it shows that the de St Venant Equations can be derived from the integral relations; Finally, it introduces supplementary lateral inflow, empirical resistance laws, and

boundary data requirements to deal with the practical application of the mathematical model.

The fundamental hypotheses used in the mathematical modelling of 1-D unsteady open channel flow are the de St Venant (1871) hypotheses. The de St Venant equations for unsteady flow are based upon the following series of assumptions [6,13]:

1. The flow is one-dimensional. This means that the velocity over the cross section is uniform and the water level across the cross section is horizontal.

2. The streamline curvature is small and the vertical accelerations are negligible. Hence, the vertical pressure distribution is hydrostatic.

3. The effects of boundary friction and turbulence can be accounted for through resistance laws which are analogous to those used for steady flow.

4. The average channel bed slope is small, i.e. the angle α between the channel bed and the horizontal plane is sufficiently small so that $\sin\alpha \cong \tan\alpha$.

The cross sections of the channel can be of arbitrary shape and may vary along the longitudinal axis, although the variation is limited by the condition of small streamline curvature.

One-dimensional unsteady flow in an open channel can be described by two dependent variables: for example, the water stage Z and the discharge Q at any given channel cross section. These dependent variables define the state of the flow along the channel and in time; they are the function of two independent variables: x for space and t for time.

Since two dependent variables are sufficient to describe one-dimensional flow, two equations with each of them representing a physical law are required to solve for the two variables.

Because the conservation of mass and the conservation of momentum laws can be applied to both discontinuous and continuous flow situations while the mass-energy laws can not, the derivation of equations will be based on mass-momentum conservation laws in this thesis.

2.2. Integral Relations

Let us consider a control volume in a channel between sections $x = x_1$ and $x = x_2$, as shown in Figure 6 to illustrate the integral relations [6,13].

The net inflow of mass into the control volume between times $t = t_1$ and $t = t_2$ is defined by the time integral of the difference between the mass flow rates $(\rho uA)_{x_1}$ entering and $(\rho uA)_{x_2}$ leaving the control volume:

$$\int_{t_1}^{t_2} [(\rho uA)_{x_1} - (\rho uA)_{x_2}] \, dt \tag{2.1}$$

This net inflow must be equal to the change of storage in the reach during the same time interval:

$$\int_{x_1}^{x_2} [(\rho A)_{t_2} - (\rho A)_{t_1}] \, dx \tag{2.2}$$

where ρ = water density; $u = u(x, t)$ = uniform cross-sectional velocity; $A = A(x, t)$ = wetted cross-sectional area. Consequently, the mass continuity integral relation for constant density is

$$\int_{x_1}^{x_2} [(A)_{t_2} - (A)_{t_1}]\, dx + \int_{t_1}^{t_2} [(Q)_{x_2} - (Q)_{x_1}]\, dt = 0 \tag{2.3}$$

where $Q = uA$.

The conservation of momentum in the x-direction requires that the change of momentum in the control volume between times t_1 and t_2 be equal to the sum of the net inflow of momentum into the control volume and the integral of the external forces acting on it over the same time interval. Momentum flux through the flow section is a product of the mass flow rate and velocity, or

$$\text{momentum flux} = \rho uA \times u = \rho u^2 A \tag{2.4}$$

The net momentum flux into the control volume is

$$(\rho u^2 A)_{x_1} - (\rho u^2 A)_{x_2} \tag{2.5}$$

and the net momentum inflow between t_1 and t_2 is

$$M_f = \int_{t_1}^{t_2} [(\rho u^2 A)_{x_1} - (\rho u^2 A)_{x_2}]\, dt \tag{2.6}$$

The momentum contained in the control volume at any instant is

$$\int_{x_1}^{x_2} \rho uA\, dx \tag{2.7}$$

and the net increase from t_1 to t_2 is

$$\Delta M = \int_{x_1}^{x_2} [(\rho uA)_{t_2} - (\rho uA)_{t_1}]\, dx \tag{2.8}$$

It is assumed that the only important external forces acting upon the control volume in the x-direction are pressure, gravity, and frictional resistance. The pressure force

F_{p1} is the difference of pressure forces F_{p1}^1 and F_{p1}^2 applied at boundaries x_1 and x_2 of the reach. At any cross-section x with free surface elevation $Z(x)$, the pressure force is expressed under the hydrostatic pressure distribution hypothesis by

$$F_{p1}^1 = g\int_0^{h(x)} \rho\,[h(x) - \eta]\,\sigma(x, \eta)\,d\eta \tag{2.9}$$

where η = depth integration variable along the Z -axis; $h(x, t)$ = water depth; $\sigma(x, \eta)$ = width of the cross section such that $\sigma(x, h) = b(x)$ = free surface width. Thus the time integral of the net pressure force F_{p1} , when F_{p1}^1 is expressed as in Equation (2.9), is

$$\int_{t_1}^{t_2} F_{p1}\,dt = \int_{t_1}^{t_2} (F_{p1}^1 - F_{p1}^2)\,dt = g\int_{t_1}^{t_2} [(\rho I_1)_{x_1} - (\rho I_1)_{x_2}]\,dt \tag{2.10}$$

$$I_1 = \int_0^{h(x)} [h(x) - \eta]\,\sigma(x, \eta)\,d\eta \tag{2.11}$$

where I_1 is a function of water stage Z.

For an infinitesimal channel length dx , the increase of the pressure force due to the width variation is represented by the increase of the wetted area $d\sigma\,d\eta$ for constant $h = h_0$ times the distance of its centroid from the free surface $h(x) - \eta$:

$$\rho g\,[(\frac{\partial \sigma}{\partial x})dx\,d\eta]_{h=h_0}\,[h(x) - \eta] \tag{2.12}$$

In Figure 6, F_{p2}^1 and F_{p2}^2 represent this type of pressure forces acting on the lateral boundary of the control volume. These forces are to be integrated between $\eta = 0$ and $\eta = h(x)$ for a given cross section, and from x_1 to x_2 to obtain the total lateral pressure force F_{p2} acting on the control volume. The total integral along the contour of the control volume and for the time interval t_1 to t_2 is

$$\int_{t_1}^{t_2} (F_{p2}^1 + F_{p2}^2)\,dt = \int_{t_1}^{t_2}\int_{x_1}^{x_2} \rho g \int_0^{h(x)} [h(x) - \eta]\left[\frac{\partial \sigma(x, \eta)}{\partial x}\right]_{h_0} d\eta\,dx\,dt \tag{2.13}$$

or

$$\int_{t_1}^{t_2} F_{p2}\, dt = g \int_{t_1}^{t_2} \int_{x_1}^{x_2} \rho I_2\, dx\, dt \tag{2.14}$$

in which

$$F_{p2} = F_{p2}^1 + F_{p2}^2, \qquad I_2 = \int_0^{h(x)} (h - \eta) \left[\frac{\partial \sigma}{\partial x}\right]_{h = h_0} d\eta \tag{2.15}$$

where I_2 is a function of the width variation between two sections and of the water stage.

The body force F_g due to gravity is evaluated by assuming that the channel bottom slope $S_0 = -\dfrac{\partial Z_b}{\partial x} = \tan \alpha$ is small (Z_b being bottom elevation above datum), so that $\tan \alpha \cong \sin \alpha$:

$$\int_{t_1}^{t_2} F_g\, dt = \int_{t_1}^{t_2} \int_{x_1}^{x_2} \rho g A S_0\, dx\, dt \tag{2.16}$$

A frictional resistance force F_f is applied to the control volume through shear force along the channel bed and banks. In order to treat the shear force, it is expressed as $\rho g A S_f$ per unit length of the channel. S_f is the so-called friction slope, i.e. the energy gradient needed to overcome the frictional resistance in steady flow. The time integral of the resistance force on the control volume is then

$$\int_{t_1}^{t_2} F_f\, dt = \int_{t_1}^{t_2} \int_{x_1}^{x_2} \rho g A S_f\, dx\, dt \tag{2.17}$$

Therefore, the statement of conservation of momentum leads to

$$\Delta M = M_f + \int_{t_1}^{t_2} F_{p1}\, dt + \int_{t_1}^{t_2} F_{p2}\, dt + \int_{t_1}^{t_2} F_g\, dt - \int_{t_1}^{t_2} F_f\, dt \tag{2.18}$$

or, for constant density ρ , the momentum equation is expressed as:

$$\int_{x_1}^{x_2} [(uA)_{t_2} - (uA)_{t_1}]dx = \int_{t_1}^{t_2} [(u^2A)_{x_1} - (u^2A)_{x_2}] dt$$

$$+ g\int_{t_1}^{t_2} [(I_1)_{x_1} - (I_1)_{x_2}] dt$$

$$- g \int_{t_1}^{t_2} \int_{x_1}^{x_2} I_2 \, dx \, dt \qquad (2.19)$$

$$+ g \int_{t_1}^{t_2} \int_{x_1}^{x_2} A(S_0 - S_f) \, dx \, dt$$

Equations (2.3) and (2.19) together are the integral form of the unsteady flow relations based on the de St Venant hypothesis [6,13]. The two differential equations describe the gradually varied one-dimensional unsteady flows in natural channels with arbitrary shapes.

2.3. Differential Form of de St Venant Equations

The differential equations of gradually varied unsteady flow may be obtained from integral equations if the dependent variables are assumed to be continuous and differentiable functions [6,13,14]. By Taylor series expansions, they are written as:

$$(A)_{t_2} = (A)_{t_1} + \frac{\partial A}{\partial t}\Delta t + \frac{\partial^2 A}{\partial t^2}\frac{\Delta t^2}{2} + \cdots \qquad (2.20)$$

$$(Q)_{x_2} = (Q)_{x_1} + \frac{\partial Q}{\partial x}\Delta x + \frac{\partial^2 Q}{\partial x^2}\frac{\Delta x^2}{2} + \cdots \qquad (2.21)$$

By retaining only first order derivatives and assuming that Δx and Δt approach zero, it follows:

$$\lim_{t_2 \to t_1} \int_{x_1}^{x_2} [(A)_{t_2} - (A)_{t_1}]\, dx = \int_{x_1}^{x_2} \int_{t_1}^{t_2} \frac{\partial A}{\partial t}\, dt\, dx \tag{2.22}$$

$$\lim_{x_2 \to x_1} \int_{t_1}^{t_2} [(Q)_{x_2} - (Q)_{x_1}]\, dt = \int_{t_1}^{t_2} \int_{x_1}^{x_2} \frac{\partial Q}{\partial x}\, dx\, dt \tag{2.23}$$

And the continuity Equation (2.3) becomes:

$$\int_{x_1}^{x_2} \int_{t_1}^{t_2} \left[\frac{\partial A}{\partial t} + \frac{\partial Q}{\partial x} \right] dt\, dx = 0 \tag{2.24}$$

In a similar way one may write

$$(u^2A)_{x_2} - (u^2A)_{x_1} = \frac{\partial (u^2A)}{\partial x} \Delta x + \frac{\partial^2 (u^2A)}{\partial x^2} \frac{\Delta x^2}{2} + \cdots$$

$$(uA)_{t_2} - (uA)_{t_1} = \frac{\partial Q}{\partial t} \Delta t + \frac{\partial^2 Q}{\partial t^2} \frac{\Delta t^2}{2} + \cdots \tag{2.25}$$

$$(I_1)_{x_2} - (I_1)_{x_1} = \frac{\partial I_1}{\partial x} \Delta x + \frac{\partial^2 I_1}{\partial x^2} \frac{\Delta x^2}{2} + \cdots$$

By substituting the first terms of expansions (2.25) into Equation (2.19) and then letting Δx and Δt approach zero ($\Delta x \to 0$, $\Delta t \to 0$), one obtains

$$\int_{x_1}^{x_2} \int_{t_1}^{t_2} \left[\frac{\partial Q}{\partial t} + \frac{\partial (u^2A)}{\partial x} \right] dt\, dx$$

$$= -g \int_{x_1}^{x_2} \int_{t_1}^{t_2} \left[\frac{\partial I_1}{\partial x} - I_2 - A(S_0 - S_f) \right] dt\, dx \tag{2.26}$$

If the relations (2.24) and (2.26) are to hold everywhere in the (x, t) plane, they must hold for an infinitely small volume, and one can write two differential equations:

continuity equation

$$\frac{\partial A}{\partial t} + \frac{\partial Q}{\partial x} = 0 \tag{2.27}$$

momentum equation

$$\frac{\partial Q}{\partial t} + \frac{\partial (u^2 A)}{\partial x} + g\frac{\partial I_1}{\partial x} = g\,A\,(S_0 - S_f) + g\,I_2 \tag{2.28}$$

combining the x derivatives in Equation (2.28) and replacing u by (Q/A) , the momentum equation becomes:

$$\frac{\partial Q}{\partial t} + \frac{\partial}{\partial x}\left(\frac{Q^2}{A} + g\,I_1\right) = g\,A\,(S_0 - S_f) + g\,I_2 \tag{2.29}$$

Equations (2.27) and (2.29) are written in this kind of special form, often called the divergent form of partial differential equations. Because all dependent variables are assumed differentiable, the derivative of the $g\,I_1$ term in Equation (2.29) can be evaluate as:

$$\frac{\partial}{\partial x}(g\,I_1) = g\frac{\partial}{\partial x}\int_0^{h(x)} [h(x) - \eta]\,\sigma(x, \eta)\,d\eta \tag{2.30}$$

Applying the Leibniz theorem for differentiation of an integral, and knowing that $\sigma(x,h) = b(x)$ and $\int_0^h \sigma\,d\eta = A$, one obtains

$$\frac{\partial}{\partial x}(gI_1) = g\int_0^{h(x)} \frac{\partial [h(x) - \eta]}{\partial x}\sigma(x, \eta)\,d\eta + g\int_0^{h(x)} [h(x) - \eta]\frac{\partial \sigma}{\partial x}d\eta$$

$$= g\frac{\partial h}{\partial x}\int_0^{h(x)} \sigma(x, \eta)d\eta + g\int_0^{h(x)} [h(x) - \eta]\left[\frac{\partial b}{\partial x}\right]_{h=const} d\eta \tag{2.31}$$

$$\frac{\partial}{\partial x}(gI_1) = g\,A(x)\frac{\partial h}{\partial x} + gI_2 \tag{2.32}$$

Consequently, Equation (2.28) may be rewritten as:

$$\frac{\partial Q}{\partial t} + \frac{\partial}{\partial x}(u^2 A) + gA\frac{\partial h}{\partial x} + gI_2 = gA(S_0 - S_f) + gI_2 \tag{2.33}$$

Thus one obtains the momentum equation generally used in engineering practices,

$$\frac{\partial Q}{\partial t} + \frac{\partial}{\partial x}(uQ) + gA(\frac{\partial h}{\partial x} - S_0) + gAS_f = 0 \tag{2.34}$$

which is commonly refered to as the dynamic equation. For convenience, the discharge $Q(x,t)$ and water surface elevation $Z(x,t)$ are usually chosen as the two dependent variables. Because water depth $h = Z - Z_b$, where $Z_b(x)$ is the bottom elevation of the channel, hence

$$\frac{\partial A(h)}{\partial t} = \frac{\partial A}{\partial h}\frac{\partial h}{\partial t} = B_T\frac{\partial h}{\partial t}$$

$$\frac{\partial h}{\partial t} = \frac{\partial Z}{\partial t} \tag{2.35}$$

$$\frac{\partial h}{\partial x} = \frac{\partial Z}{\partial x} - \frac{\partial Z_b}{\partial x} = \frac{\partial Z}{\partial x} + S_0$$

where $B_T = B_T(y)$, $A = A(y)$.

B_T is a so-called storage-width of the channel.

Substitution of Equation (2.35) into Equations (2.27) and (2.34) leads to the system

$$\frac{\partial Q}{\partial x} + B_T\frac{\partial Z}{\partial t} = 0 \tag{2.36}$$

$$\frac{\partial Q}{\partial t} + \frac{\partial}{\partial x}\left(\frac{Q^2}{A}\right) + gA\frac{\partial Z}{\partial x} + gAS_f = 0 \tag{2.37}$$

2.4. Supplementary Terms and Coefficients

Lateral Inflow

If a continuous lateral inflow q per unit length is added to the channel flow and u_q is the longitudinal velocity component of the lateral inflow, Equations (2.36) and (2.37) become [6]:

$$\frac{\partial Q}{\partial x} + B_T\frac{\partial Z}{\partial t} = q \tag{2.38}$$

$$\frac{\partial Q}{\partial t} + \frac{\partial}{\partial x}\left(\frac{Q^2}{A}\right) + gA\left(\frac{\partial Z}{\partial x} + S_f\right) - q\left(u_q - \frac{Q}{A}\right) = 0 \tag{2.39}$$

Empirical Friction Laws

The friction slope S_f is used to represent any one of the empirical friction laws. Most of these empirical laws are based on a relationship between discharge and friction losses in the following general form [4]:

$$Q = K\sqrt{S_f} \tag{2.40}$$

i.e. $$S_f = \frac{Q|Q|}{K^2} \tag{2.41}$$

where $|Q|$ is the absolute value of Q, $K = K(Z)$ is the so-called conveyance factor of the channel and S_f is the slope of the energy grade line in steady flow. Therefore, the friction slope S_f is a function of dependent variables $Q(x,t)$ and $Z(x,t)$. This makes the dynamic equation non-linear. Assuming that the velocity of the lateral inflow is normal to the x-direction, and substituting Equation (2.41) into (2.39), the continuity and dynamic equations of unsteady flow in open channel are written in the following form:

$$\frac{\partial Q}{\partial x} + B_T \frac{\partial Z}{\partial t} = q \tag{2.42}$$

$$\frac{\partial Q}{\partial t} + \frac{\partial}{\partial x}\left(\frac{Q^2}{A}\right) + gA\frac{\partial Z}{\partial x} + gA\frac{Q|Q|}{K^2} + \frac{Q}{A}q = 0 \tag{2.43}$$

These are so-called de St Venant equations which are the governing equations for the mathematical model used in this study. Mathematically, these kind of equations are classified as a hyperbolic non-linear equations. They do not have a closed form solution. Therefore, numerical method is used to solve them.

The empirical friction law used for this study is the Manning's equation [4,6]:

$$Q = \frac{1}{n} A R^{\frac{2}{3}} \sqrt{S_f} \tag{2.44}$$

where n is Manning's roughness coefficient, in metric units. R, the hydraulic radius, is defined by the relation:

$$R = \frac{A}{P} \tag{2.45}$$

where P is the wetted perimeter of the cross section. The conveyance factor is expressed as:

$$K = \frac{1}{n} A R^{\frac{2}{3}} \tag{2.46}$$

2.5. Boundary data requirements

In order to solve the de St Venant equations, some data for the boundaries of the solution domain must be given. The subcritical flow computations with which this thesis exclusively deals require one-point data at the upstream boundary, one-point data at the downstream boundary and two-point along the $t = 0$ line. Generally, boundary data can be given as any functional relationships between the dependent variables and their derivatives with respect to x and t. However, from a practical point of view, the most common and attractive approach is directly to give the values of the two dependent variables. For example, the system of equations (2.42) and (2.43) is supplemented with initial condition $Q(x,0)$ and $Z(x,0)$, upstream boundary condition $Q(x_1,t)$, and downstream boundary condition $Z(x_2,t)$ which are used for numerical calculation in this thesis. It is important that these imposed boundary conditions must not depend on what happens within the model.

Chapter 3. Numerical Method

3.1. Discretization of de St Venant Equations

The characteristics method [1,14], the finite difference method [8,18,19,20,22], and the finite element method [9,10,11,12] are commonly used in the numerical solution of the de St Venant Equations. In this study, the finite difference method is chosen since the geometry of the navigation channel is relatively simple. The Preissmann implicit scheme is used as a basic discreteization scheme because of its independence of time interval Δt and some other merits [6,15]. Preissmann scheme, as shown in Figure 7, is a 4-point scheme of finite differences in which variable $f(x,t)$ in the space interval is evaluated by its mean value between j and $j + 1$, but in the time interval it is evaluated by its weighted average between n and $n + 1$:

$$f = f(x + \frac{\Delta x}{2}; t + \theta\Delta t) \cong \frac{\theta}{2}(f_{j+1}^{n+1} + f_j^{n+1}) + \frac{1-\theta}{2}(f_{j+1}^{n} + f_j^{n}) \tag{3.1}$$

where f_j^n represents the value of the grid function at point x_j and at time t_n and $0 \le \theta \le 1$ is a weighting coefficient. When $\theta = 1$, equation (3.1) becomes the most

stable implicit scheme; when $\theta = 0.5$, the approximation is of second order; when $\theta = 0$, equation (3.1) becomes an explicit scheme. Based on the criteria of stability and computational accuracy, $\theta = 0.55$ was chosen after several θ values were tried.

The corresponding discreteization of the derivatives of the variable is represented by the following approximations:

$$\frac{\partial f}{\partial t} \cong \frac{(f_{j+1}^{n+1} + f_j^{n+1}) - (f_{j+1}^n + f_j^n)}{2\Delta t} \tag{3.2}$$

$$\frac{\partial f}{\partial x} \cong \theta \frac{f_{j+1}^{n+1} - f_j^{n+1}}{\Delta x} + (1 - \theta)\frac{f_{j+1}^n - f_j^n}{\Delta x} \tag{3.3}$$

Because the de St Venant equation systems are non-linear, the finite difference analogues of the basic differential equations also become non-linear algebraic systems which cause some difficulties. The actual discreteizations of every term in Equations (2.42) and (2.43), according to the Preissmann Scheme, are as follows [5,14,23]:

$$\frac{\partial Q}{\partial x} \cong \theta \frac{Q_{j+1}^{n+1} - Q_j^{n+1}}{\Delta x} + (1 - \theta) \frac{Q_{j+1}^n - Q_j^n}{\Delta x};$$

$$B_T \frac{\partial Z}{\partial t} \cong \left[\frac{\theta}{2} (B_{Tj+1}^{n+1} + B_{Tj}^{n+1}) + \frac{1 - \theta}{2} (B_{Tj+1}^n + B_{Tj}^n) \right]$$

$$\times \left(\frac{Z_{j+1}^{n+1} - Z_{j+1}^n}{2\Delta t} + \frac{Z_j^{n+1} - Z_j^n}{2\Delta t} \right);$$

$$q = q_j + \theta \Delta q_j;$$

$$\frac{\partial Q}{\partial t} \cong \frac{Q_{j+1}^{n+1} - Q_{j+1}^n}{2\Delta t} + \frac{Q_j^{n+1} - Q_j^n}{2\Delta t}; \tag{3.4}$$

$$\frac{\partial}{\partial x}\left(\frac{Q^2}{A}\right) \cong \frac{\theta}{\Delta x}\left[\frac{(Q_{j+1}^{n+1})^2}{A_{j+1}^{n+1}} - \frac{(Q_j^{n+1})^2}{A_j^{n+1}}\right] + \frac{(1-\theta)}{\Delta x}\left[\frac{(Q_{j+1}^{n})^2}{A_{j+1}^{n}} - \frac{(Q_j^{n})^2}{A_j^{n}}\right];$$

$$gA\frac{\partial Z}{\partial x} \cong g\left[\frac{\theta}{2}(A_{j+1}^{n+1} + A_j^{n+1}) + \frac{1-\theta}{2}(A_{j+1}^{n} + A_j^{n})\right]$$

$$\times\left[\theta\frac{Z_{j+1}^{n+1} - Z_j^{n+1}}{\Delta x} + (1-\theta)\frac{Z_{j+1}^{n} - Z_j^{n}}{\Delta x}\right];$$

$$gA\frac{Q|Q|}{K^2} \cong g\left[\frac{\theta}{2}(A_{j+1}^{n+1} + A_j^{n+1}) + \frac{(1-\theta)}{2}(A_{j+1}^{n} + A_j^{n})\right]$$

$$\times\left\{\frac{\theta}{2}\left[\frac{Q_{j+1}^{n+1}|Q_{j+1}^{n+1}|}{(K_{j+1}^{n+1})^2} + \frac{Q_j^{n+1}|Q_j^{n+1}|}{(K_j^{n+1})^2}\right]\right.$$

$$\left.+\frac{1-\theta}{2}\left[\frac{Q_{j+1}^{n}|Q_{j+1}^{n}|}{(K_{j+1}^{n})^2} + \frac{Q_j^{n}|Q_j^{n}|}{(K_j^{n})^2}\right]\right\};$$

$$\frac{Q}{A}q \cong \left[\frac{\theta}{2}\left(\frac{Q_{j+1}^{n+1}}{A_{j+1}^{n+1}} + \frac{Q_j^{n+1}}{A_j^{n+1}}\right) + \frac{1-\theta}{2}\left(\frac{Q_{j+1}^{n}}{A_{j+1}^{n}} + \frac{Q_j^{n}}{A_j^{n}}\right)\right](q_j + \theta\Delta q_j);$$

In Equations (3.4), the frictional resistance force term $\frac{Q|Q|}{K^2}$ is discretized by weighted average of $\frac{1}{K^2}$. In the computer program, subroutine *COEFA* uses this form. The frictional term can also be discretized by weighted average of K^2, which is included in subroutine *COEFB*.

Equations (3.4) need to be further linearized. In doing this, it is assumed that all functions $f(Z,Q)$ in the discretized non-linear algebraic equations are known at time level $n\Delta t$ and are differentiable with respect to Z and Q . Then, any such function at time level $(n + 1)\Delta t$ can be evaluated by a Taylor power series expansion:

$$f^{n+1} = f^n + \Delta f = f^n + \frac{\partial f}{\partial Z}\Delta Z + \frac{\partial f}{\partial Q}\Delta Q + \frac{\partial^2 f}{\partial Z^2}\frac{\Delta Z^2}{2} + \frac{\partial^2 f}{\partial Q^2}\frac{\Delta Q^2}{2} + \cdots \quad (3.5)$$

where ΔZ and ΔQ are the increments of water stage Z and discharge Q during the time step Δt.

Then, neglect the terms of second and higher orders, keep only the first-order term, and use the following approximation relations:

$$\frac{1}{f + \Delta f} = \frac{1}{f(1 + \frac{\Delta f}{f})} \cong \frac{1}{f}(1 - \frac{\Delta f}{f});$$

$$\frac{1}{(f + \Delta f)^2} = \frac{1}{f^2(1 + \frac{\Delta f}{f})^2} \cong \frac{1}{f^2}(1 - 2\frac{\Delta f}{f});$$

$$(f + \Delta f)^2 \cong f^2 + 2f\Delta f;$$

$$(f + \Delta f)|f + \Delta f| \cong f|f| + 2|f|\Delta f; \quad (3.6)$$

$$\Delta A \cong \frac{\partial A}{\partial Z}\Delta Z = B_T \Delta Z;$$

$$\Delta K \cong \frac{\partial K}{\partial Z}\Delta Z;$$

$$\Delta B_T \cong \frac{\partial B_T}{\partial Z}\Delta Z.$$

Thus, Equations (2.42) and (2.43) can be written as the following two algebraic equations in terms of ΔZ_j, ΔQ_j, ΔZ_{j+1}, and ΔQ_{j+1} for every pair of adjacent points $(j, j+1)$:

$$\frac{\Delta x_j(B_{Tj+1} + B_{Tj})}{4\Delta t}(\Delta Z_{j+1} + \Delta Z_j) + \theta(\Delta Q_{j+1} - \Delta Q_j)$$

$$= \Delta x_j(q_j + \theta\Delta q_j) - (Q_{j+1} - Q_j) \tag{3.7}$$

$$\frac{\Delta x_j}{2\Delta t}(\Delta Q_j + \Delta Q_{j+1}) - 2\theta\left(\frac{Q_j\Delta Q_j}{A_j} - \frac{Q_{j+1}\Delta Q_{j+1}}{A_{j+1}}\right)$$

$$+ \theta\left[B_{Tj}\left(\frac{Q_j}{A_j}\right)^2\Delta Z_j - B_{Tj+1}\left(\frac{Q_{j+1}}{A_{j+1}}\right)^2\Delta Z_{j+1}\right]$$

$$+ 0.5\theta g\left[(Z_{j+1} - Z_j)(B_{Tj}\Delta Z_j + B_{Tj}\Delta Z_{j+1}) - (A_j + A_{j+1})(\Delta Z_j - \Delta Z_{j+1})\right]$$

$$+ \frac{\theta g\Delta x_j}{K_j^2 + K_{j+1}^2}\left\{(A_j + A_{j+1})(|Q_j|\,\Delta Q_j - |Q_{j+1}|\,\Delta Q_{j+1}) + (Q_j|Q_j| + Q_{j+1}|Q_{j+1}|)\right.$$

$$\left.\times\left[\frac{B_{Tj}\Delta Z_j + B_{Tj+1}\Delta Z_{j+1}}{2} - \frac{A_j + A_{j+1}}{K_j^2 + K_{j+1}^2}\left(K_j\frac{dK_j}{dZ_j}\Delta Z_j + K_{j+1}\frac{dK_{j+1}}{dZ_{j+1}}\Delta Z_{j+1}\right)\right]\right\}$$

$$+ 0.5\theta\Delta x_j(q_j + \theta\Delta q_j)\left[\left(\frac{\Delta Q_j}{A_j} - \frac{\Delta Q_{j+1}}{A_{j+1}}\right) - \left(\frac{B_{Tj}Q_j}{A_j^2}\Delta Z_j + \frac{B_{Tj+1}Q_{j+1}}{A_{j+1}^2}\Delta Z_{j+1}\right)\right]$$

$$- \frac{Q_j^2}{A_j} + \frac{Q_{j+1}^2}{A_{j+1}} + 0.5g(A_j + A_{j+1})(Z_{j+1} - Z_j)$$

$$+ \frac{g\Delta x_j}{2(K_j^2 + K_{j+1}^2)}(A_j + A_{j+1})(Q_j|Q_j| + Q_j|Q_{j+1}|)$$

$$+0.5\Delta x_j(Q_j + \theta\Delta q_j)\left(\frac{Q_j}{A_j} + \frac{Q_{j+1}}{A_{j+1}}\right) = 0 \tag{3.8}$$

For N computational points, there will be a system of $2(N-1)$ such equations for $2N$ unknowns. With the addition of two boundary conditions, the system of $2N$ algebraic equations for $2N$ unknowns (ΔQ_j, ΔZ_j) can be solved for any time step Δt.

For convenience, the linearized system may be written in the following form:

$$A_{1j}\Delta Q_j + B_{1j}\Delta Z_j + C_{1j}\Delta Q_{j+1} + D_{1j}\Delta Z_{j+1} = G_{1j} \tag{3.9}$$

$$A_{2j}\Delta Q_j + B_{2j}\Delta Z_j + C_{2j}\Delta Q_{j+1} + D_{2j}\Delta Z_{j+1} = G_{2j} \tag{3.10}$$

$$(j = 1,2, ..., N-1)$$

where

$$A_{1j} = -\theta; \qquad B_{1j} = \frac{\Delta x_j}{4\Delta t}(B_{Tj+1} + B_{Tj}); \qquad C_{1j} = \theta;$$

$$D_{1j} = B_{1j}; \qquad G_{1j} = \Delta x_j (q_j + \theta\Delta q_j) - (Q_{j+1} - Q_j);$$

$$A_{2j} = \theta\Delta x_j \left[\frac{1}{2\theta\Delta t} - \frac{2Q_j}{A_j\Delta x_j} + g|Q_j|\frac{A_j + A_{j+1}}{K_j^2 + K_{j+1}^2} + \frac{1}{2A_j}(q_j + \theta\Delta q_j) \right]; \tag{3.11}$$

$$B_{2j} = \theta B_{Tj}\left[(\frac{Q_j}{A_j})^2 + 0.5g(Z_{j+1} - Z_j) \right.$$

$$\left. + \frac{g\Delta x_j(Q_j|Q_j| + Q_{j+1}|Q_{j+1}|)}{2(K_j^2 + K_{j+1}^2)} - \frac{\Delta x_j Q_j}{2A_j^2}(q_j + \theta\Delta q_j)\right]$$

$$- \frac{g\theta\Delta x_j K_j(A_j + A_{j+1})(Q_j|Q_j| + Q_{j+1}|Q_{j+1}|)}{(K_j^2 + K_{j+1}^2)^2}\frac{dK_j}{dZ_j} - 0.5\theta g(A_j + A_{j+1});$$

$$C_{2j} = \theta \Delta x_j \left[\frac{1}{2\theta \Delta t} + \frac{2Q_{j+1}}{\Delta x_j A_{j+1}} + g|Q_{j+1}| \frac{A_j + A_{j+1}}{K_j^2 + K_{j+1}^2} + \frac{1}{2A_{j+1}} (q_j + \theta \Delta q_j) \right];$$

$$D_{2j} = \theta B_{Tj+1} \left[-\left(\frac{Q_{j+1}}{A_{j+1}}\right)^2 + 0.5g\,(Z_{j+1} - Z_j) \right.$$

$$\left. + \frac{g\Delta x_j (Q_j|Q_j| + Q_{j+1}|Q_{j+1}|)}{2(K_j^2 + K_{j+1}^2)} - \frac{\Delta x_j Q_{j+1}}{2A_{j+1}^2} (q_j + \theta \Delta q_j) \right]$$

$$- \frac{g\theta \Delta x_j k_{j+1} (A_j + A_{j+1})(Q_j|Q_j| + Q_{j+1}|Q_{j+1}|)}{(k_j^2 + k_{j+1}^2)^2} \frac{dk_{j+1}}{dZ_{j+1}} + 0.5\theta g (A_j + A_{j+1});$$

$$G_{2j} = \frac{Q_j^2}{A_j} - \frac{Q_{j+1}^2}{A_{j+1}} - 0.5g(A_j + A_{j+1})(Z_{j+1} - Z_j)$$

$$- \frac{g\Delta x_j}{2(k_j^2 + k_{j+1}^2)} (A_j + A_{j+1})(Q_j|Q_j| + {}_{j+1}|Q_{j+1}|)$$

$$-0.5\Delta x_j (q_j + \theta \Delta q_j) \left(\frac{Q_j}{A_j} + \frac{Q_{j+1}}{A_{j+1}}\right).$$

The most salient features of Preissmann's scheme are the following [6,15]:

- it is an implicit scheme, so there is no limitation on time step Δt ;
- it consistently approximates integral conservation laws;
- it calculates both unknown flow variables Q and Z at the same computational grid points;

- it links flow variables together at only two adjacent sections, x_j, x_{j+1}; thus the space intervals $x_{j+1} - x_j$, $x_{j+2} - x_{j+1}$, etc., may be variable while the accuracy of approximation is unaffected.

- it makes the discretization of the boundary condition easy to treat.

3.2. The Double-Sweep Solution Method

Equations (3.9) and (3.10), together with appropriate linearized boundary conditions, furnish a system of linear algebraic equations in terms of increment (ΔQ and ΔZ) of unknown flow variables at time level $(n + 1)\Delta t$. It must be simultaneously solved for all computational points in every time step Δt during the period of computation. However, since this computation is the most time-consuming part of the program, the double-sweep method of solution which is a time-saving procedure is applied as a solver.

The application of the double-sweep method to Preissmann scheme is explained as follows [6,14]. Suppose, in Equations (3.9) and (3.10), that for a point j there is a linear relationship of the type:

$$\Delta Q_j = E_j \Delta Z_j + F_j \tag{3.12}$$

Substitute Equation (3.12) into (3.9) and (3.10) will give

$$(A_{1j}E_j + B_{1j})\Delta Z_j + C_{1j}\Delta Q_{j+1} + D_{1j}\Delta Z_{j+1} = G_{1j} - A_{1j}F_j \tag{3.13}$$

$$(A_{2j}E_j + B_{2j})\Delta Z_j + C_{2j}\Delta Q_{j+1} + D_{2j}\Delta Z_{j+1} = G_{2j} - A_{2j}F_j \tag{3.14}$$

From Equation (3.13), the relationship between ΔZ_j and the increments of dependent variables ΔZ and ΔQ at point $j + 1$ is found:

$$\Delta Z_j = -\frac{D_{1j}}{A_{1j}E_j + B_{1j}}\Delta Z_{j+1} - \frac{C_{1j}}{A_{1j}E_j + B_{1j}}\Delta Q_{j+1} + \frac{G_{1j} - A_{1j}F_j}{A_{1j}E_j + B_{1j}} \tag{3.15}$$

Equation (3.15) can be rewritten as

$$\Delta Z_j = L_j\Delta Z_{j+1} + M_j\Delta Q_{j+1} + N_j \tag{3.16}$$

where

$$L_j = -\frac{D_{1j}}{A_{1j}E_j + B_{1j}}; \quad M_j = -\frac{C_{1j}}{A_{1j}E_j + B_{1j}}; \quad N_j = \frac{G_{1j} - A_{1j}Fj}{A_{1j}E_j + B_{1j}} \tag{3.17}$$

Eliminate the unknown increment ΔZ_j from equations (3.13) and (3.14), then express the discharge increment ΔQ_{j+1} as a function of ΔZ_{j+1} , the result is :

$$\Delta Q_{j+1} = E_{j+1}\Delta Z_{j+1} + F_{j+1} \tag{3.18}$$

where

$$E_{j+1} = -\frac{(A_{2j}E_j + B_{2j})L_j + D_{2j}}{(A_{2j}E_j + B_{2j})M_j + C_{2j}}; \quad F_{j+1} = \frac{G_{2j} - A_{2j}F_j - (A_{2j}E_j + B_{2j})N_j}{(A_{2j}E_j + B_{2j})M_j + C_{2j}} \tag{3.19}$$

Equation (3.18) is the linear relationship form which is indicated by Equation (3.12). It is shown that if the relationship expressed by Equation (3.12) is true for any point of the model, it will also be true for all the following points. Moreover, from Equation (3.19) two recurrence relationship will be obtained:

$$E_{j+1} = E(E_j); \qquad F_{j+1} = F(E_j,F_j) \tag{3.20}$$

Thus, if the linearized upstream boundary condition furnishes (E_1, F_1), all coefficients $(E_j, F_j), j = 2, 3, ..., N$ may be computed. On the other hand, the coefficients L_j, M_j, and N_j in Equation (3.16) can be computed by Equation (3.17). Therefore, as long as the increments ΔZ and ΔQ are known for point $j + 1$, the computation of ΔZ_j is feasible.

The known downstream boundary condition (at point N) will let us express ΔZ_N, then $\Delta Q_N = E_N \Delta Z_N + F_N$, $\Delta Z_{N-1} = L_{N-1} \Delta Z_N + M_{N-1} \Delta Q_N + N_{N-1}$, etc. So, ΔZ and ΔQ for all points $j = 1, 2, ...N$ can be calculated. The method is explained on the flow chart as shown in Figure 8 [14].

The key to the double-sweep method is the appropriate linearized expressions of the boundary conditions at $j = 1$ and $j = N$. This means the boundary conditions have to be expressed in the following forms:

1. At the upstream boundary, $j = 1$, we need to know the relationship

$$\Delta Q_1 = E_1 \Delta Z_1 + F_1 \tag{3.21}$$

   i.e. coefficients E_1 and F_1 must be known.

2. At the downstream boundary, $j = N$, the value of ΔZ_N has to be known.

The restriction of the double sweep technique is that a computational point j is only linked to the adjacent points j-1 and j+1. This is always true in one dimensional flow. Its coefficient expressions are different when one deals with a supercritical flow.

3.3. Boundary Conditions

The original equations based on the de St Venant hypotheses may be applied to gradually varied one-dimensional unsteady flow of natural rivers or channels. Actually, a marked discontinuity in geometrical or hydraulic characteristics in the waterway exists. Typical examples are river junctions, sudden changes in cross sections, flow over weirs or under gates, etc. Therefore, two kinds of boundary conditions are considered. One is the exterior boundary which is located at the ends of the channels to be modeled. The other is the interior boundary to which the gradually varied flow equations cannot be apply. The discontinuity in geometrical or hydraulic characteristics within the channels are defined as the interior boundary [6,14]. For example, the sudden width change of the cross-section between two reaches, junctions of river branches, weir and dam, violate the de St Venant basic hypotheses. At interior boundary, special compatibility conditions must be provided.

Exterior Boundary Conditions

The exterior boundary conditions in a computational model should furnish either the values of coefficients E_1 and F_1 or the value of the water stage increment ΔZ_N. In the practical situation, there are three kinds of exterior boundary conditions [6,14]:

1. $Z = Z(t)$ is given;

2. $Q = Q(t)$ is given;

3. $Q = Q(Z)$ is given.

Upstream Boundary Conditions: The first two conditions can be easily specified for the current problem. They are discussed here.

- $Z_1 = Z_1(t)$ is given

  The water stage at time level $n\Delta t$, Z_1^n is known as well as the water stage at time level $(n + 1)\Delta t$, $Z_1^{n+1} = Z_1(t + \Delta t)$. Consequently, ΔZ_1 is a known value. From Equation (3.12), ΔZ_1 can be written as:

$$\Delta Z_1 = \frac{\Delta Q_1}{E_1} - \frac{F_1}{E_1} \tag{3.22}$$

  Actually, ΔZ_1 should be independent of ΔQ_1. This means $(\Delta Q_1/E_1) \rightarrow 0$ and $(F_1/E_1) \rightarrow -(Z_1^{n+1} - Z_1^n)$. To achieve this, let

$$E_1 = \alpha; \qquad F_1 = -\alpha\left[Z((n + 1)\Delta t) - Z_1^n\right] \tag{3.23}$$

  where α should be very large compared with ΔQ_1, say, on the order of 10^4 to 10^6.

- $Q_1 = Q(t)$ is given

  E_1 and F_1 should be determined such that $\Delta Q_1 = Q(t_n + \Delta t) - Q_1^n$. According to Equation (3.12), ΔQ_1 depends on ΔZ_1, but it should be independent of ΔZ_1 for being used as an arbitrary boundary condition. Let

$$E_1 = 0; \qquad F_1 = Q(t^n + \Delta t) - Q_1^n \tag{3.24}$$

  Then, for whatever the computed value of ΔZ_1 is, ΔQ_1 will always be equal to the boundary condition value.

Downstream boundary condition

- $Z_N = Z(t)$ is given, then

$$\Delta Z_N = Z(t^n + \Delta t) - Z_N^n \tag{3.25}$$

- $Q_N = Q(t)$ is given, then from Equation (3.12)

$$\Delta Z_N = \frac{\Delta Q_N - F_N}{E_N} \tag{3.26}$$

- $Q_N = f(Z_n)$ is given, where $f(Z)$ is either a polynomial or a tabulated function, then

$$f(Z_N^n) + \frac{df}{dZ}\Delta Z_N = E_N \Delta Z_N + F_N + Q_N^n \tag{3.27}$$

therefore,

$$\Delta Z_N = \frac{f(Z_N^n) - F_N - Q_N^n}{E_N - \frac{df}{dZ}} \tag{3.28}$$

Interior Boundary Condition

At an interior boundary, two compatibility conditions are needed to link the reaches in which the de St Venant equations are applicable. One is the continuity equation and the other is the dynamic equation for the particular hydraulic features. Usually, the second kind of condition concerns the compatibility of the water stage or the total energy. In this thesis, only interior boundaries such as the junctions where lateral concentrated inflows occured are considered.

In order to perform the double sweep method through an interior boundary section j, usually an additional section $j + 1$ has to be added to the channel at the position very close to the interior boundary. One can consider that the distance between sections j and $j + 1$ equals zero. A concentrated discharge flowing into the channel or out of the channel at cross-section j is shown in Figure 9.

The coefficients E_j and F_j are computed by Equations (3.19) from known E_{j-1} and F_{j-1}. To continue the computations, the coefficients E_{j+1} and F_{j+1} are needed. Then, the coefficients $(E, F)_{j+2}$ etc. can be computed by the recurrence Equations (3.19). The coefficients L_j, M_j, and N_j are also needed to compute ΔZ_j when ΔZ_{j+1} and ΔQ_{j+1} are known. All of these coefficients depend upon the characteristics of the transition relationship. For simplification, the total energy at the section j is always supposed to be the same as the total energy at the section $j + 1$ because the section $j + 1$ is considered to have the same location as the section j.

The energy equation at section j and section $j + 1$ is

$$Z_j^{n+1} + \frac{(u_j^{n+1})^2}{2g} = Z_{j+1}^{n+1} + \frac{(u_{j+1}^{n+1})^2}{2g} \tag{3.29}$$

The continuity equation between sections j and $j + 1$ is

$$Q_{j+1}^{n+1} = Q_j^{n+1} + Q_c^{n+1} \tag{3.30}$$

where Q_c is the concentrated side discharge flowing into or out of the channels at the junction section j.

According to the Taylor power series expansion, Equation (3.5), the velocity at time level $(n + 1)\Delta t$ may be expressed as following:

$$u^{n+1} = u^n + (\frac{\partial u}{\partial Z})^n \Delta Z + (\frac{\partial u}{\partial Q})^n \Delta Q \tag{3.31}$$

Since

$$u = \frac{Q}{A} \tag{3.32}$$

one may obtain

$$\frac{\partial u}{\partial Q} = \frac{1}{A} \tag{3.33}$$

$$\frac{\partial u}{\partial Z} = -\frac{Q}{A^2}\frac{\partial A}{\partial Z} = -\frac{uB}{A} \tag{3.34}$$

Substituting the following equations into Equations (3.29) and (3.30),

$$Z^{n+1} = Z^n + \Delta Z \tag{3.35}$$

$$Q^{n+1} = Q^n + \Delta Q \tag{3.36}$$

$$u^{n+1} = u^n - \frac{uB}{A}\Delta Z + \frac{1}{A}\Delta Q \tag{3.37}$$

and neglecting the terms of second order, one obtains following Equations:

$$Q_{j+1} + \Delta Q_{j+1} = Q_j + \Delta Q_j + Q_c^{n+1} \tag{3.38}$$

$$Z_j + \Delta Z_j + \frac{u_j^2}{2g} - \frac{u_j^2}{gA_j}B_j\Delta Z_j + \frac{u_j}{gA_j}\Delta Q_j$$

$$= Z_{j+1} + \Delta Z_{j+1} + \frac{u_{j+1}^2}{2g} - \frac{u_{j+1}^2}{gA_{j+1}}B_{j+1}\Delta Z_{j+1} + \frac{u_{j+1}}{gA_{j+1}}\Delta Q_{j+1} \tag{3.39}$$

Substituting Equation (3.12) into Equation (3.38) yields

$$\Delta Z_j = \frac{1}{E_j}\Delta Q_{j+1} + \frac{Q_{j+1} - Q_j - Q_c^{n+1} - F_j}{E_j} \tag{3.40}$$

By comparing Equation (3.40) with Equation (3.16), one can write the coefficients as the following:

$$L_j = 0; \quad M_j = \frac{1}{E_j}; \quad N_j = \frac{Q_{j+1} - Q_j - Q_c^{n+1} - F_j}{E_j} \tag{3.41}$$

By the same process, from Equation (3.39) the recurrence coefficients can be written as follows:

$$E_{j+1} = -\frac{D}{\beta}; \quad F_{j+1} = \frac{G - \alpha N_j - AF_j}{\beta} \tag{3.42}$$

where

$$\alpha = AE_j + B; \quad \beta = \frac{\alpha}{E_j} + C; \quad A = \frac{u_j}{gA_j}; \quad B = 1 - \frac{u_j^2 B_j}{gA_j};$$

$$C = -\frac{u_{j+1}}{gA_{j+1}}; \quad D = \frac{u_{j+1}^2 B}{gA_{j+1}} - 1; \quad G = Z_{j+1} - Z_j + \frac{u_{j+1}^2 - u_j^2}{2g}. \tag{3.43}$$

3.4. Program Development

The program is developed in interactive mode [23]. It has two sub-packages. The sub-package PCDCCR is for pre-processing topographic data. It consists of one main program and five subroutines. The channels involved in the model may be distinguished

into three categories: trapezoidal prismatic channels, arbitrary shaped prismatic channels, and irregular natural channels. The original topographic data can be described either by bottom width b and side slope m (for trapezoidal channel) or coordinates (for irregular natural channel). The function of PCDCCR is to generate a data file of A(x,h), B_T (x,h), R(x,h), K(x,h) and n(x,Q). The data file is prepared for the sub-package MYBCY. The function of each subroutine are described as follows:

- PCDCCR

  Main program, control operation and generate the data file of A(x,h), B_T(x,h), R(x,h), K(x,h) and n(x,Q).

- CPABR

  Calculate A(h), B_T(h), and R(h) for a trapezoidal channel.

- HABRJN

  Calculate A(h), B_T(h), and R(h) for one section of a irregular channel.

- HABRXN

  Calculate A(x,h), B_T(x,h), and R(x,h) for all sections of the channel.

- COMKN

  Calculate K(x,h) or n(x,Q).

- TYPE11

  Output A(x,h), $B_T(x,h)$, and R(x,h).

The sub-package MYBCY is the main part of the program. It contains a main program and seventeen subroutines. Their functions are listed as following:

- MYBCY

  Main program, control operation, select parameters, generate the data files for calculated results of Q(x,t), Z(x,t), h(x,t), and U(x,t).

- PCABR

  Read pre-processed topographic data file calculated by PCDCCR.

- NUMIN1

  Input hydraulic data file which includes the number of time steps, initial water depthes h(x,0), initial discharge Q(x,0), Manning roughness coefficients n(x,Q), upstream boundary condition Q(0,t) or Z(0,t), and downstream boundary condition Q(L,t), Z(L,t), or Q(L,Z).

- INTER

  Judge interior boundaries.

- NUMIN2

  Input interior boundary conditions which are discharge hydrographs for concentrated inflow (or outflow).

- CHABR

  Calculate A, B_T, and R for known water depth h at one section.

- LAQP

  Subroutine for interpolation.

- IMPREI

Preissmann's implicit scheme.

- ZHQU

  Calculate Z^{n+1}, H^{n+1}, U^{n+1}, and Q^{n+1} by $f^{n+1} = f^n + \Delta f$.

- UBZTQT

  Calculate E_1 and F_1 at upstream boundary by Equations (3.23) or (3.24).

- LBZTQT

  Calculate $\Delta Z(N)$ and $\Delta Q(N)$ at downstream boundary by Equations (3.25), (3.26), or (3.28).

- DZDQ

  The backward sweep procedure of double sweep method, calculate $\Delta Z(j)$ and $\Delta Q(j)$, $j = 1,2, \ldots\ldots, N-1$, by Equations (3.12) and (3.16).

- DKDDZ

  Calculate dK/dZ at each calculation point.

- CKCRI

  Calculate K at each section by Equation (2.46).

- SWEEPA

  The forward procedure of the double sweep method, calculate E_j, F_j, L_j, M_j, and N_j $j = 1, 2, \ldots\ldots, N-1$ by Equation (3.19) and (3.17).

- DQSX

Calculate pre-coefficients.

- COEFA

  Method 1 to calculate A_{1j} , B_{1j} , ..., G_{2j} by equation (3.11).

- COEFB

  Method 2 to calculate A_{1j} , B_{1j} , ..., G_{2j}.

The mathematical model is programmed to be suitable for studying both regular prismatic channels and irregular natural channels. The channel system may be a single channel or a branched channel system (also called 'tree-like'). The upstream boundary condition can be described by a water stage-time relationship or a discharge hydrograph. The downstream boundary condition can be described by a water stage-time relationship, a discharge hydrograph, or a rating curve (stage-discharge relationship). So, there are six possible combinations under consideration. Two formulas of discretization for the frictional resistance force term are derived to make the modelling technique more flexible. The best features of the model are its stability and time-saving because of the use of the Preissmann implicit scheme and the double sweep algorithm method.

Chapter 4. Model Calibration, Verification, and Application

4.1. Data Needs for Calibration

A mathematical model is a simplified, discrete representation of a complex and continuous physical flow situation. Natural three-dimensional feature of flow is represented by one-dimensional elements in this study. The physics of flow are assumed to be governed by the de St Venant Equations in which certain empirical coefficients are involved. Model calibration and verification are the processes of judging the rationality of the simplified one-dimensional approach and determining the values of empirical hydraulic coefficients so that flow characteristics simulated by the model will reproduce as faithfully as possible the comparable natural events. In the modelling practice, unsteady flow calibration and verification involve in adjusting model features which include the representations of the cross-sections and the values of Manning's roughness coefficients in such a way as to obtain coincidence between observed and computed water surface elevation variations with respect to time.

A model's potential for reproducing and predicting real flow events essentially depends on the suitability of the governing equations used and the amount and quality of topographical and hydraulic data available for calibration and verification. The basic data required for an unsteady flow model can be grouped into two classes: topographic and hydraulic. Topographic data describe the geometry features of the channel system to be simulated. They have to supply accurate information necessary to define widths, cross-sectional areas, hydraulic radius, and bed slopes, etc. at representative cross-sections along the channels where the computational points are established. Usually, the width $B_T(h)$, wetted area $A(h)$, and conveyance $K(h)$ at a section are functions of water depth. The Manning's roughness coefficients $n(Q)$ are the function of discharges. Hydraulic data consist of measurement of water stage and discharge hydrographs. These data serve two purposes: the establishment of model initial and boundary conditions and the indirect determination of channel roughness coefficients. Discharge hydrograph at the upstream boundary and the water stage-time relationship at the downstream boundary are required for the model of the Third Navigation Channel. Discharge and water stage observations as a function of time at various stations are needed for calibration and verification of the model.

4.2. Prototype Test

In early 1983, the Lock Operation Office of the Yangtze River Navigation Administration organized a prototype test in which approximately two hundred people were involved. The purpose of the test was to obtain the field topographic and hydraulic data [7]. Under the full consideration of the field situation and mathematical model, ten water level observation stations were established along the channel with an additional dis-

charge observation station located at cross-section *No.*1. The arrangement of the observation stations for the field test and the computational sections for the mathematical model is shown in Figure 10.

The cross sections of all observation stations and computational points are surveyed and the plots of cross-sectional profiles are shown in Figure 11 through Figure 15. At each observation station, water levels were recorded every minute for two and half hours for each test. The discharge hydrograph released from the lock chamber was also measured at cross section No.1. During the test, water levels were about 60*m* and 39*m* at upstream and downstream of the dam respectively. The maximum instantaneous discharge measured at section *No.*1 was $545m^3/s$.

4.3. Calibration and verification

For the mathematical model, there are fourteen computational points. Some of them are exactly placed at the observation stations. These computational points are carefully chosen so that the width, wetted area, and roughness at a section represent not only this particular section, but also the entire reach ΔX between two adjacent cross sections. Therefore, the space steps between two computational points are not constant and their range is from 187*m* to 346*m*. It is believed that each of the computational points chosen in the model adequately represents the characteristic features of the entire reach in which the point is located. The procedure of calibtration becomes such a process to adjust the Manning's roughness coefficients in order to achieve the best overall agreement between the calculated water stage and the measured water stage at all observation stations for the entire simulation time period. When the mathematical model simulates the prototype test situation, the upstream boundary condition used is the

measured discharge hydrograph as shown in Figure 16 by the scattered points and the downstream boundary condition is the measured water stage-time relationship as shown in Figure 17 also by the scattered poinds [23]. The initial condition is a static situation, that is, the initial water depths are the differences between the horizontal water surface elevations and the bed elevations and the initial discharges are zero everywhere.

In the man-made channel with smooth bed surface composed by very fine sand, Manning's roughness coefficient is within the range of 0.01 to 0.02. When Manning's roughness coefficient n equals 0.015 at all computational points, the calculated water level variations coincide with the measured field data quite well in the calibration process. With the adaption of $n = 0.015$, the results of a verification case are shown in Figure 18 to Figure 21 in terms of time variation of water level [23]. The maximum variance between observed data and calculated values is on the order of 10 cm. It is noticed that the variances of the first wave at section No.2 are only 4 cm. Therefore, the performance of the mathematical model is considered to be fair to good. The next step is to simulate the unsteady flow for various situations.

4.4. Simulation

Using the mathematical model calibrated and verified previously, a simulation has been made base on initial water elevation in the main stream of the Yangtze River of $39m$ above mean sea level. The calculated water surface elevation profiles in the Third Navigation Channel are shown in Figure 22. The profiles indicate the water surface elevation vary with respect to time and distance. From the figure, one can see that when $t = 5$ minutes, the water surface profile is higher than the initial water elevation and the maximum water level increase $\Delta Z = +0.8m$ occured at $x = 800m$. When $t = 20$

minutes, the water surface profile is lower than the initial condition and the maximum water level decrease $\Delta Z = -0.7m$ occured at the upstream boundary. When $t = 40$ minutes, the water surface profile rises again. At $t = 60$ minutes, the water surface profile still oscillates. When water elevation is much lower than $39m$, obviously the water depth is inadequate and may be dangerous for navigation.

Research to seek for methods to improve the navigation condition in the Third Navigation Channel is the purpose of this study. According to the analysis of the data requirements for the mathematical model, all hydraulic and topographic parameters are to be studied in order to come up with viable methods. They are listed as follows:

- Upstream boundary condition. In the mathematical model, the discharge hydrograph, $Q(0,t)$, released from the lock chamber is used to describe the upstream boundary conditions. By controlling the valve opening time, the upstream boundary condition would vary in terms of change in peak discharge and lock emptying time.

- Side discharge. The side discharge is the flow released from the lock chamber and transported through conduits to downstream points of cross section *No.*1. In the model, the side discharge is considered as the interior boundary condition. The side discharge may be the total discharge or part of the discharge released from the lock chamber and distributed at downstream sections.

- Channel bed roughness. By using different values of Manning's roughness coefficient in model simulation, one can compare the effects of smooth bed and rough bed on the characteristics of unsteady flow in the channel.

- Topographic condition. By modifying the channel's cross-sections through changes in depth, shape and side slopes, etc. one can assess changes in water stages and velocities in the channel.

Upstream Boundary Condition

Water in the lock chamber is discharged into the channel through a culvert system as shown in Figure 23. The unsteady flow occured in the channel is a result of non-constant discharge from the lock chamber. The lock chamber emptying time should be kept as short as possible because the emptying time is an important factor related to the cost and efficiency of the Yangtze River navigation. However, the degree of oscillation of water surface elevation and water velocity caused by unsteady flow is a function of the emptying time. In order to analyze the influence of the emptying time on the unsteady flow in the channel, a discharge hydrograph formula is derived in order to vary the upstream boundary conditions.

For simplicity, assume that the water is discharged from the lock chamber through a single culvert, as shown in Figure 24. At a given time t, the head difference between the water levels inside and outside the lock chamber is H. Energy considerations yield the following equation [16]:

$$H = [K_i + K_f + K_o + K_v - (\frac{a}{A_c})^2 + (\frac{a}{A_d})^2]\frac{Q^2}{2ga^2} \tag{4.1}$$

where a is the valve opening area which varies with respect to time; K_i, K_f, K_o, and K_v are head loss coefficients due to inlet, boundary friction, outlet, and valve constriction, respectively; A_c and A_d are the flow areas in the lock chamber and the channel, respectively. The instantaneous discharge is

$$Q = a\sqrt{2gH}\frac{1}{\sqrt{K_l + K_f + K_o + K_v - (\frac{a}{A_c})^2 + (\frac{a}{A_d})^2}} \tag{4.2}$$

All loss coefficients may be combined into a single coefficient C_D which varies with the head difference H. Therefore the coefficient C_D is expressed as:

$$C_D = \frac{1}{\sqrt{K_l + K_f + K_o + K_v - (\frac{a}{A_c})^2 + (\frac{a}{A_d})^2}} = C\frac{H}{H_0} \tag{4.3}$$

where H_0 is the initial head difference. The discharge is then expressed by the following formula:

$$Q = C\,a\sqrt{2g}\frac{H}{H_0}H^{0.5} \tag{4.4}$$

where the coefficient C is less than unity.

Assume the valve has an opening w wide by h high as shown in Figure 25. The valve is normally opened gradually rather than instantaneously. The speed of the valve opening is assumed to be constant during the total opening time period T. At a given time step i ($i = 1, 2, ..., M$), the valve opening angle is expressed as:

$$\theta = \frac{\pi\ i\Delta t}{2\ \ T} \tag{4.5}$$

At time $i\Delta t$, the height of the opening B is expressed as:

$$B = h(1 - \cos\theta) \tag{4.6}$$

The valve opening area at time $i\Delta t$ is:

$$a = wh(1 - \cos\theta) \tag{4.7}$$

The discharge at any time $i\Delta t$ may be expressed by the following formula:

$$Q = C\,w\,h\,(1 - \cos\frac{\pi i\Delta t}{2T})\,2g\frac{H}{H_0}H^{0.5} = f(i\,\Delta t, H^i, T) \tag{4.8}$$

Equation (4.8) shows that the discharge hydrograph is a function of the head difference H^i at time $i\Delta t$ and the total valve opening time period T. The water volume flowing out of the chamber during a time interval Δt is $Q\Delta t$. It is approximately equal to $A\Delta H$, where A is the horizontal cross-section area of the lock chamber and it is known $A = 280 \times 34m^2$ based on the dimensions of the lock chamber. The decrease in water level inside the lock chamber during a time interval Δt is :

$$\Delta H = \frac{Q\Delta t}{A} = \frac{Q\Delta t}{9520} \tag{4.9}$$

By neglect of the water surface variation in the channel, the head difference at the next time step $i + 1$, becomes

$$H^{i+1} = H^i - \Delta H \tag{4.10}$$

If the initial head difference H_0 between the lock chamber and the Third Navigation Channel is known and the valve opening time period T is determined, the discharge hydrograph at the upstream boundary may be calculated step by step until the head difference H^{i+1} becomes zero. The flow chart for calculating the hydrograph is shown in Figure 26.

Figure 16 shows the discharge hydrographs due to water release from the lock chamber. The solid line is the calculated values by Equation (4.8) with the initial head

difference of $H_0 = 60 - 39 = 21m$ and the total valve opening time period $T = 10$ minutes. The scattered points are the measured data. It is shown that the calculated values and the measured data match quite well. Therefore, the formula derived to calculate the upstream boundary discharge hydrograph is considered reasonable. In Figure 27, three other discharge hydrographs are plotted. They are calculated based on Equation (4.8) with the design head $H_0 = 63 - 39 = 24m$, the velocity coefficient $C = 0.8$, the total opening area $a = 240m^2$, and the total valve opening time $T = 5$, 10, and 20 minutes, respectively. These hydrographs will be used as the upstream boundary conditions when the effects of the valve opening time on unsteady flow in the channel are simulated.

The three different valve opening times are simulated under the following conditions:

- Initial conditions: $Q(j,0) = 0$, $Z(j,0) = 39m$, $j = 1,2,.....,14$.

- Manning's roughness coefficient: $n = 0.015$ for all sections.

- Downstream boundary conditions: $Z(14,t) = 39m$

- Upstream boundary conditions: The discharge hydrographs released from lock chamber shown in Figure 27 represent three different total valve opening times of 5, 10, and 20 minutes, respectively.

The results of these simulations are shown in Figure 28 through Figure 31. For the sake of comparison, the computational results for the case of valve opening time being 10 minutes are used as a reference for other simulations. The average amplitudes of variation of water surface elevation are about $1.2m$, $1.0m$, and $0.7m$ at the cross-section *No.*2 for 5, 10, and 20 minutes valve opening time, respectively. At the cross-section

*No.*11, they are 0.6*m*, 0.5*m*, *and*0.4*m*, respectively. The distinct differences among them, either at the section *No.*2 or *No.*11, occur when the first waves arrive there. Then, the differences gradually become smaller.

In the mathematical model, two dependent variables are water elevation $Z(x,t)$ and discharge $Q(x,t)$. Figure 32 which corresponds to 10 minutes valve opening time shows the calculated discharge hydrographs at the section *No.*2 and *No.*11. Positive Q occures when water flows from the Third Navigation Channel into the Yangtze River. Negative Q values mean water flows from Yangtze River into the channel. This variation in discharge is more significant for sections near the downstream boundary than other upstream sections. This explains that larger oscillations of the velocity occured at section *No.*11 than that at the section *No.*2 as shown in Figure 5.

Side Discharge

From the discussion made in the previous paragraphs, it is known that the larger the peak discharge released from the lock chamber is, the larger the amplitude of the water level variation in the channel would be. In order to reduce the amplitude, it is reasonable to try to avoid this type of concentrated discharge at the head of the channel.

The side discharge is to distribute the discharge released from the lock chamber through distribution pipes to the different downstream sections instead of total discharge concentrated at the upstream boundary only. Two distribution methods are considered. One deals with an uniform distribution at every downstream section, the other deals with a nonuniform distribution at every downstream section.

Uniform distribution: In engineering practice, this alternative may be approached by designing different port sizes at different downstream sections along a large single pipe.

Two cases have been simulated. For the first case, total discharge released from the lock chamber is equally distributed at thirteen sections except the downstream boundary. The uniform side discharge hydrograph at each section is shown in Figure 33. For the second case, one half of total discharge is equally distributed at twelve downstream sections and the other half remains at the upstream boundary. The discharge hydrograph at the upstream boundary and the side discharge hydrographs at every downstream sections are are shown in Figure 34. The variations of water surface elevation at section *No.*2 and *No.*11 for both cases together with the case of no side discharge are shown in Figure 35 and Figure 36.

Obviously the total discharge being uniformly distributed as side discharges is the best among the three cases. The average amplitude of the water surface elevation caused by the total discharge being uniformly distributed is only one half of the average amplitude caused by the case of no side discharge. The velocity variations for the three cases are shown in Figure 37 and Figure 38. At section *No.*2, the velocity variation caused by total discharge being uniformly distributed rapidly reaches zero after 10 minutes. At section *No.*11, the amplitude is less than one half of the amplitude caused by the case of no side discharge.

Nonuniform distribution: 25% and 50% of the total discharge distributed to twelve downstream sections with a nonuniform distribution are two alternatives investigated. In other words, the discharge hydrographs at upstream boundary are 75% and 50% of the total discharge, respectively. Again, the case of no side discharge is included as a reference case for the purpose of comparison with two alternatives.

In the distribution pipes, the water travels through a long distances between the lock chamber and the downstream outlets. Therefore, the minor losses and outlet loss are relatively unimportant and may be neglected in the energy equation. Approximately,

the head difference between water levels in the lock chamber and the channel equals to the friction loss:

$$H = f\frac{l}{d}\frac{V^2}{2g} \tag{4.11}$$

or

$$V = \sqrt{\frac{2gHd}{fl}} \tag{4.12}$$

During a time interval Δt, the head H is treated as a constant for all distribution pipes.

Suppose that all distribution pipes have the same in diameter and material. Therefore, the flow rate in a single distribution pipe is propotional to the inverse of the square root of its length l:

$$Q = \frac{C}{\sqrt{l}} \tag{4.13}$$

where

$$C = \frac{\pi d^{2.5}}{4}\sqrt{\frac{2gH}{f}} \tag{4.14}$$

Therefore, the total discharge Q distributed to the downstream sections may be expressed as:

$$Q = \sum_{j=1}^{12} Q_{sj} \qquad j = 1,2,.....,12. \tag{4.15}$$

where Q_{sj} is the side discharge flowing into the $(j + 1)th$ section. Q_{sj} may be expressed as the following form:

$$Q_{sj} = C_j \frac{Q}{12} \tag{4.16}$$

where C_j is the side discharge weighting coefficient. It is assumed to be propotional to the inverse of the square root of the pipe length between the upstream boundary and the $(j + 1)th$ cross-section. Therefore, C_j may be expressed as:

$$C_j = \frac{K}{\sqrt{l_j}} \tag{4.17}$$

and an additional limitation is assumed as:

$$\sum_{j=0}^{12} C_j = 12 \tag{4.18}$$

Solving Equations (4.17) and (4.18), one obtains the parameter $K = 34.65$. Then, all weighted coefficients at every section can be calculated by Equation (4.15). All weighted coefficients are listed in Table 1.

Table 1. Side discharge weighting coefficients

A_1	A_2	A_3	A_4	A_5	A_6	A_7	A_8	A_9	A_{10}	A_{11}	A_{12}
1.95	1.45	1.26	1.11	0.99	0.91	0.84	0.77	0.73	0.69	0.66	0.64

With 25% of the total discharge released from the lock chamber are distributed at downstream sections, the side discharge hydrographs at sections *No.*1, *No.*2, and *No.*5 are shown in Figure 39. Figure 40 shows the side discharge hydrographs with 50% of total discharge distributed as the side discharges.

The mathematical simulation results are shown in Figure 41 through Figure 44. The case of no side discharge represents the reference case. Comparison of these figures shows that the larger the side discharges are, the smaller the amplitudes of both water surface and velocity variations are.

The cases of 50% side discharges for both uniform and nonuniform distributions are compared in Figure 45 through Figure 48. There are almost no significant differences in water elevation and velocity variations between the two cases.

To compare the methods of uniform side discharge along the channel with the concentrated discharge at the upstream boundary, an additional simulation has been made. Assuming the allowable maximum amplitude in water surface elevation variation under design condition is ± 0.25 m. This requirement can be met by either 5 minutes valve opening time with uniform side discharge or 55 minutes valve opening time without side discharge. The comparisons of the two approaches are shown in Figure 49 through Figure 52. For this example, the side discharge method has saved the lock emptying time by 50 minutes. Thus, it greatly increases the shipping capacity through the lock systems at the Gezhouba Water Control Project.

Manning's Roughness Coefficient

Three cases with n = 0.012, 0.015, and 0.02 are simulated. The results are shown in Figure 53 through Figure 56. These figures reveal that there are no phase differences at all. At the beginning of the water wave propagation and near the head of the channel, the water surface and velocity variations are very much independent of the n value. The differences in amplitude become larger while the waves propagate downstream and as time increases. As expected, the larger the n value is, the smaller the amplitudes are.

But the influence of bed roughness on the unsteady flow in the channel seems insignificant.

Channel's Topographic Condition

For the existing navigation channel at the Gezhouba Water Control Project, it is possible to modify the channel's cross-sectional profiles at various reaches. From the engineering point of view, the channel's cross-sections may be modified through changes in depth, shape and side slopes, etc. The proposed channel modifications are shown in Figure 12 through Figure 16 by the dot and dash lines. The comparisons of water surface elevation and velocity variations in the modified channel with the existing channel are shown in Figure 57 through Figure 60. The phase differences are obvious. But they have little effect on the improvement in navigation conditions. The amplitudes of wave propagation are almost the same for each other. Therefore, the method of modifying the channel's cross-sections seems not improving the navigation condition.

Chapter 5. Conclusions

The following conclusions are drawn from this study:

1. Any significant variation of water surface elevation and velocity in a navigation channel, in general, is hazardous to navigation. The variations during the lock operation are mainly caused by the unsteady discharge from the lock chamber. The peak discharge at the upstream boundary of the channel is dictated by the lock emptying time (shown in Figure 27). Longer emptying time will yield smaller peak discharge and hence produce smaller amplitudes for water surface elevation and velocity variation.

2. The de St Venant Equations have been shown to be a good representation of the complex one-dimensional unsteady flow in the Third Navigation Channel. The mathematical model which is based on these governing equations, calibrated and verified using the prototype test data is a useful tool to analyze the flow in the channel and to seek for methods to improve the navigation condition.

3. The input data for the mathematical model include the hydraulic and topographic parameters such as discharge hydrograph at the upstream boundary, downstream water level, channel roughness and channel's cross-sections. According to the results from a series of mathematical simulations, changes in discharge characteristics at the upstream boundary have the most significant effects on the amplitudes and phases of wave propagation in the navigation channel. The rest of the parameters seem to have less effects on the Third Navigation Channel.

4. Instead of concentrated discharge at the upstream boundary, the side discharges which distribute the water released from the lock chamber along the entire length of the navigation channel has been shown to greatly reduce the variations in water surface elevation and velocity. With the side discharge scheme, lock emptying time can be shortened and hence the shipping capacity through the lock systems is increased.

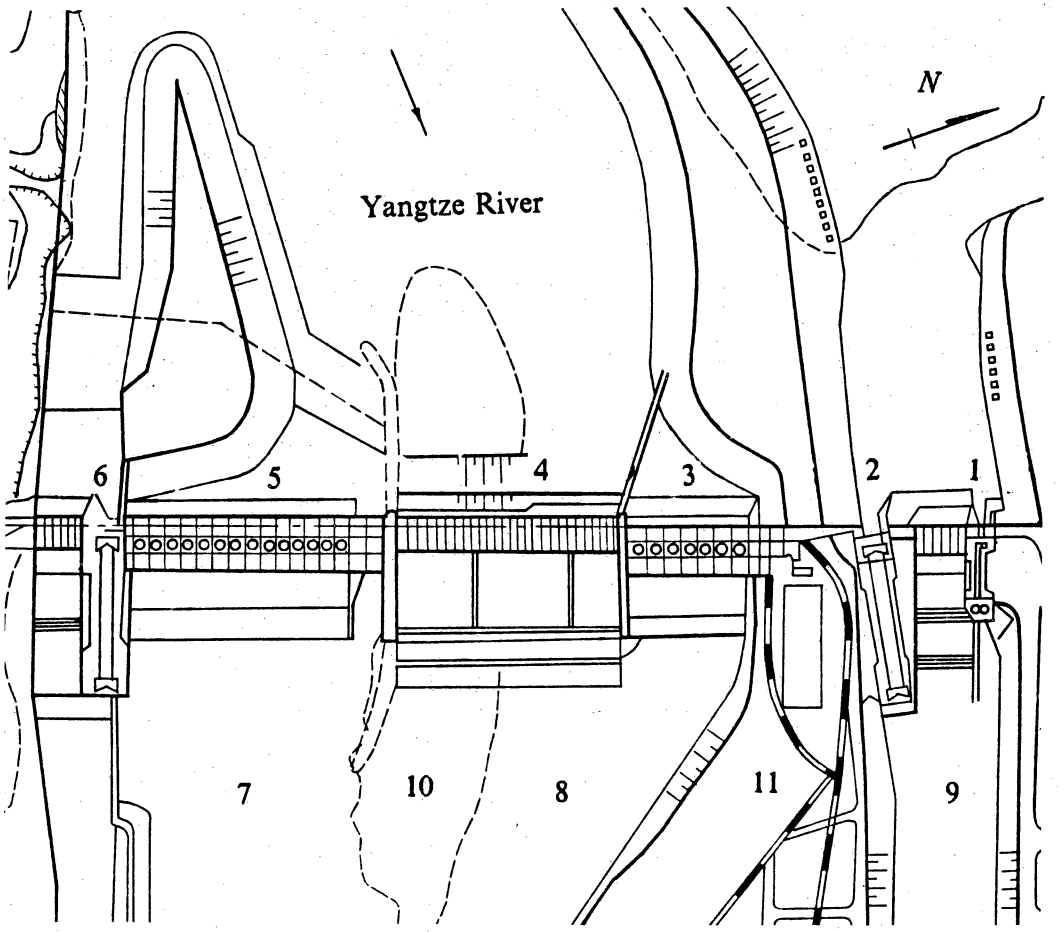

1. Lock *No.*3
2. Lock *No.*2
3. Power station on the Second Channel
4. Spillway
5. Power station on the Grand Channel
6. Lock *No.*1
7. The Grand Channel
8. The Second Channel
9. The Third Channel
10. Gezhouba island
11. Xiba island

Figure 1. The Gezhouba Water Control Project (plan view)

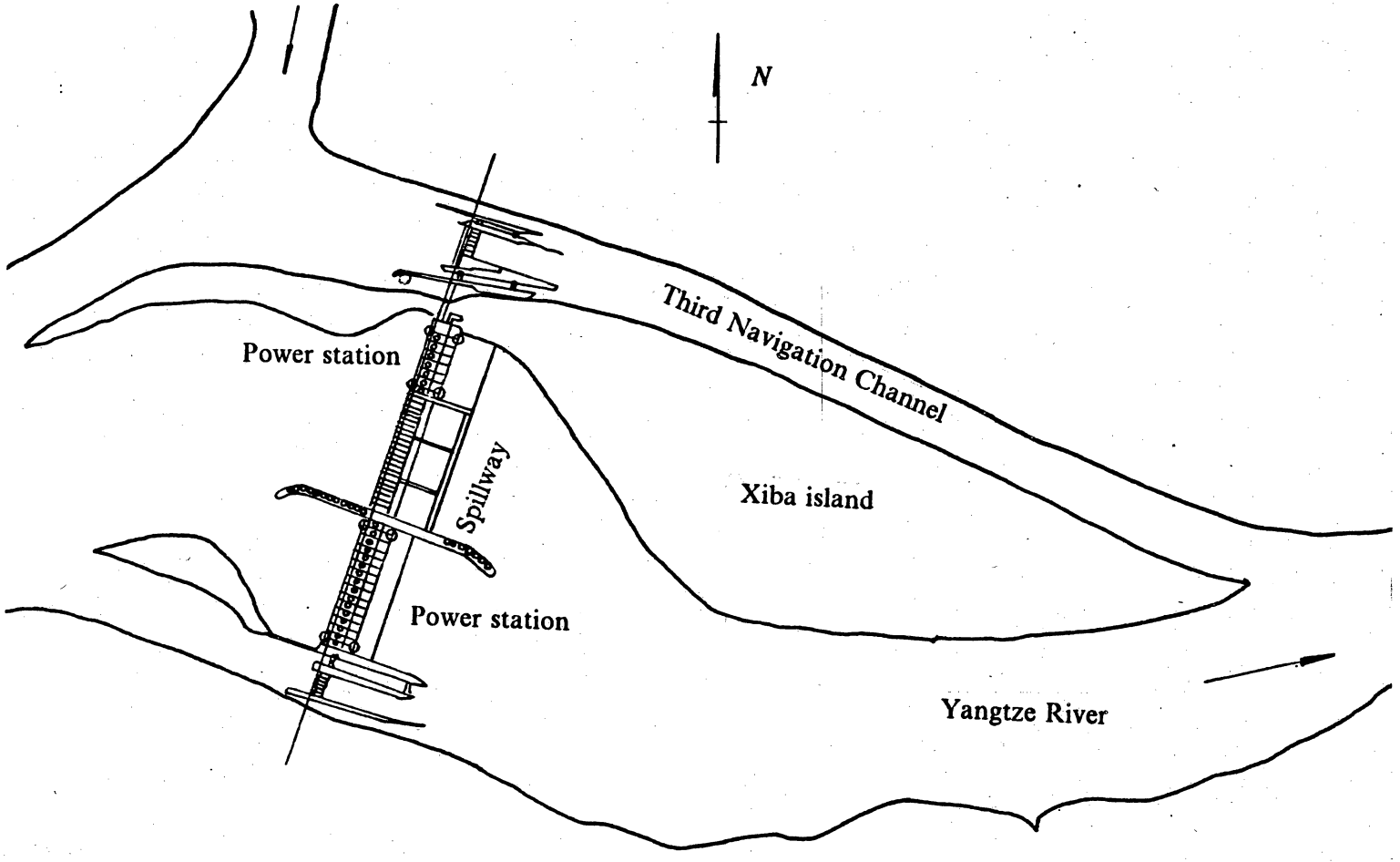

Figure 2. The Third Navigation Channel

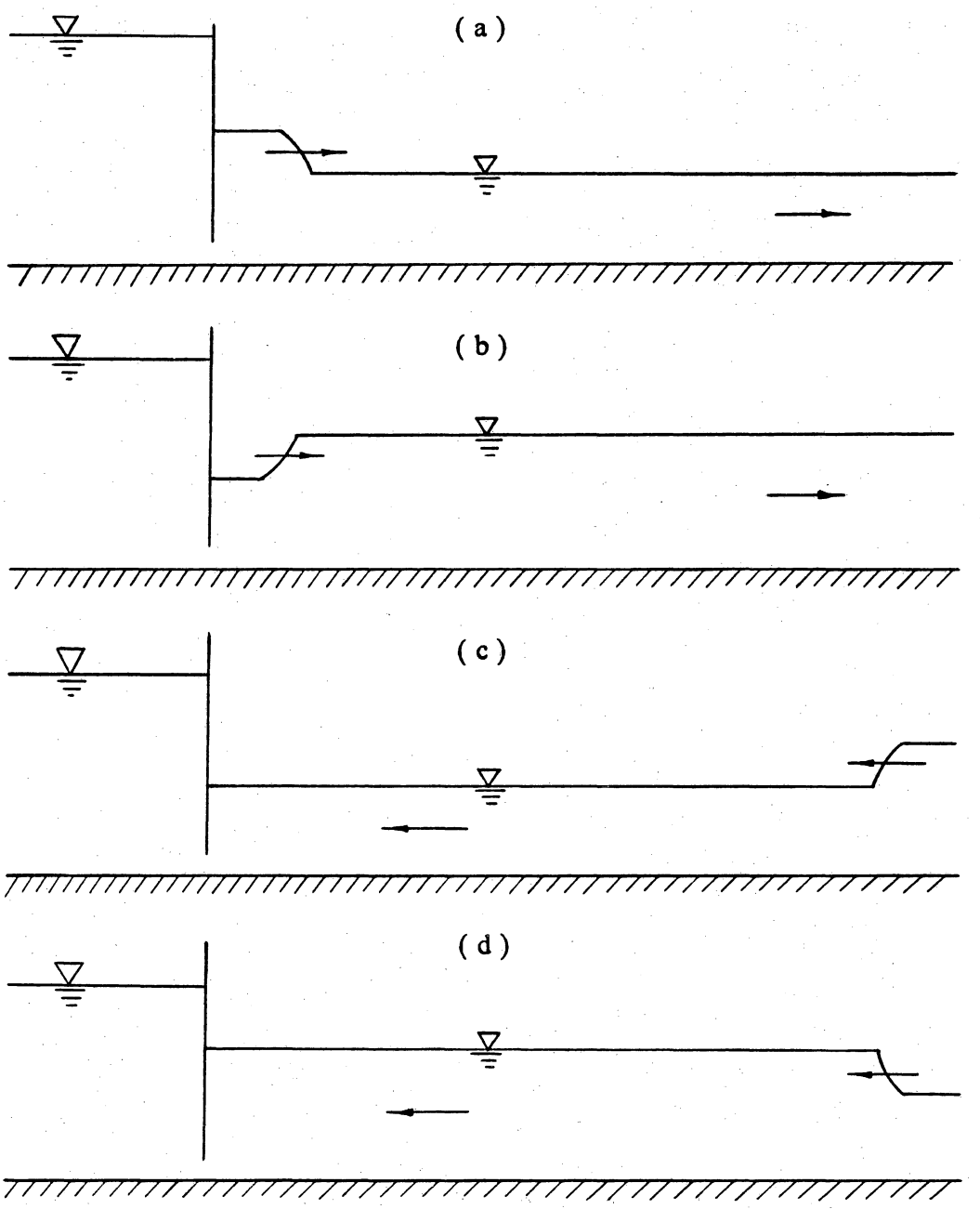

(a) Positive wave with positive velocity (c) Positive wave with negative velocity

(b) Negative wave with positive velocity (d) Negative wave with negative velocity

Figure 3. Water wave propagation in the Third Navigation Channel

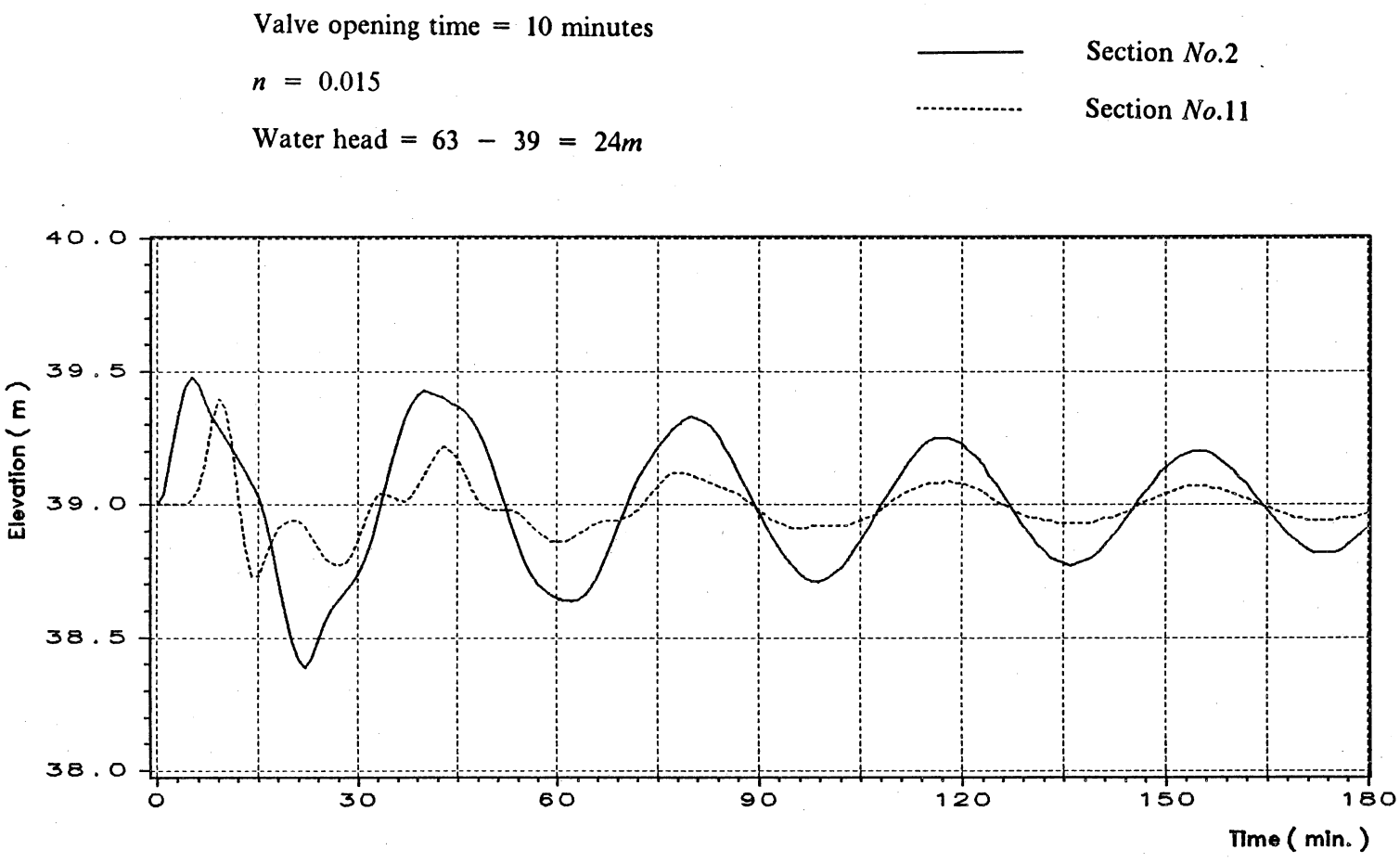

Figure 4. Water surface elevation variations at different sections

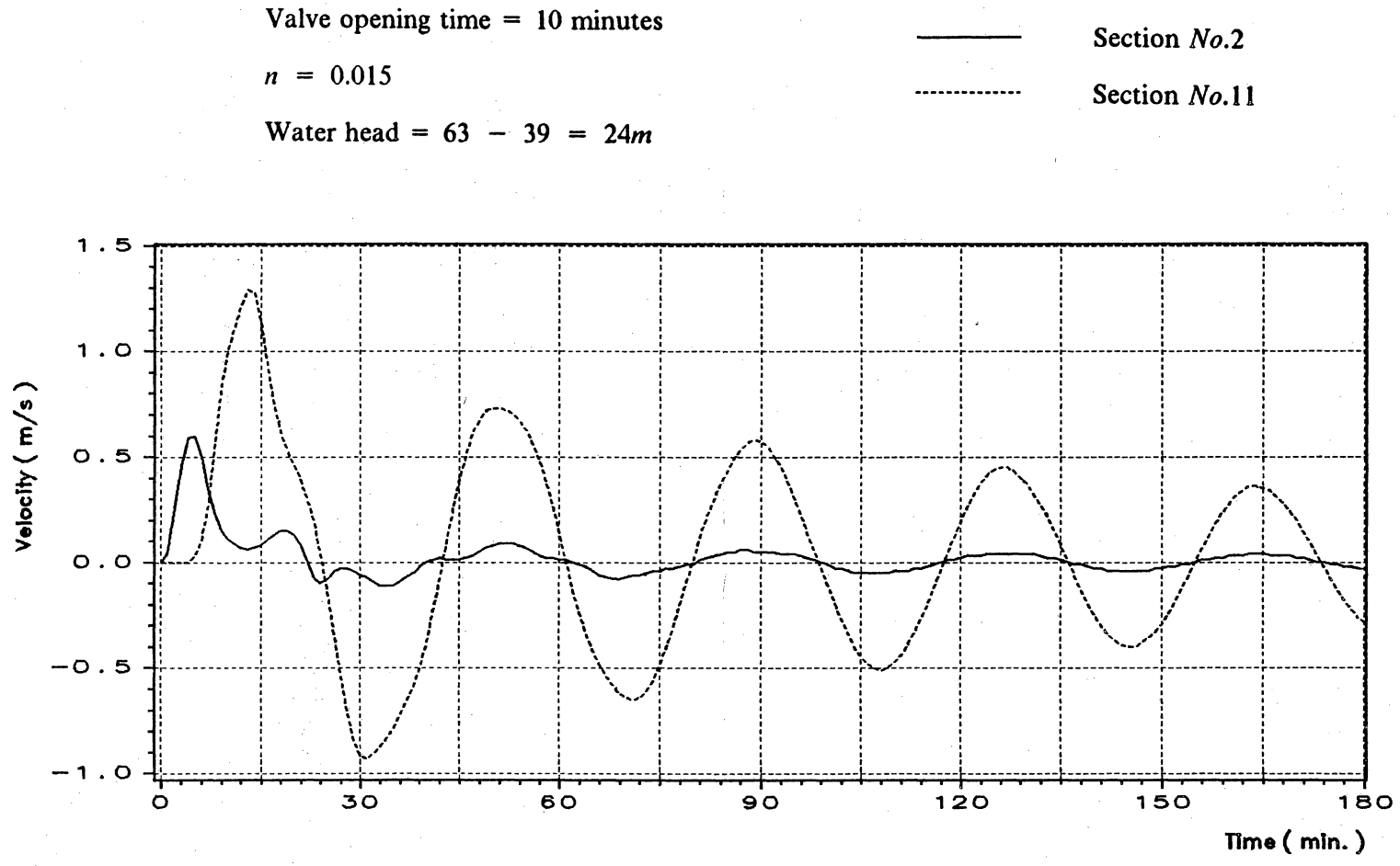

Figure 5. Water velocity variations at different sections

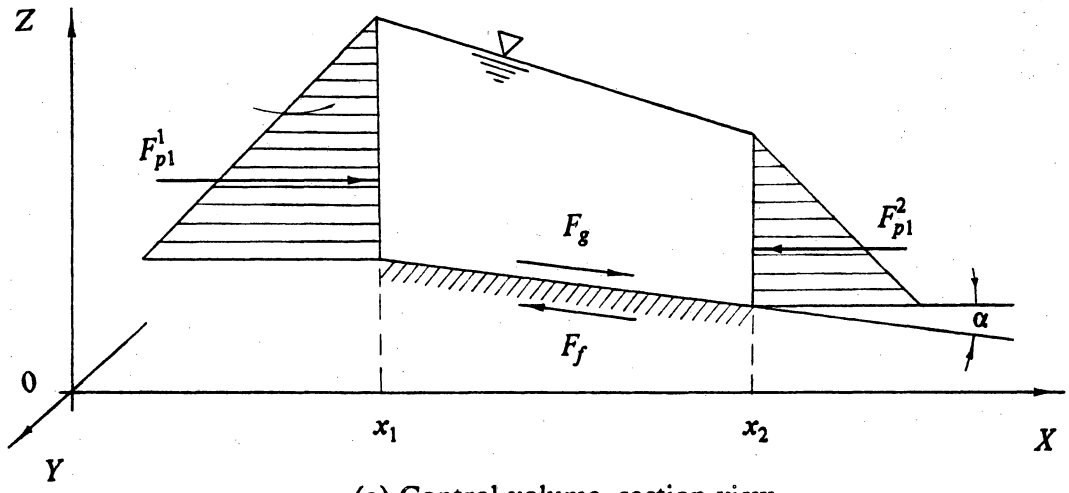

(a) Control volume, section view

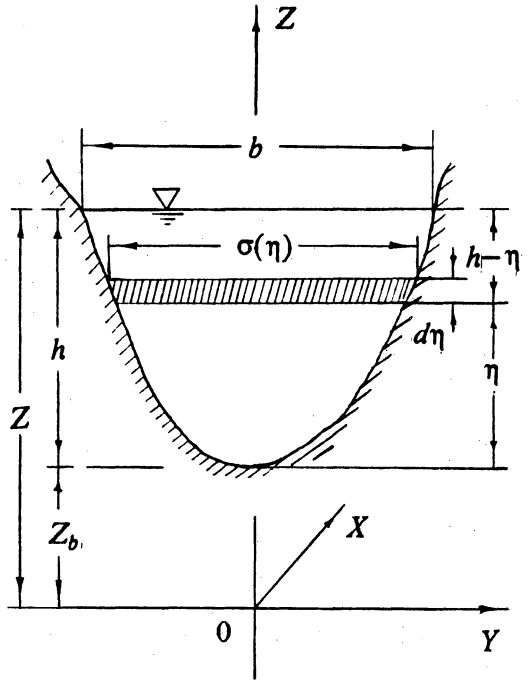

(b) Cross-section

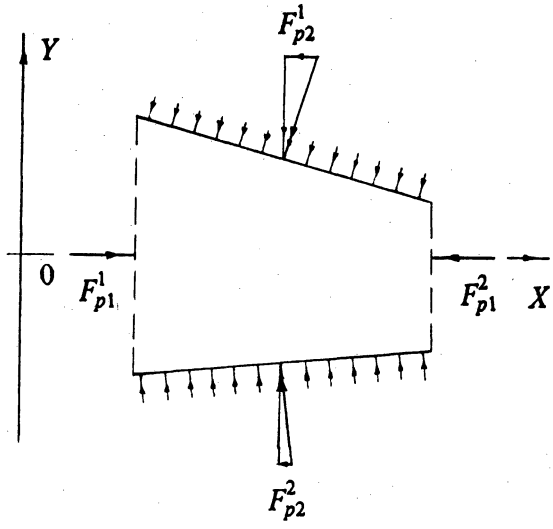

(c) Pressure force, plan view

Figure 6. Definition sketches for the derivation of unsteady flow equations

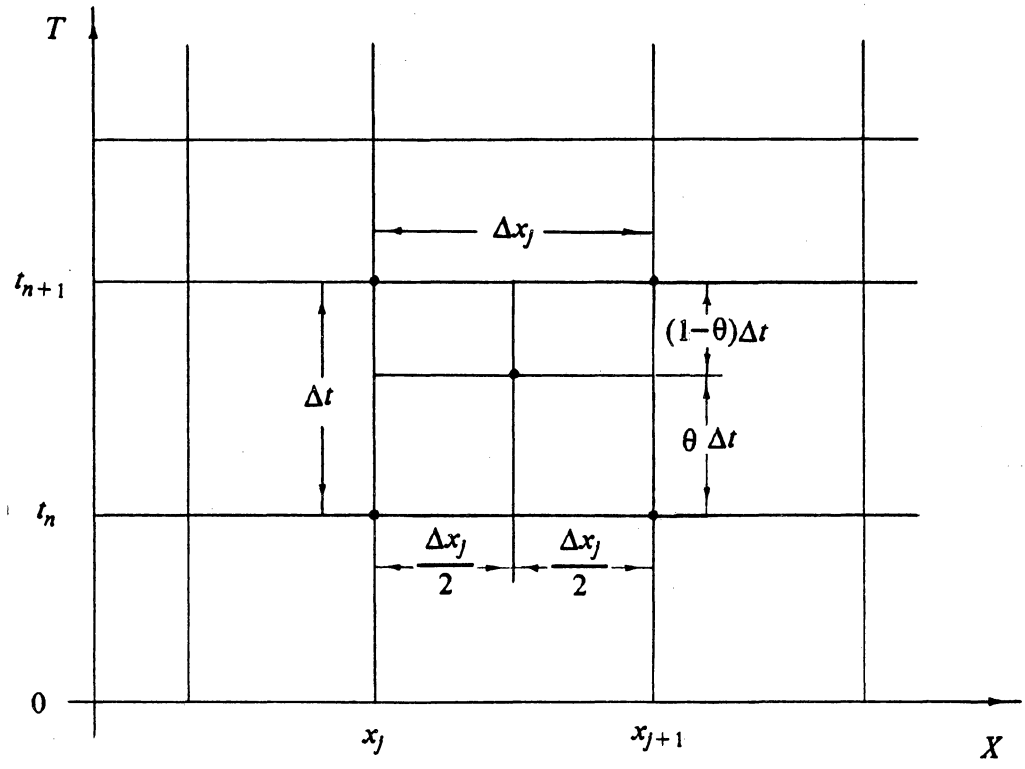

Figure 7. Preissmann implicit scheme

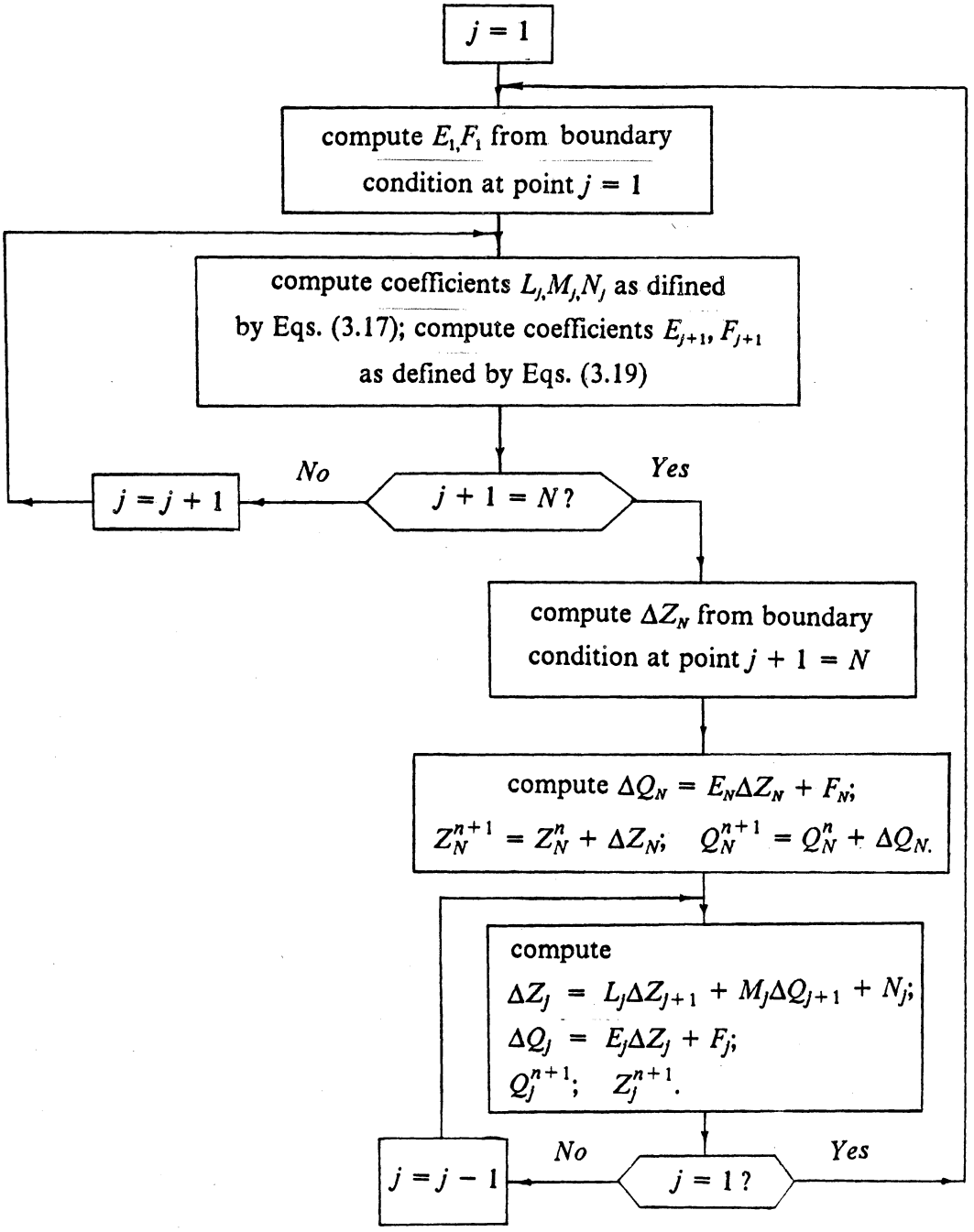

Figure 8. Flow chart for the Double-sweep method

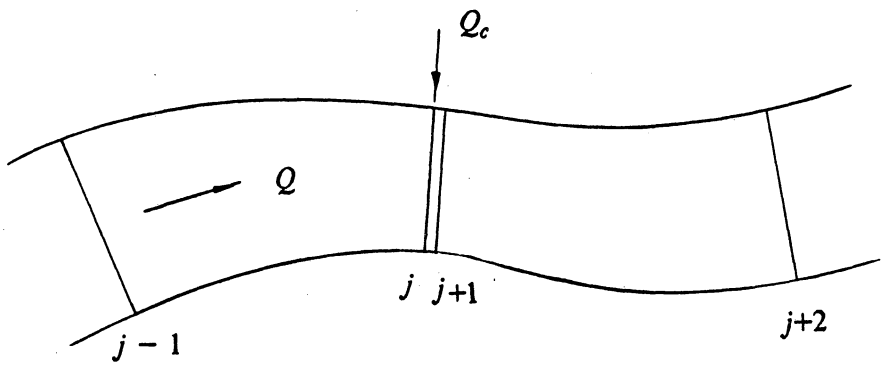

Figure 9. Junction as the interior boundary condition

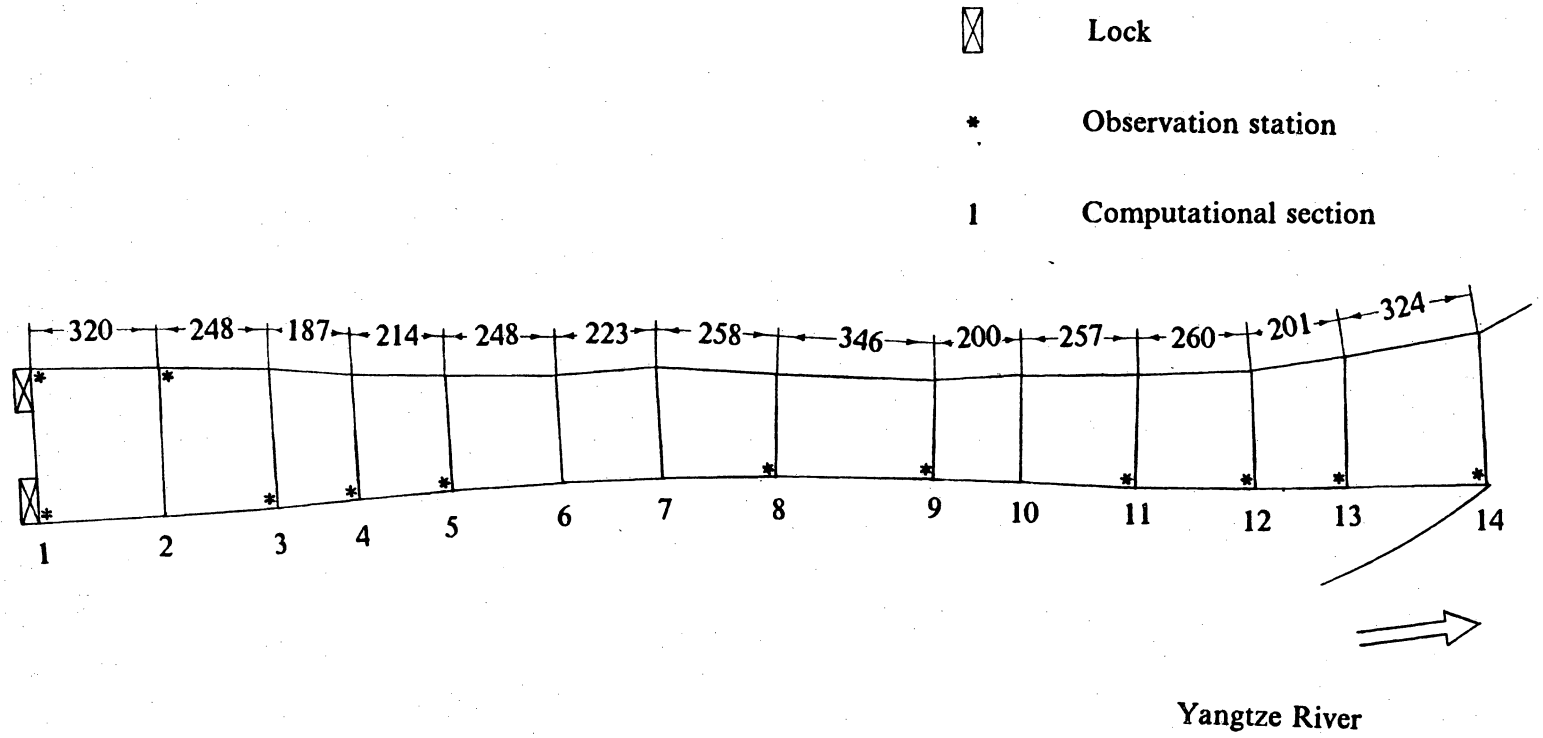

Figure 10. The locations of the observation stations and the computational sections

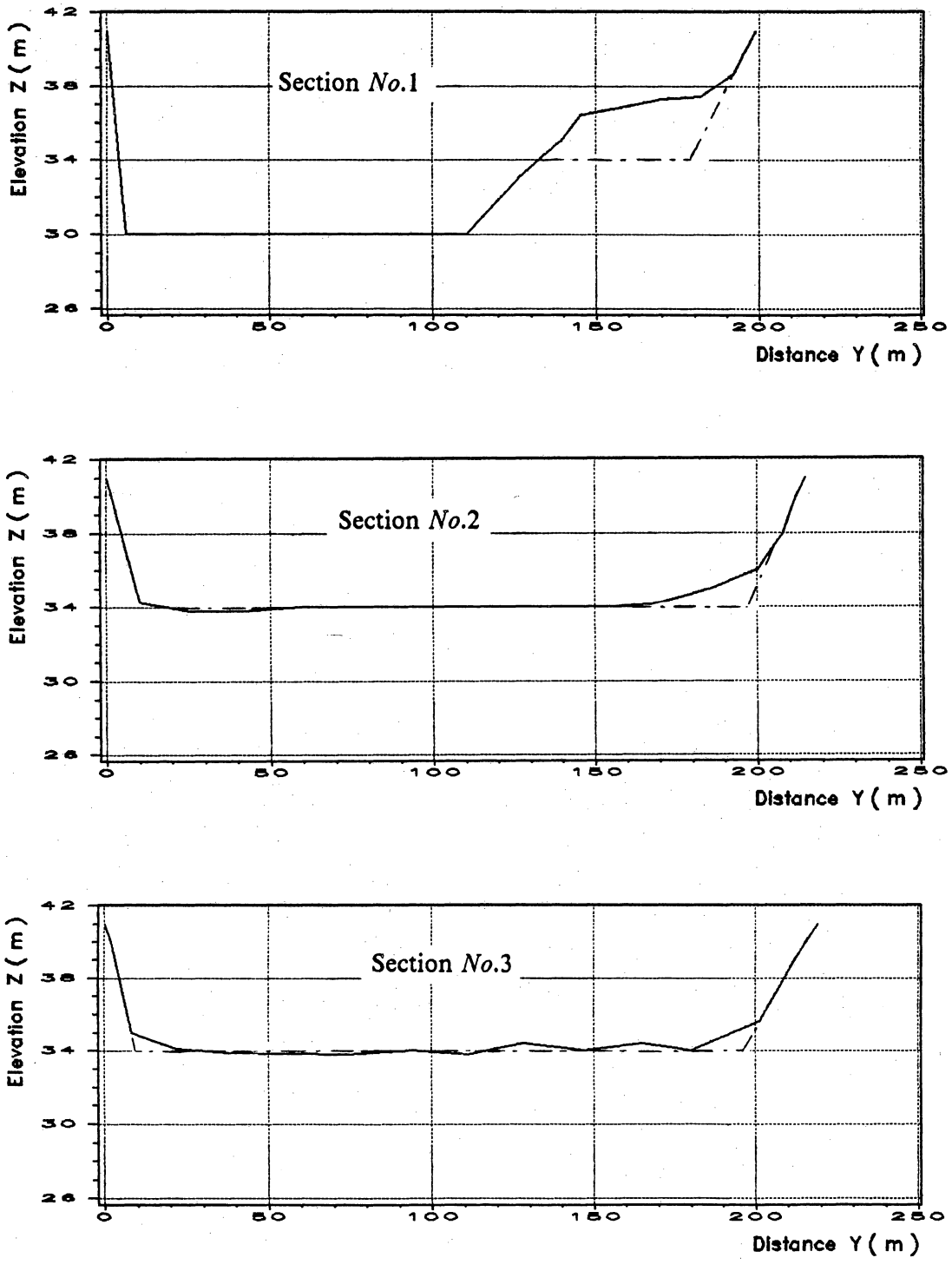

Figure 11. Profiles of cross-sections *No.*1, *No.*2, and *No.*3

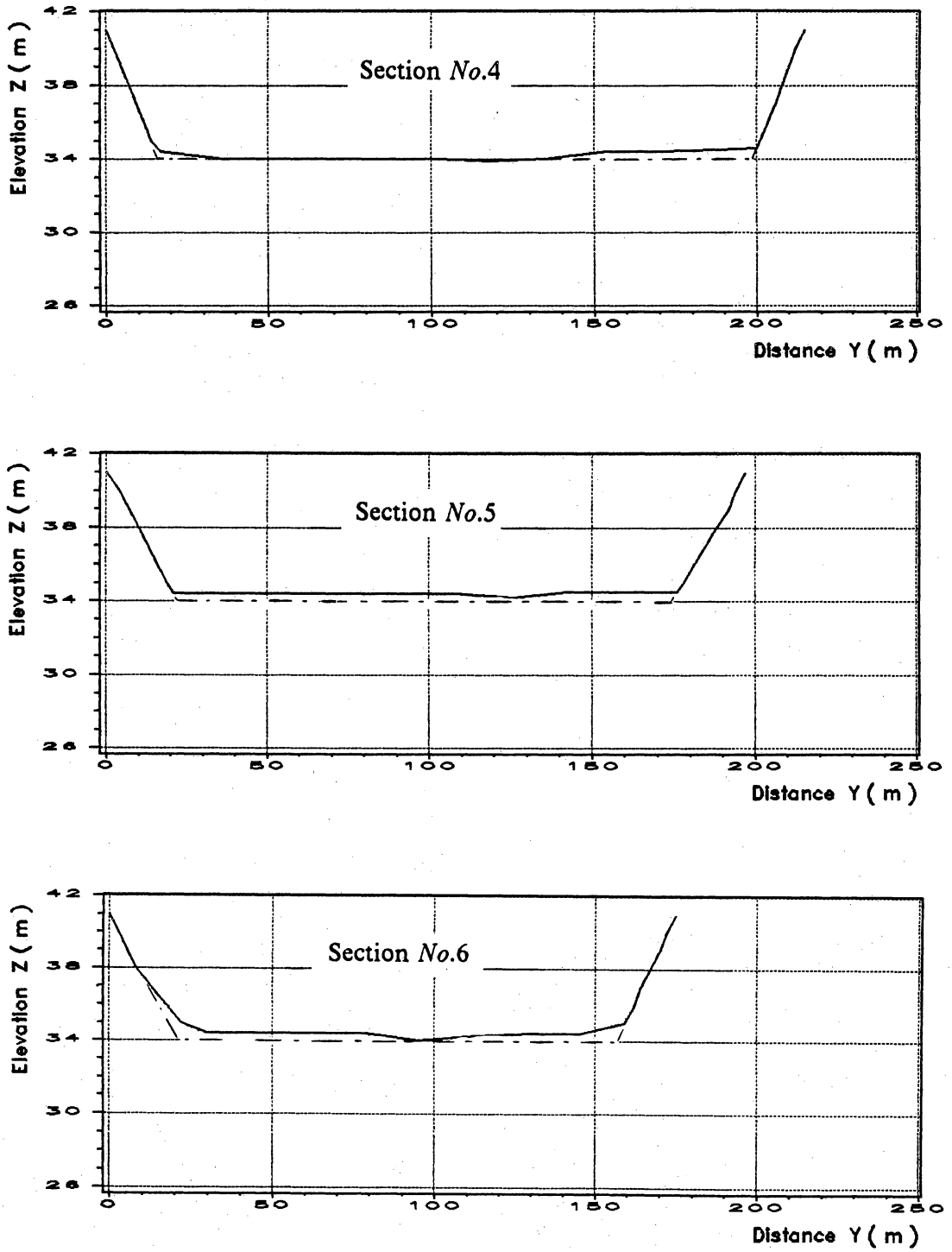

Figure 12. Profiles of cross-sections *No.*4, *No.*5, and *No.*6

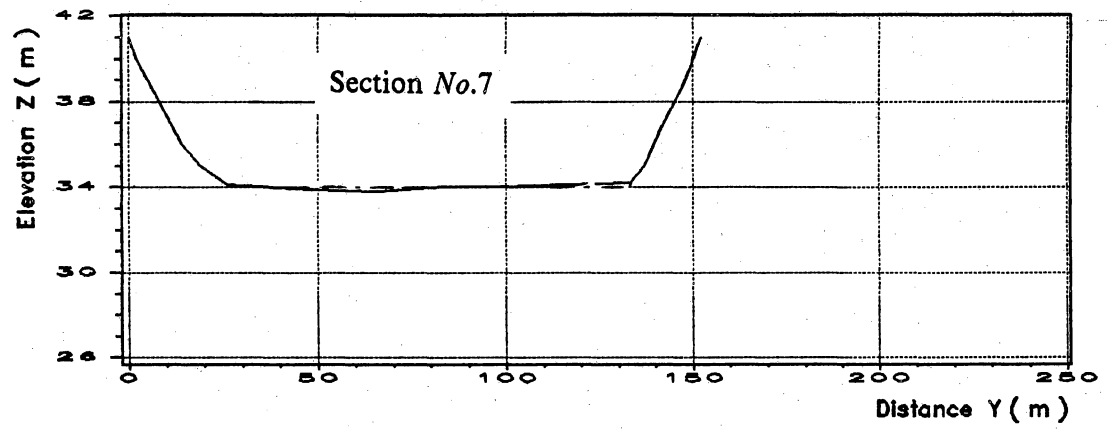

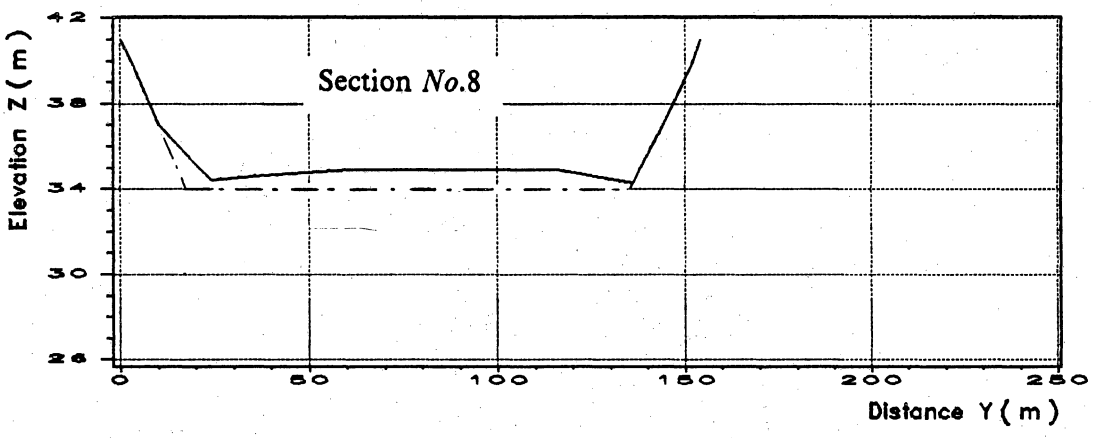

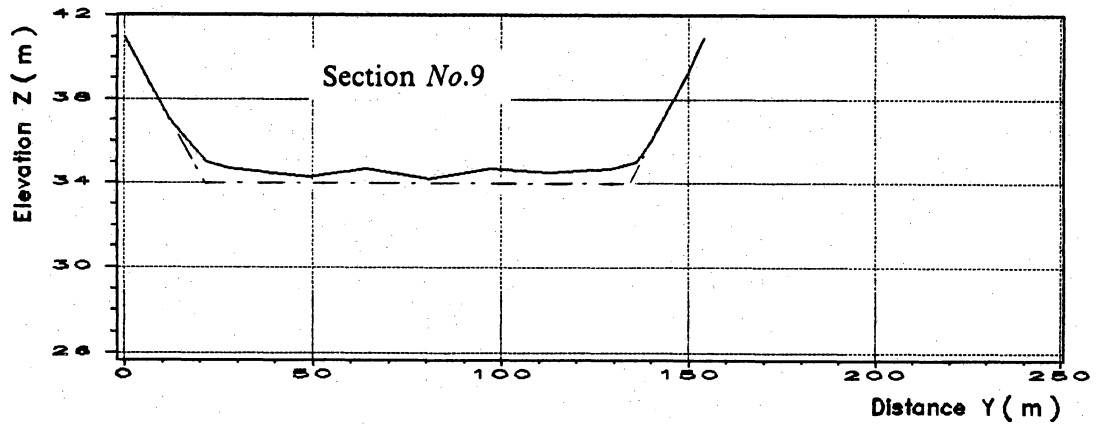

Figure 13. Profiles of cross-sections *No.*7, *No.*8, and *No.*9

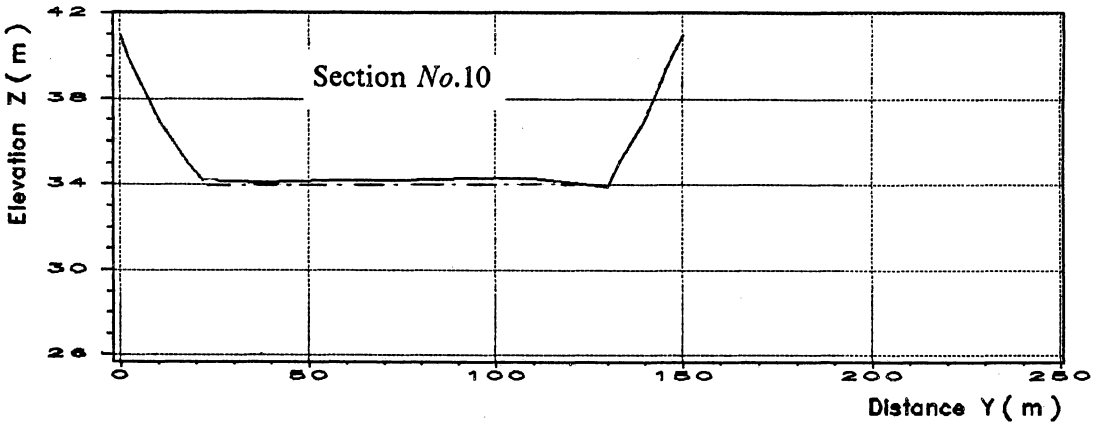

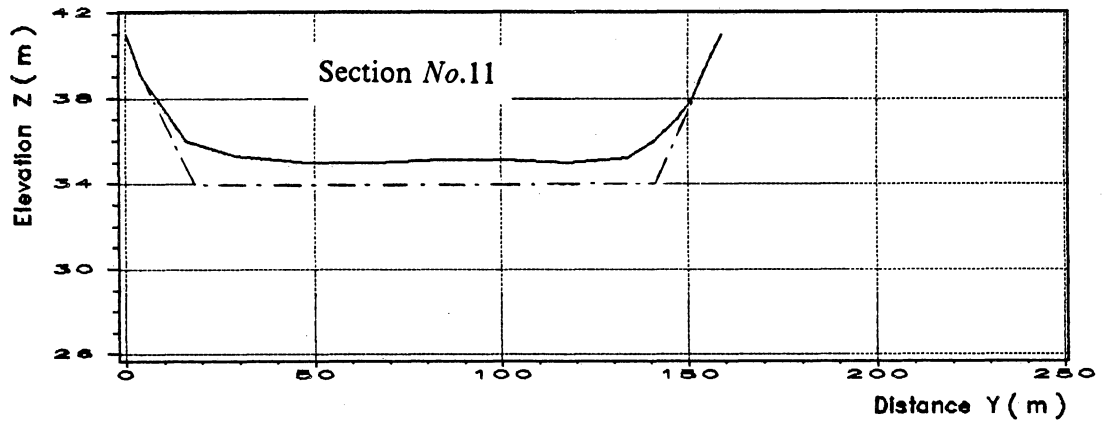

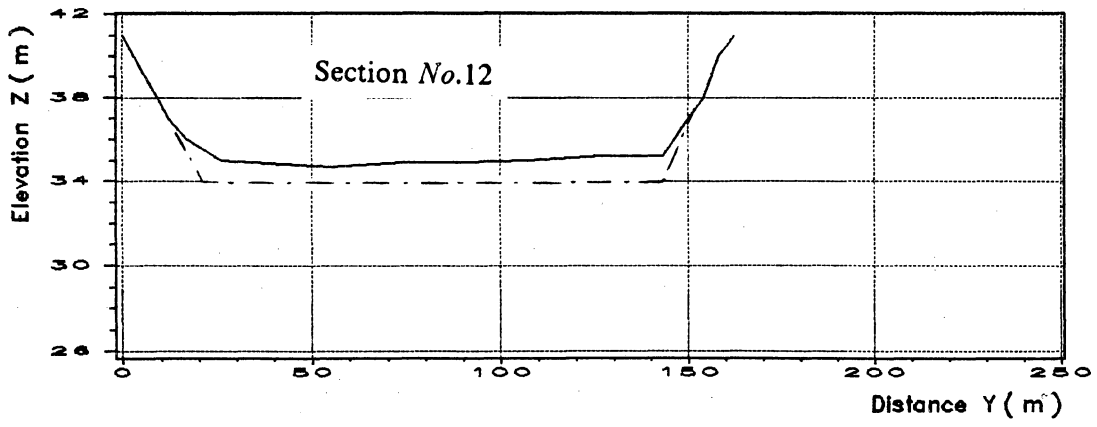

Figure 14. Profiles of cross-sections *No.*10, *No.*11, and *No.*12

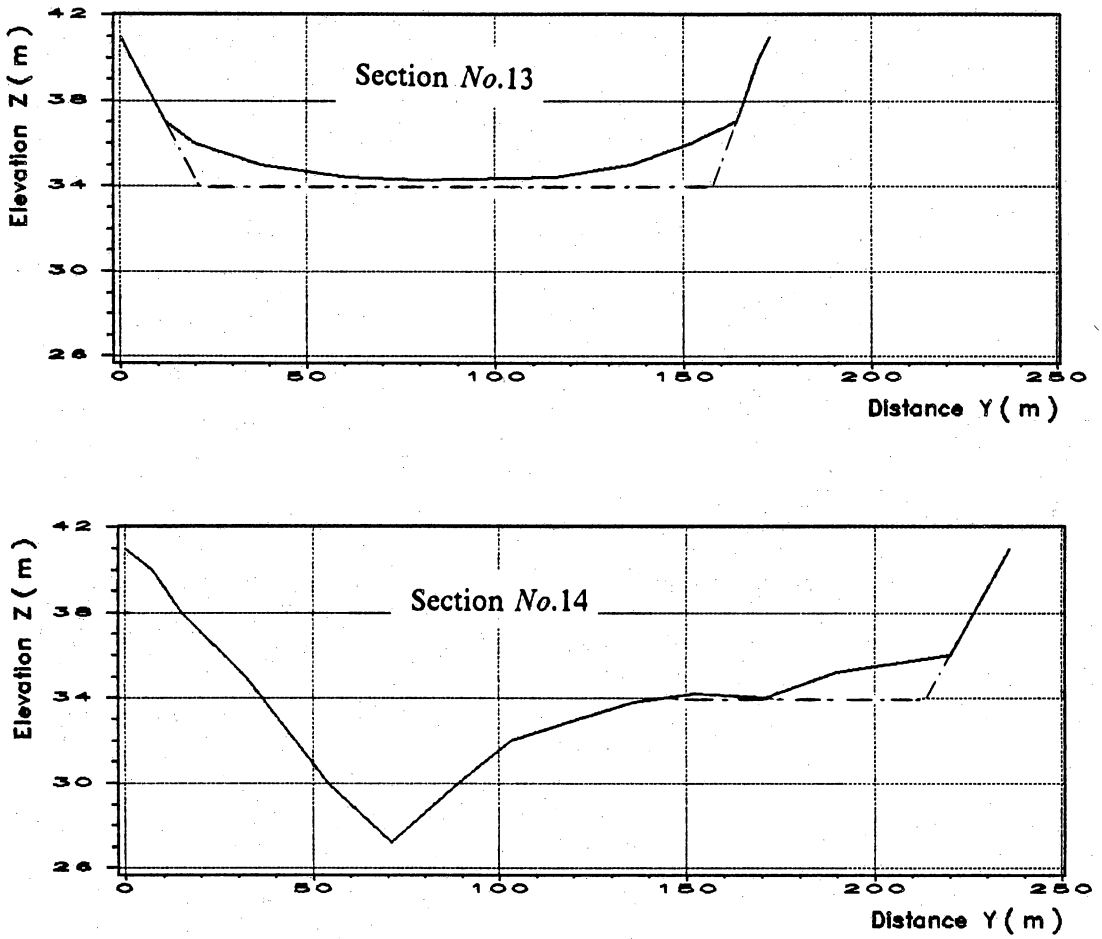

Figure 15. Profiles of cross-sections *No.*13 and *No.*14

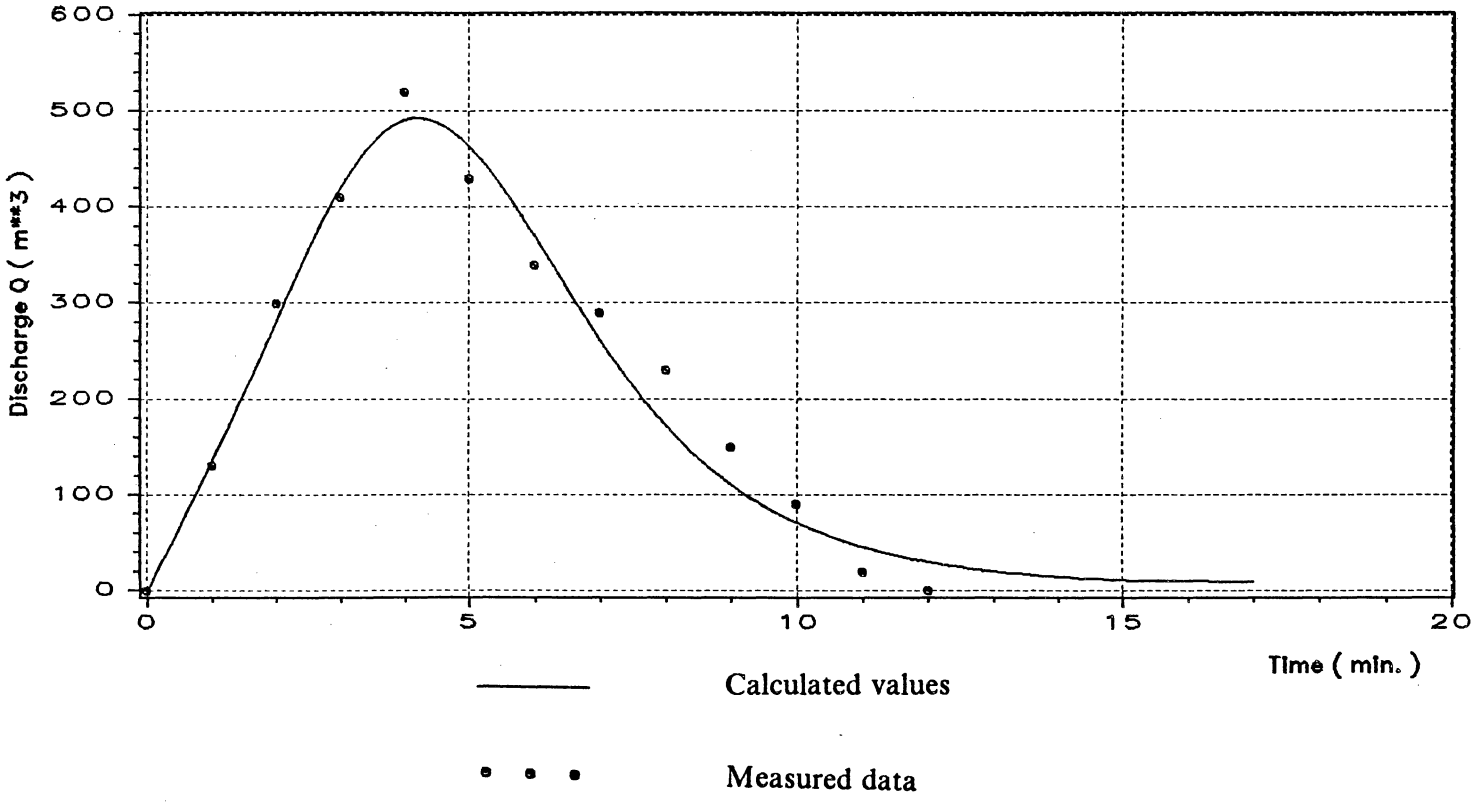

Figure 16. Comparison of the calculated and measured discharge hydrographs (at upstream boundary)

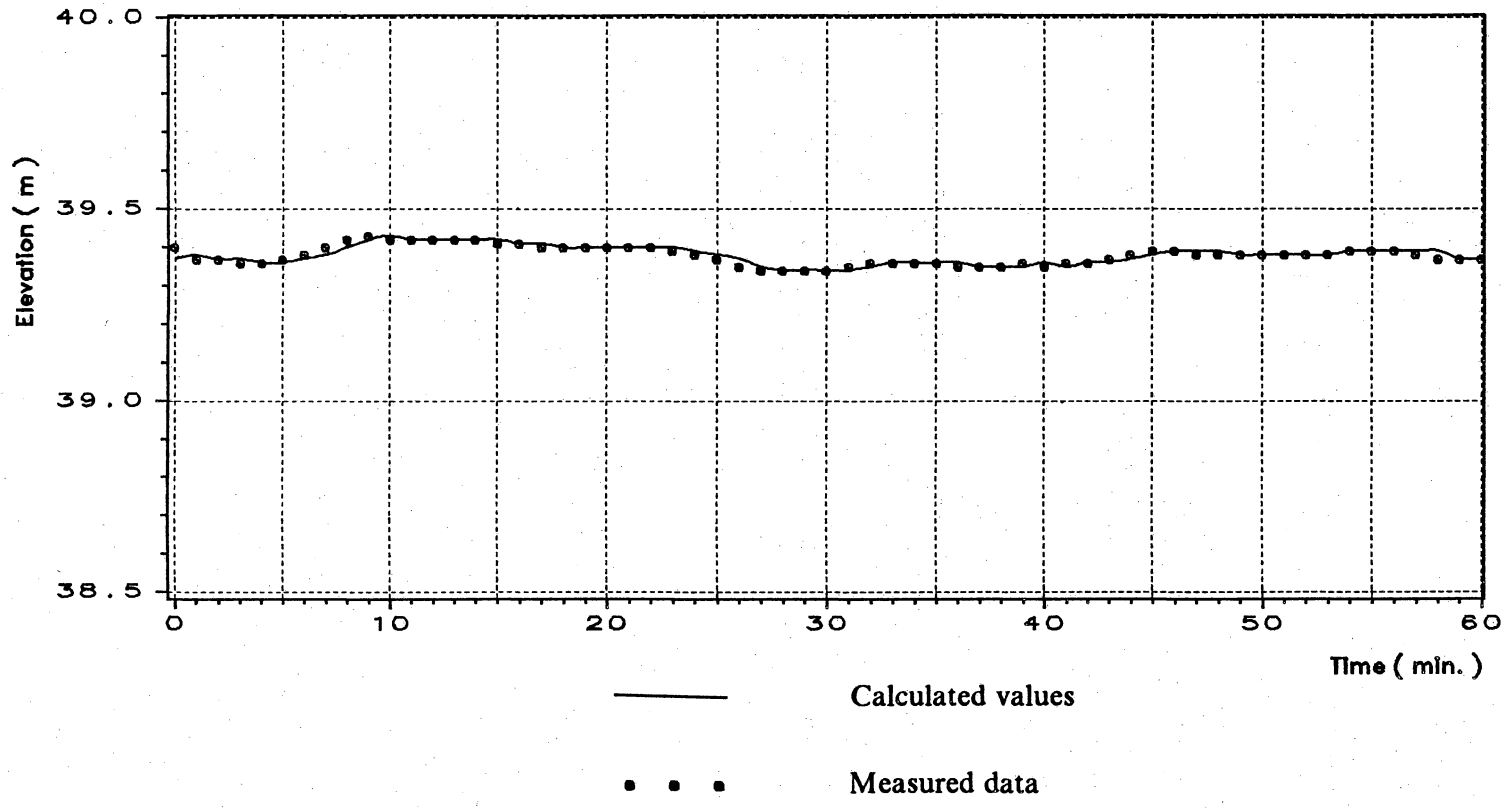

Figure 17. Comparison of the calculated and measured water elevation hydrographs (at the downstream boundary)

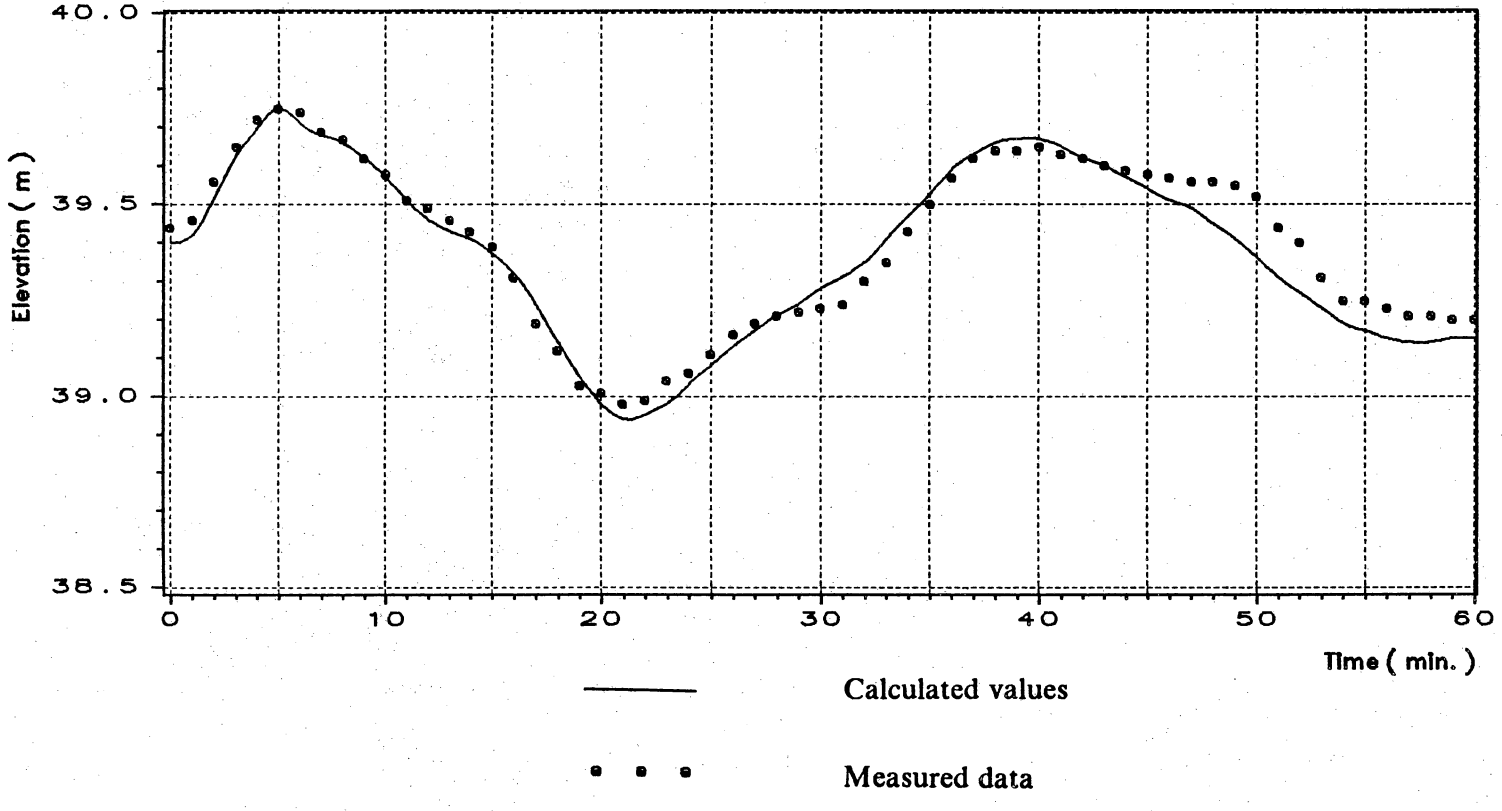

Figure 18. Verification of the mathematical model of the Third Navigation Channel (Section *No.*2)

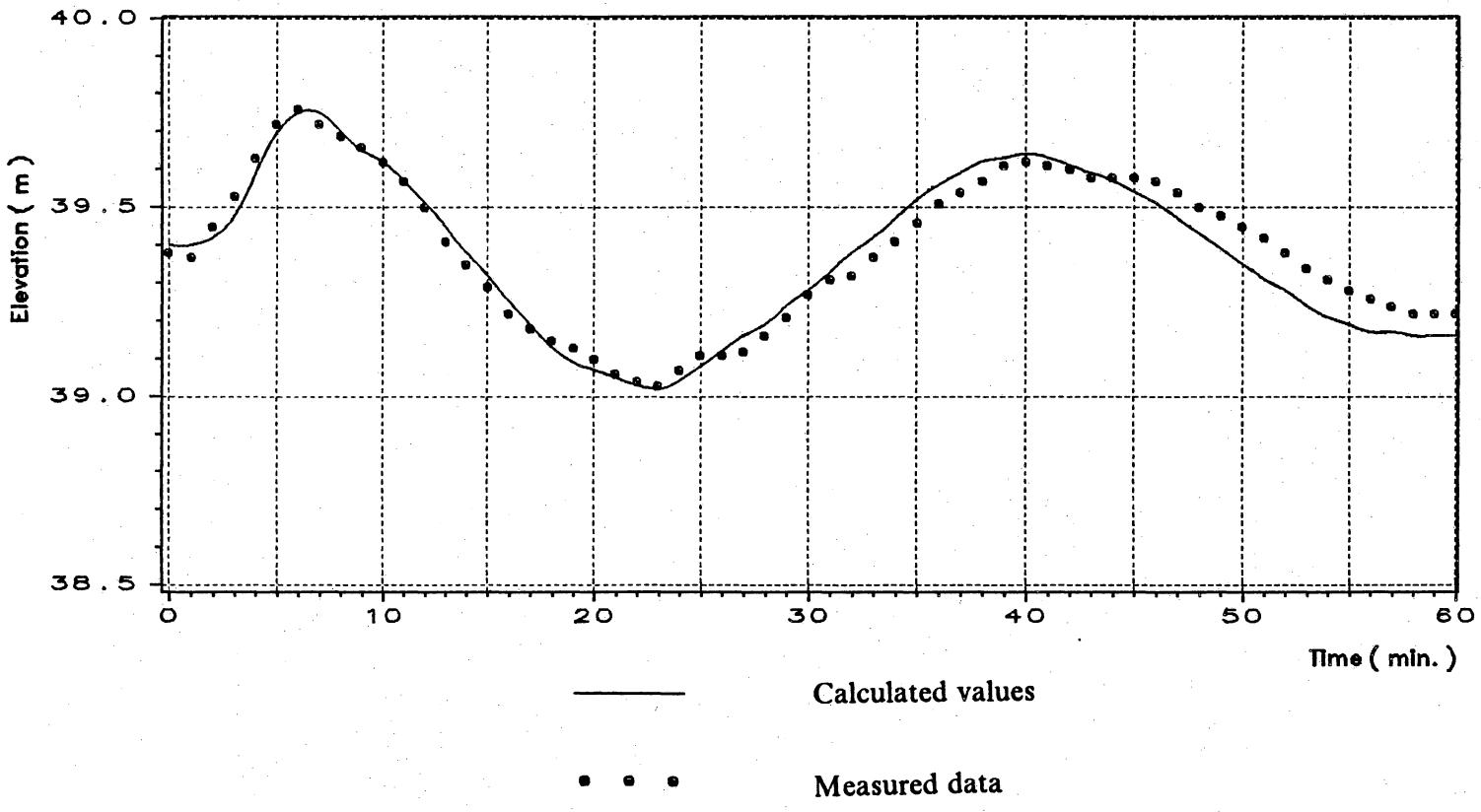

Figure 19. Verification of the mathematical model of the Third Navigation Channel (Section *No.*5)

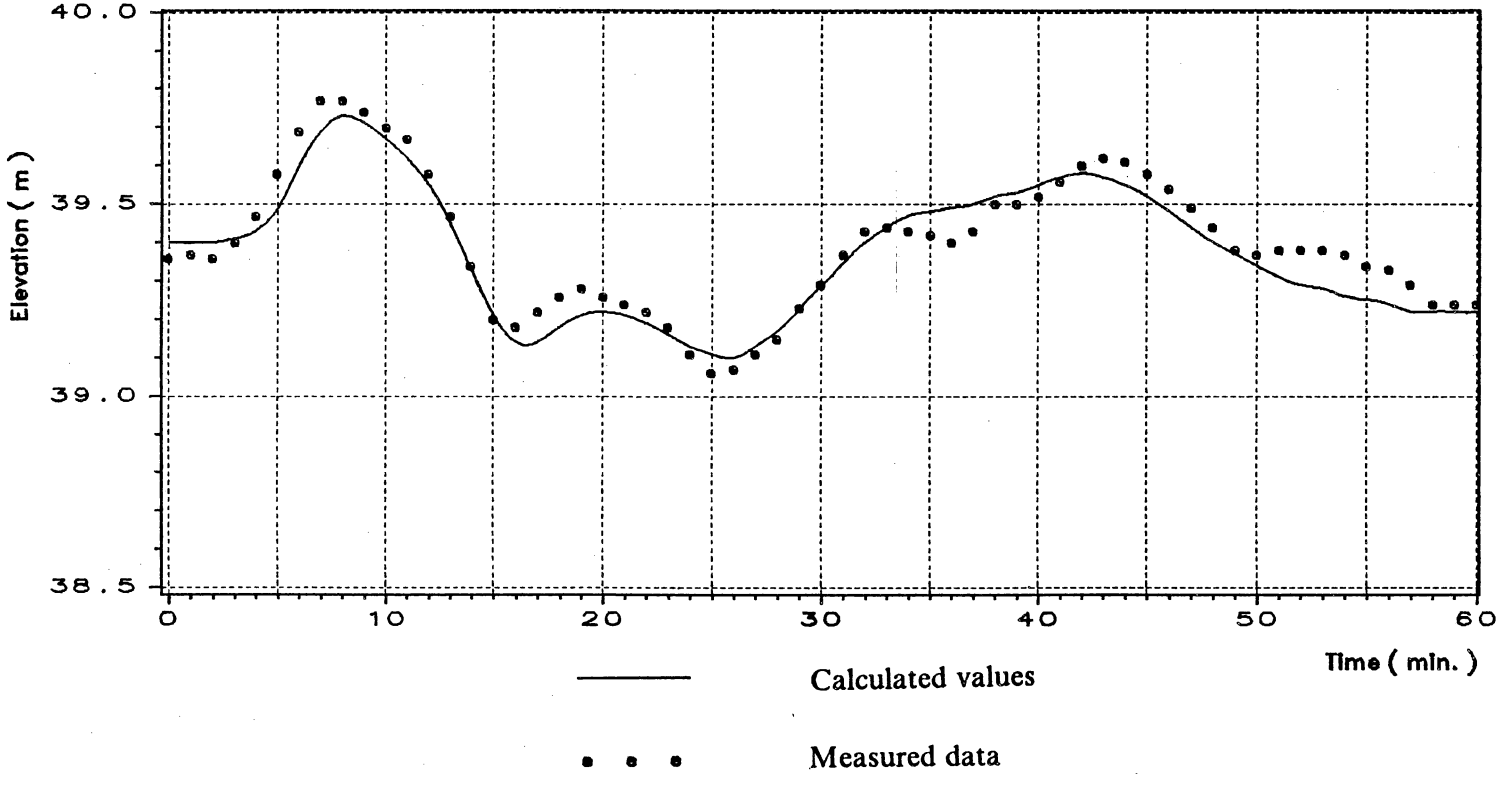

Figure 20. Verification of the mathematical model of the Third Navigation Channel (Section *No.*8)

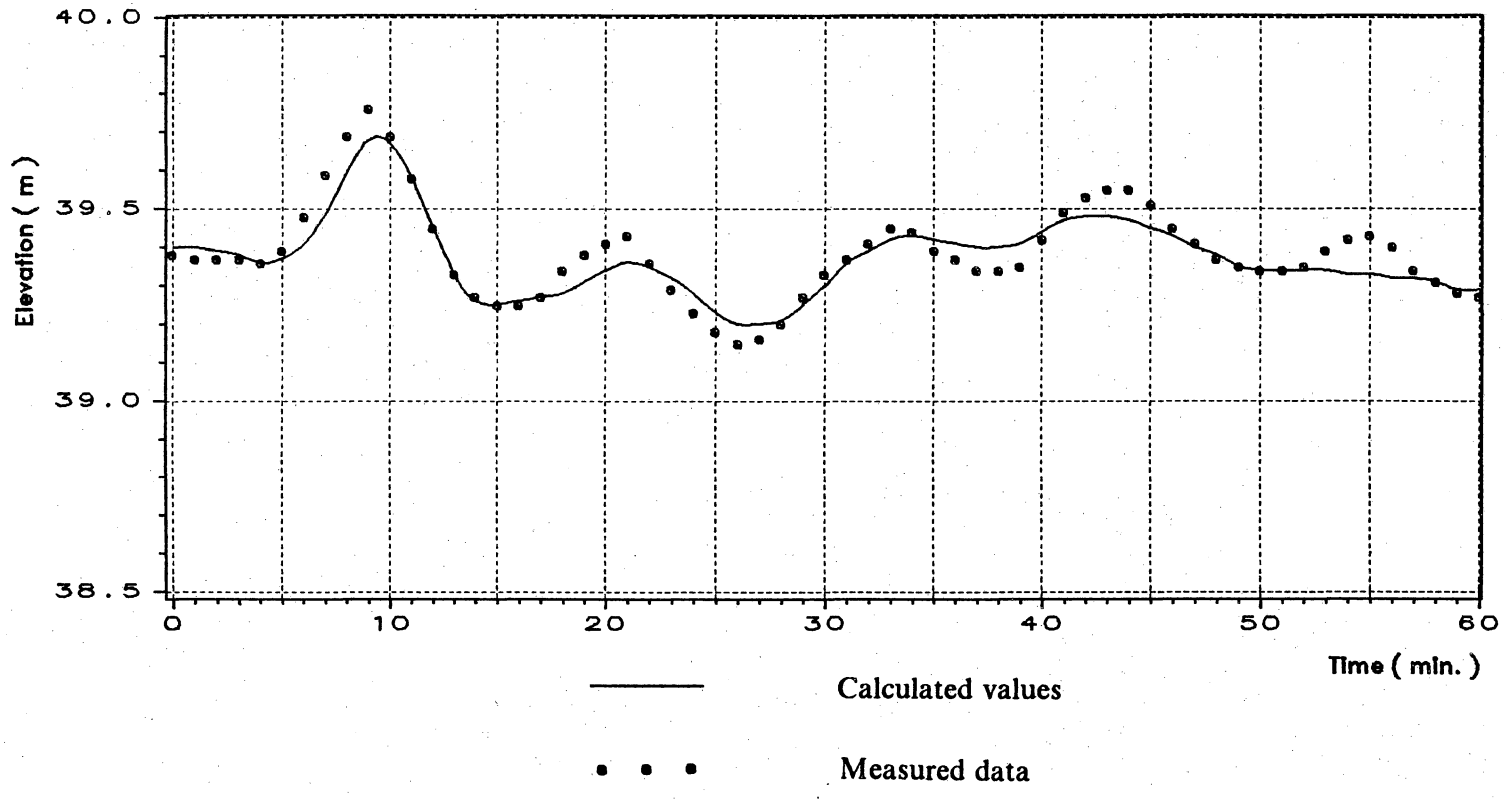

Figure 21. Verification of the mathematical model of the Third Navigation Channel (Section *No.*11)

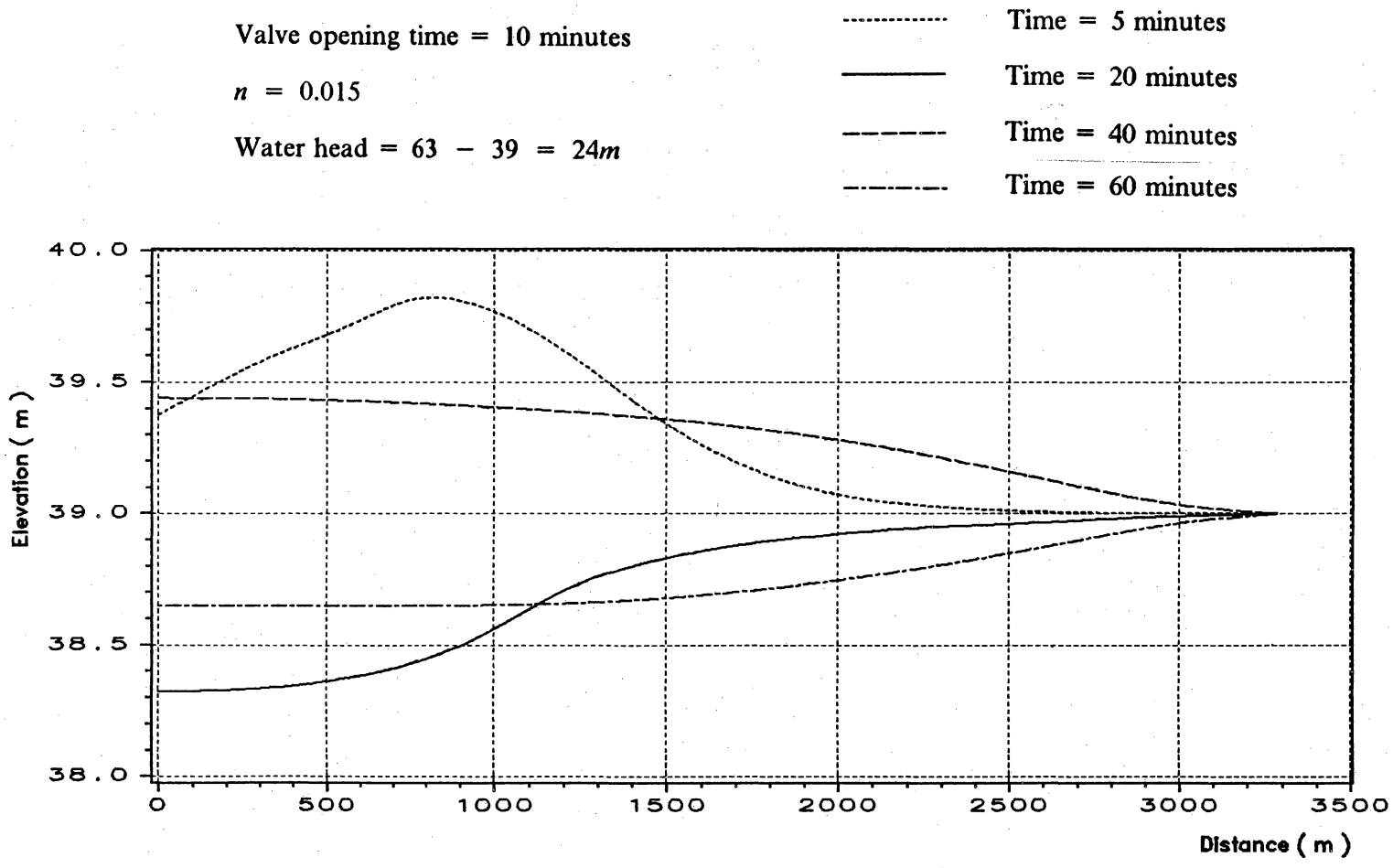

Figure 22. Water surface elevation profiles at different time levels

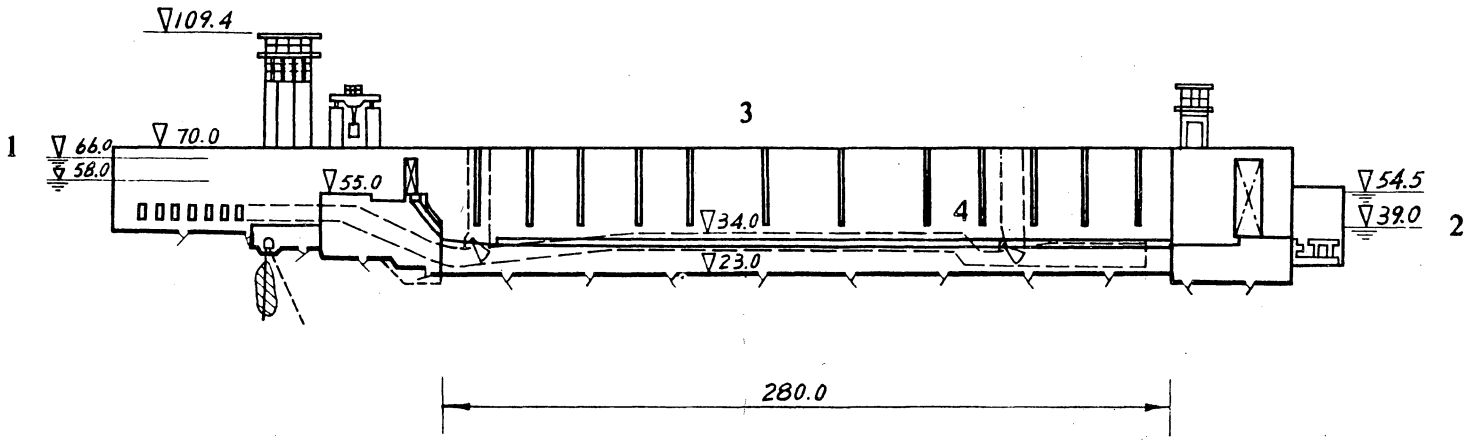

1. Designed water elevation
2. Lowest water elevation for navigation
3. Lock chamber
4. Culvert system

Figure 23. The culvert system for Lock *No.*2 filling and emptying

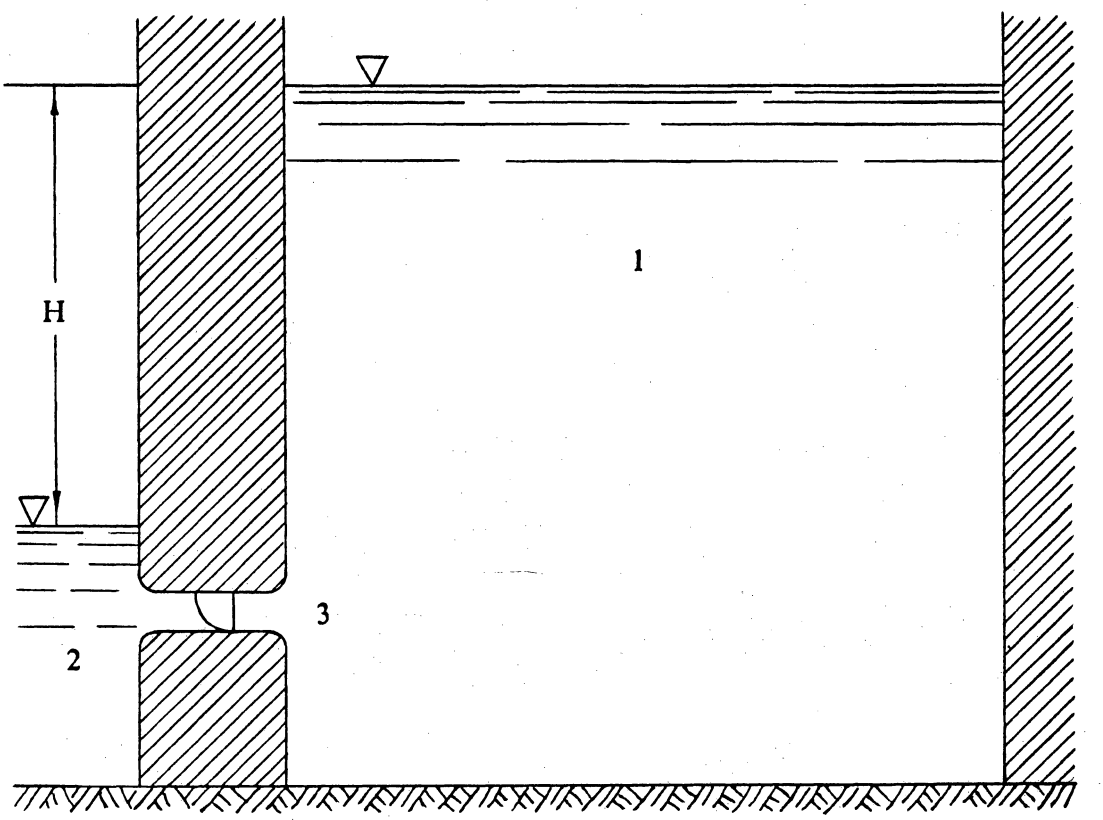

1. Lock chamber
2. The Third Navigation Channel
3. Valve

Figure 24. Lock chamber emptying through a single culvert

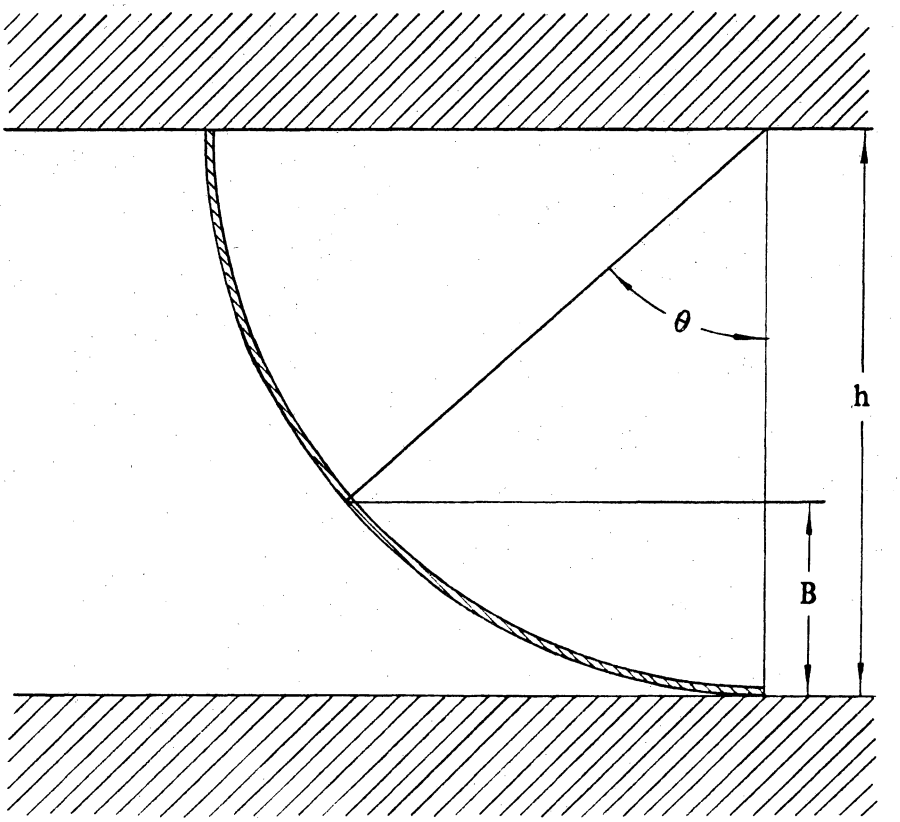

Figure 25. The sketch of the valve opening

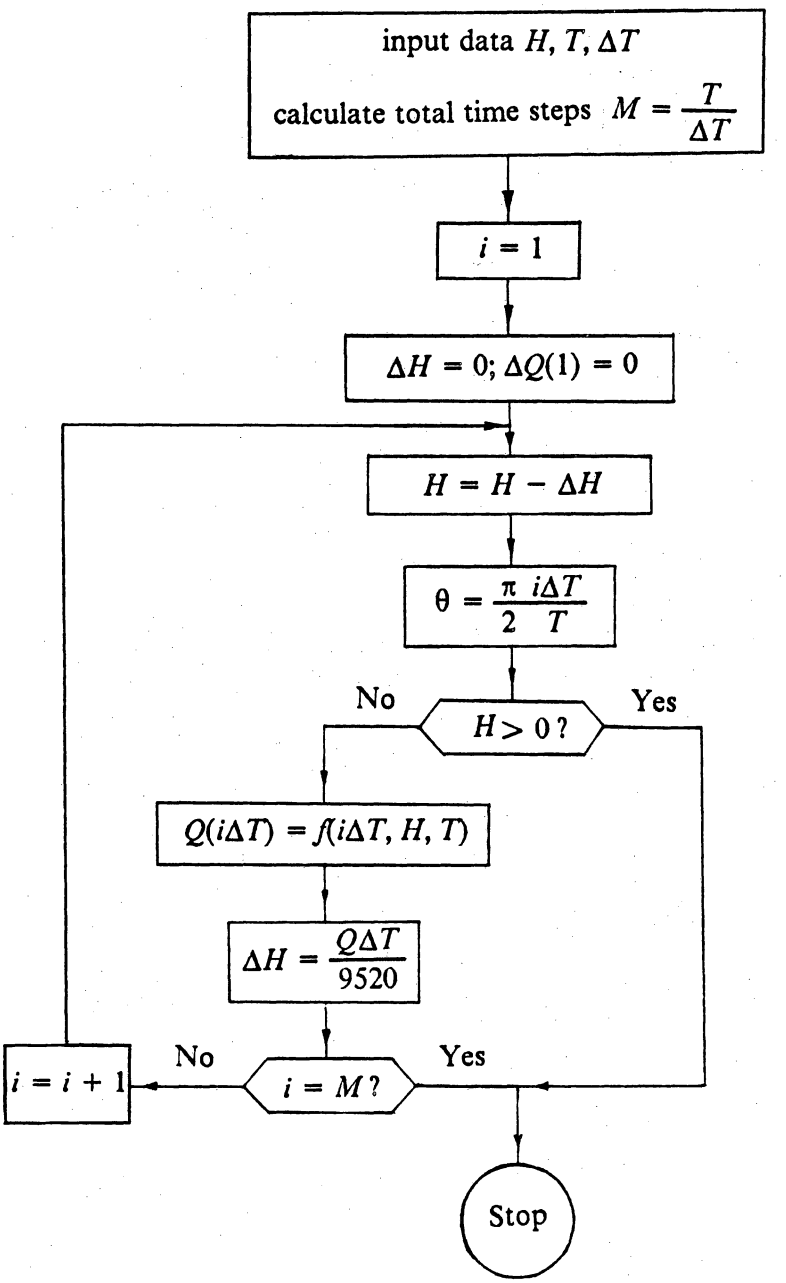

Figure 26. Flow chart for computation of the hydrographs at the upstream boundary

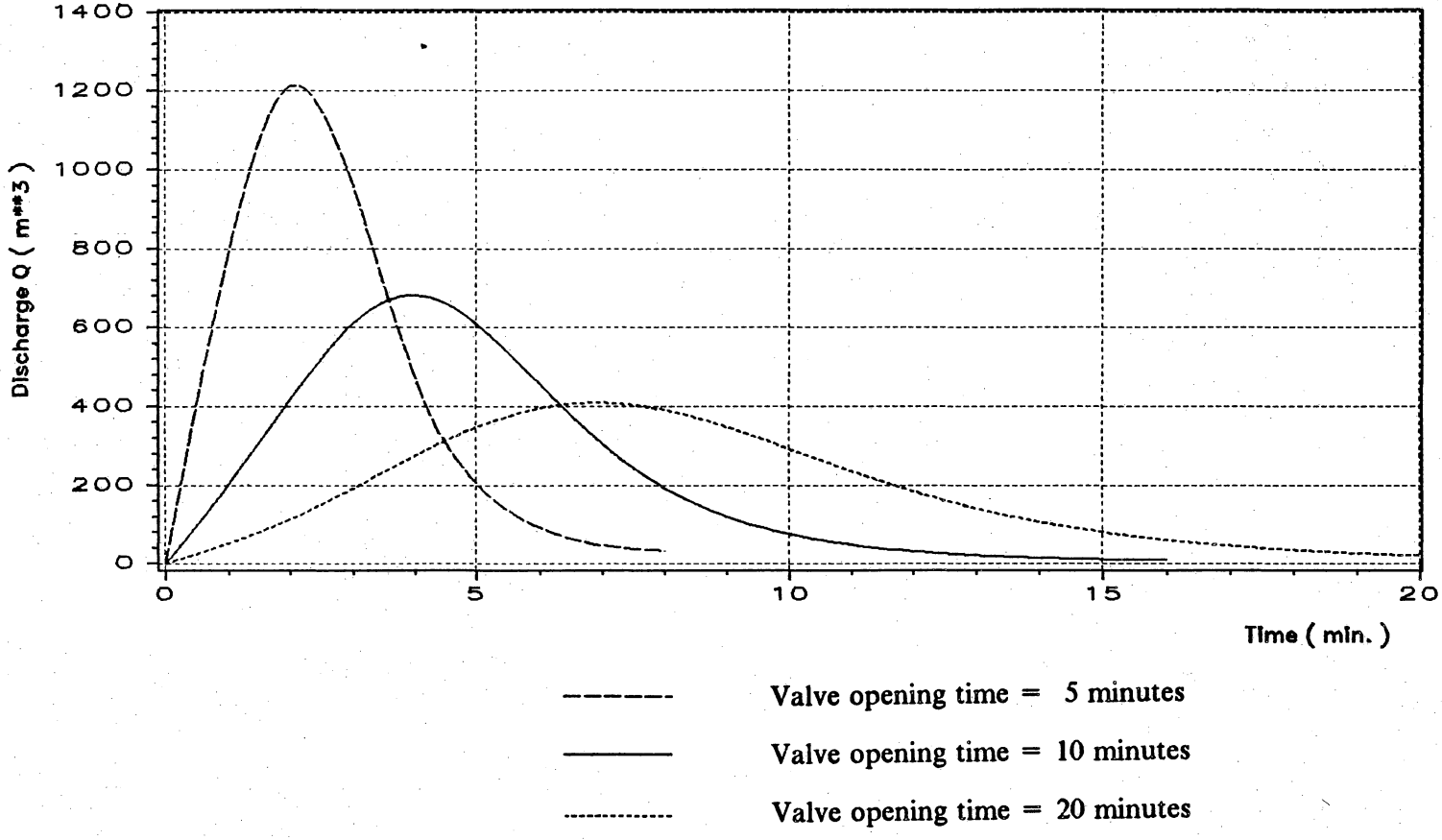

Figure 27. Calculated hydrographs as the uptream boundary conditions by different valve opening times

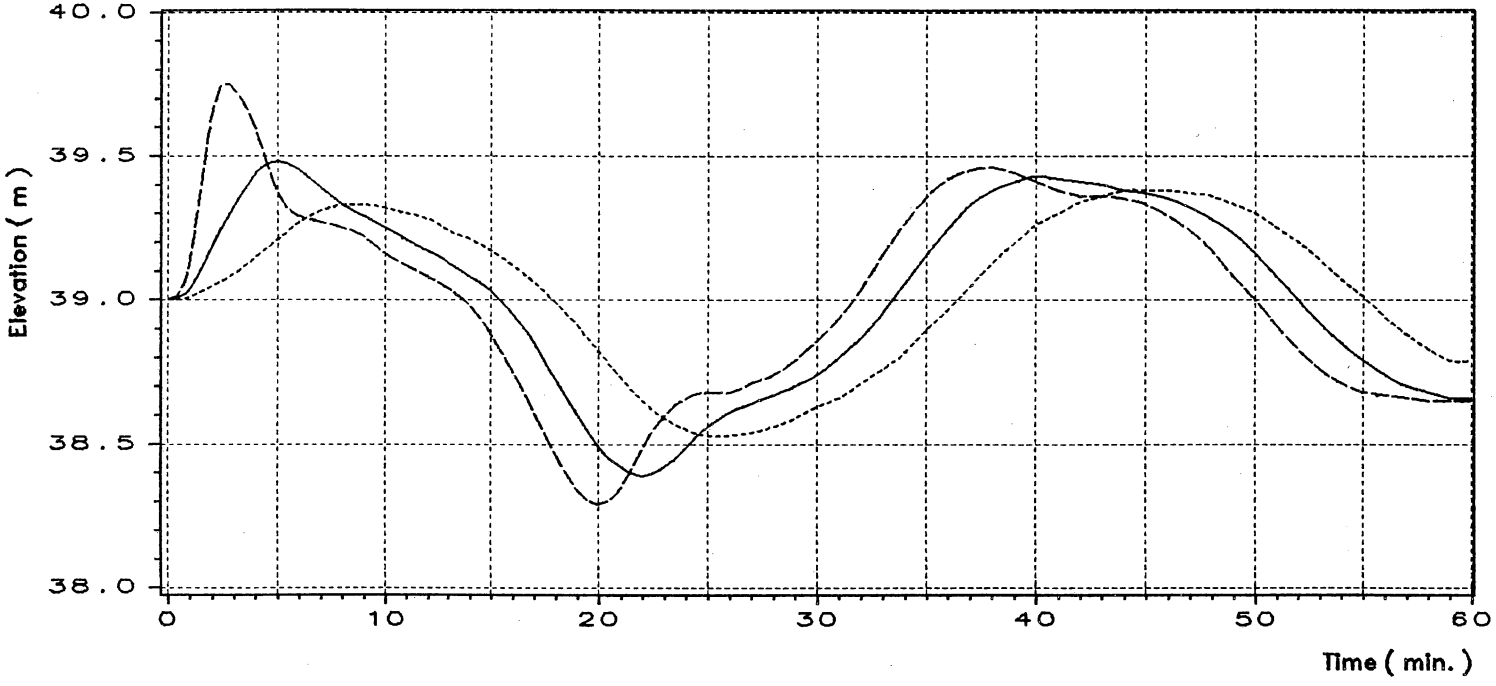

Figure 28. Comparison of water surface elevation variation by different valve opening times (at cross-section *No.*2)

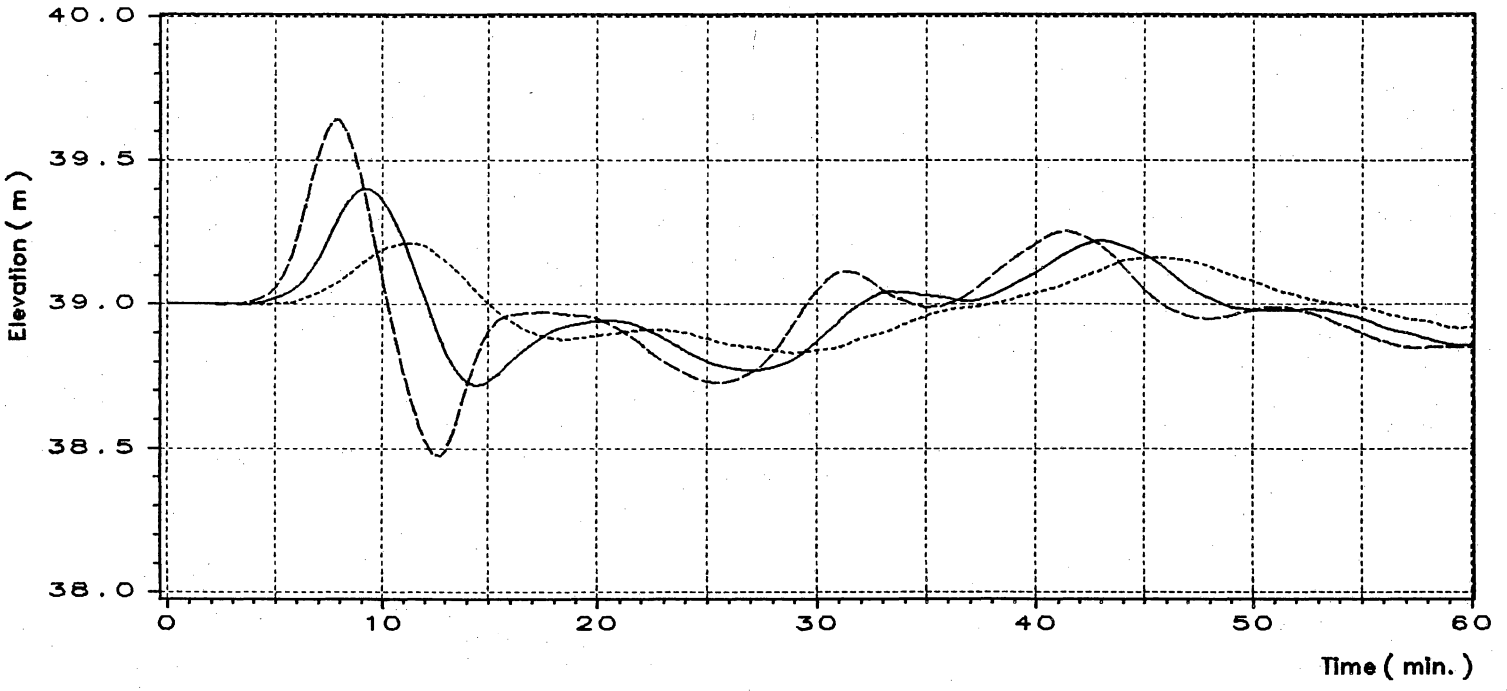

n = 0.015

Water head = 63-39 = 24 m

------ Valve opening time = 5 minutes

——— Valve opening time = 10 minutes

---------- Valve opening time = 20 minutes

Figure 29. Comparison of water surface elevation variation by different valve opening times (at cross-section *No.*11)

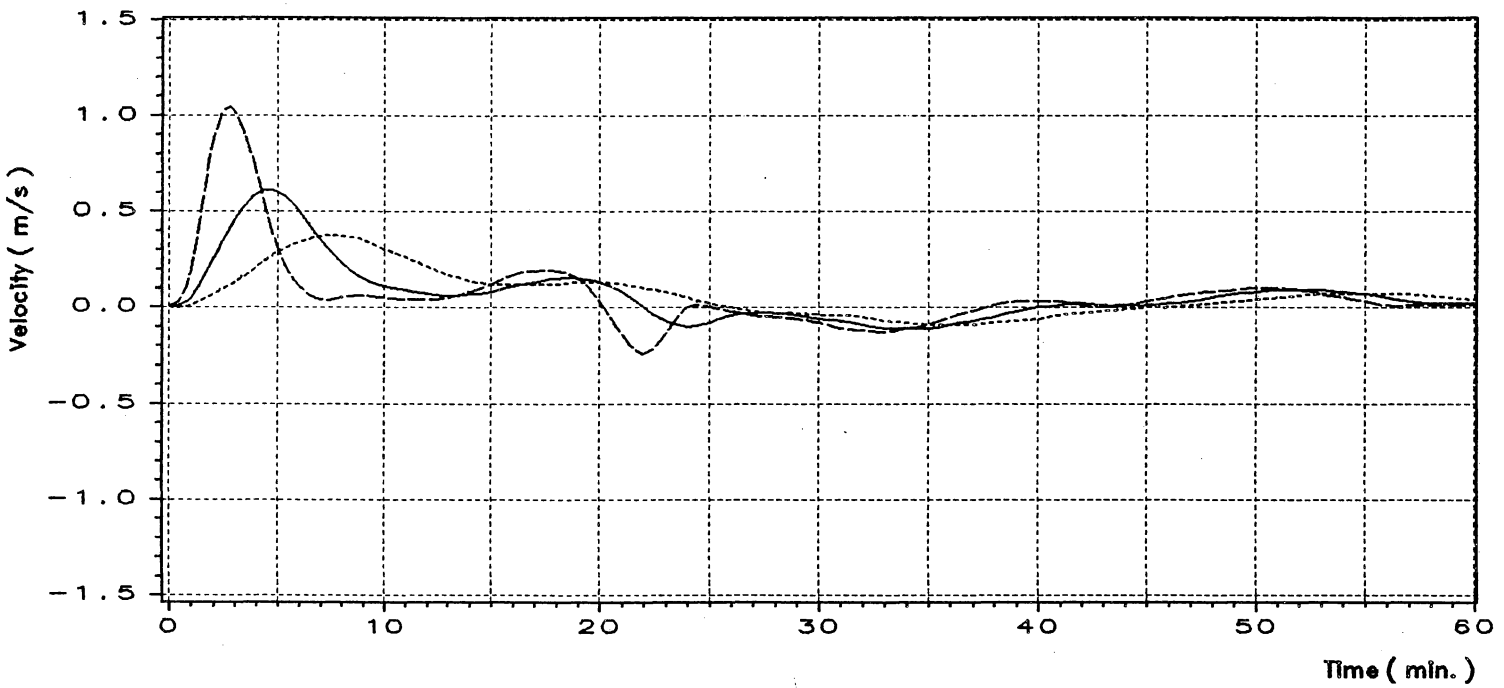

n = 0.015

Water head = 63-39 = 24 m

------ Valve opening time = 5 minutes

——— Valve opening time = 10 minutes

---------- Valve opening time = 20 minutes

Figure 30. Comparison of velocity variation by different valve opening times

(at cross-section *No.*2)

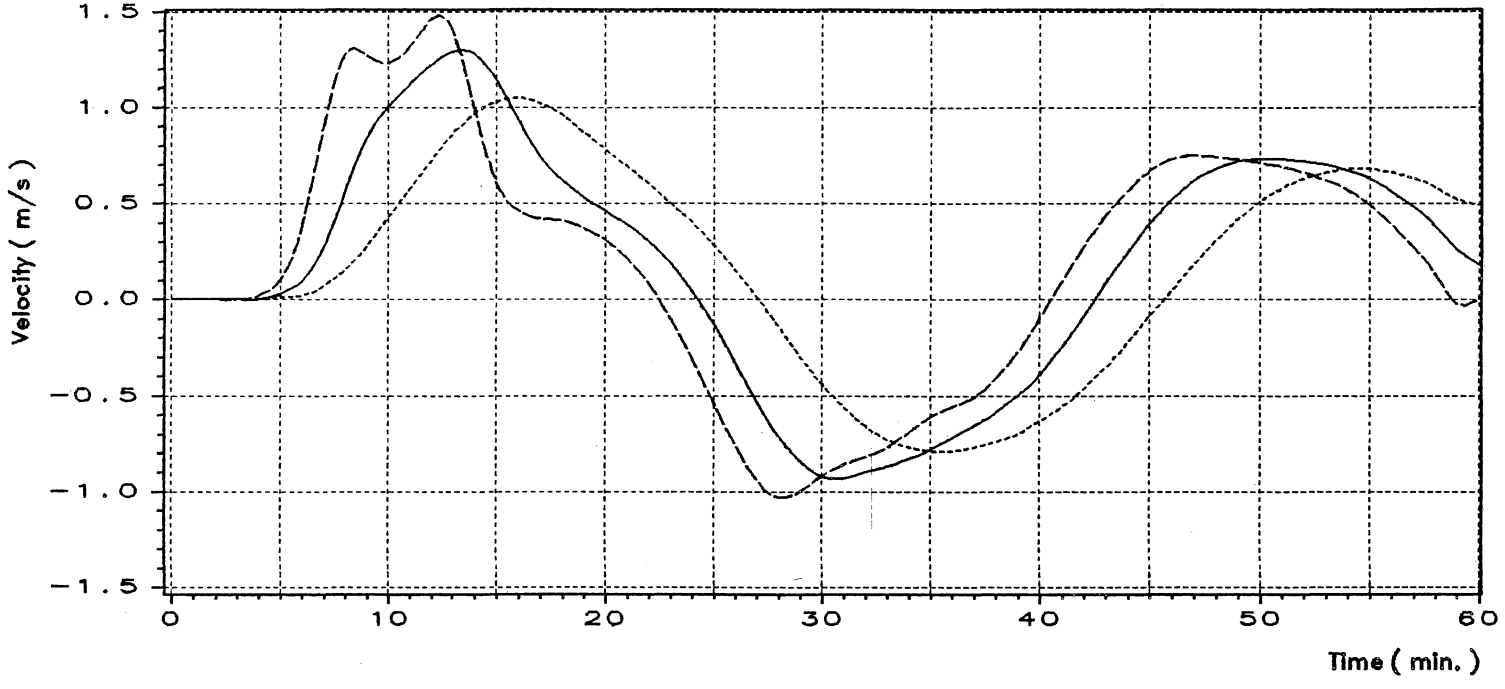

n = 0.015

Water head = 63-39 = 24 m

------- Valve opening time = 5 minutes

——— Valve opening time = 10 minutes

---------- Valve opening time = 20 minutes

Figure 31. Comparison of velocity variation by different valve opening times

(at cross-section *No.*11)

Valve opening time = 10 minutes

n = 0.015

Water head = 63-39 = 24 m

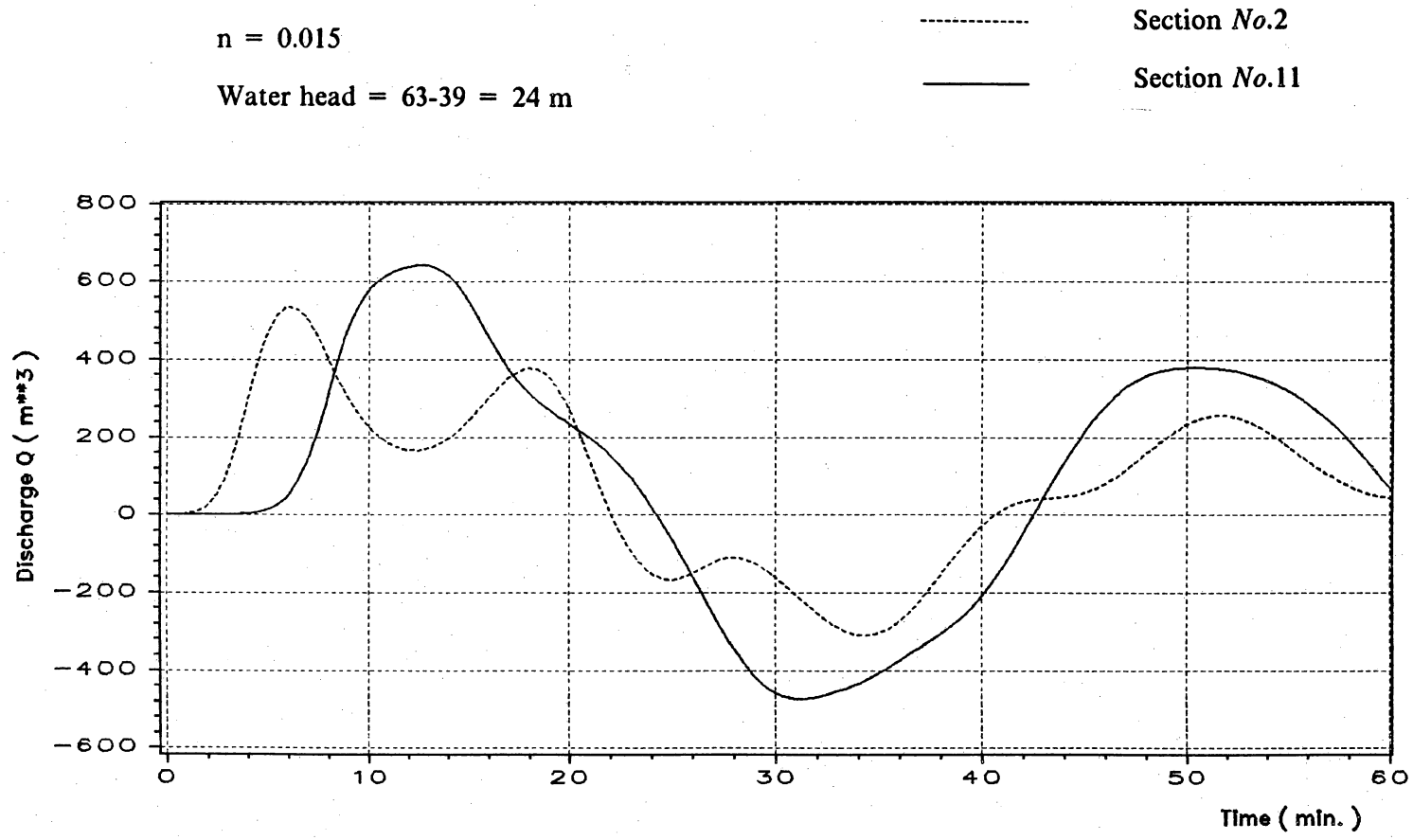

Figure 32. Calculated discharge hydrographs at different sections

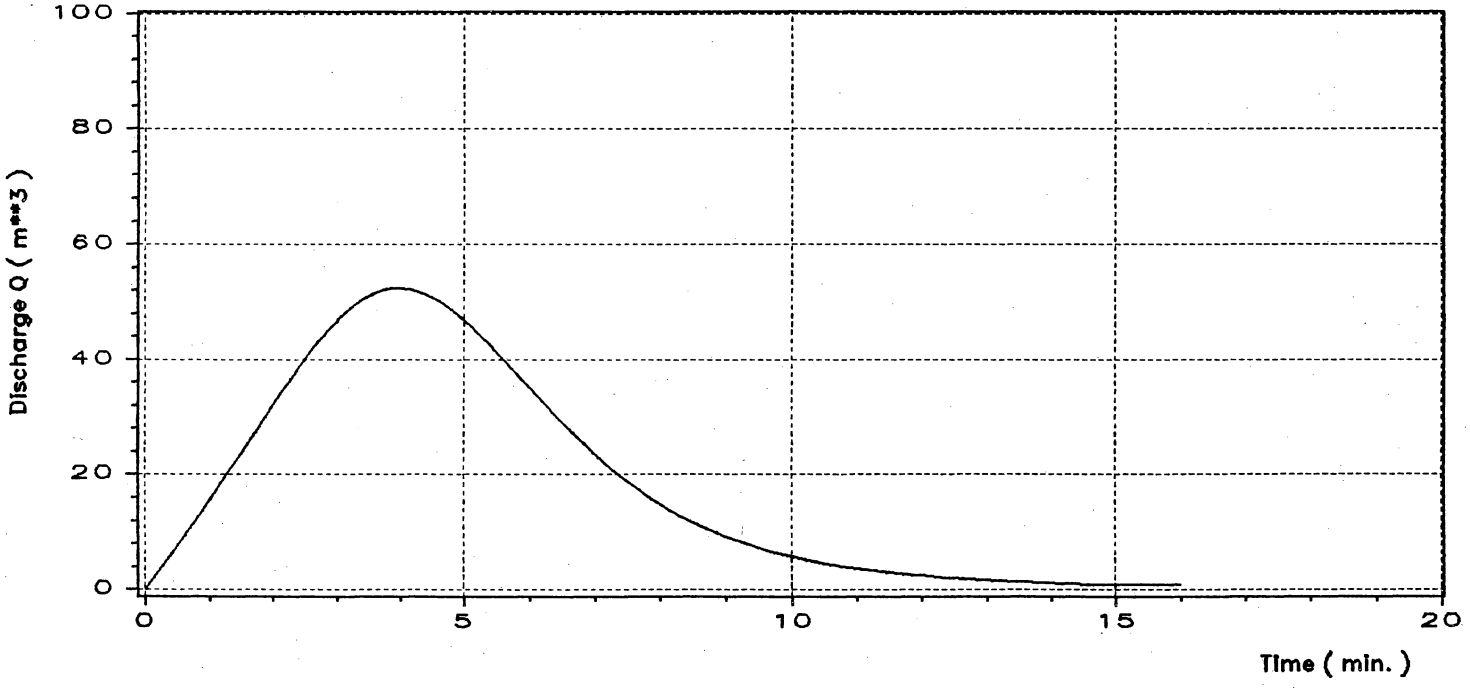

Figure 33. Uniform side discharge hydrograph at each section

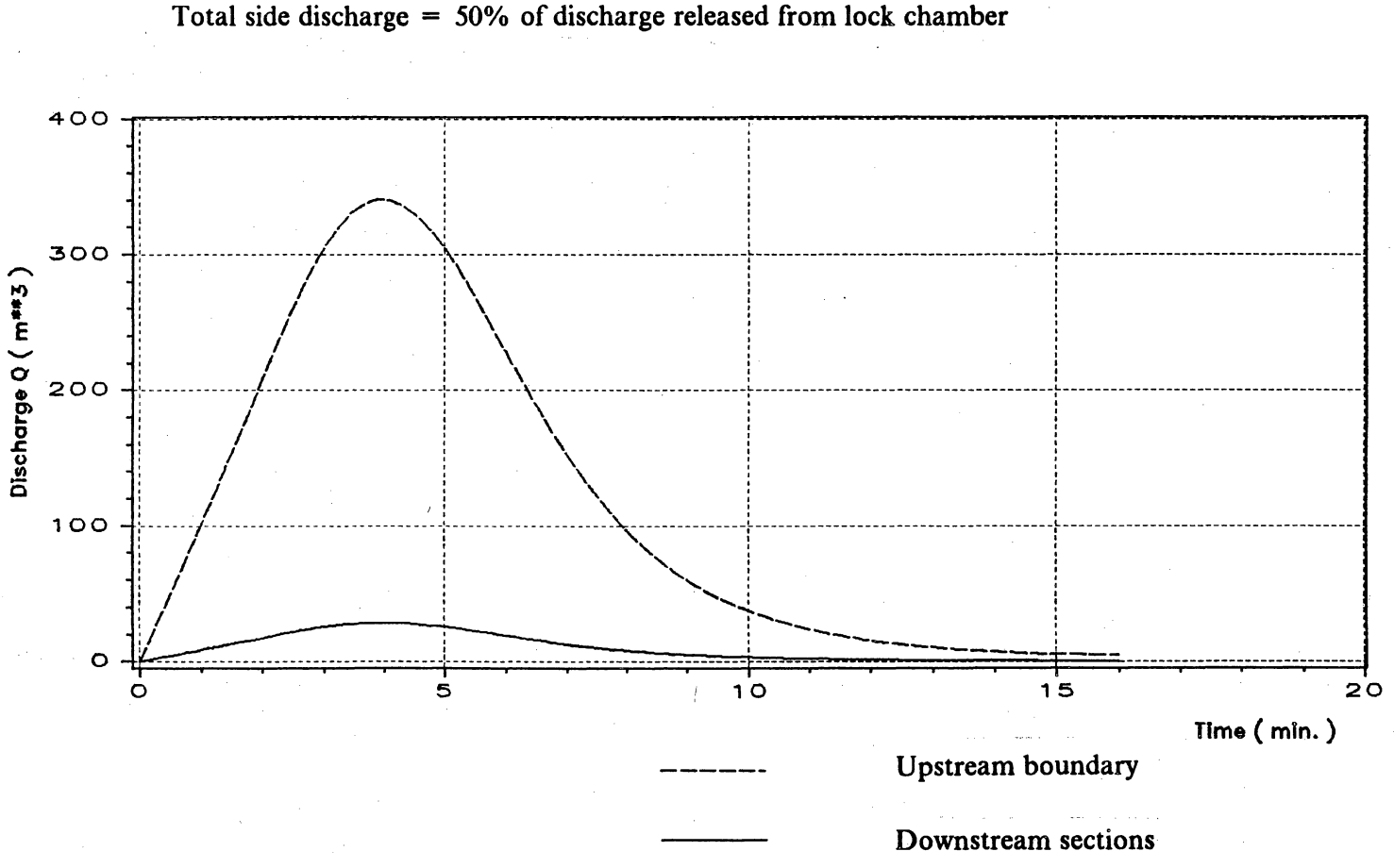

Figure 34. Uniform side discharge hydrographs at upstream boundary and downstream sections

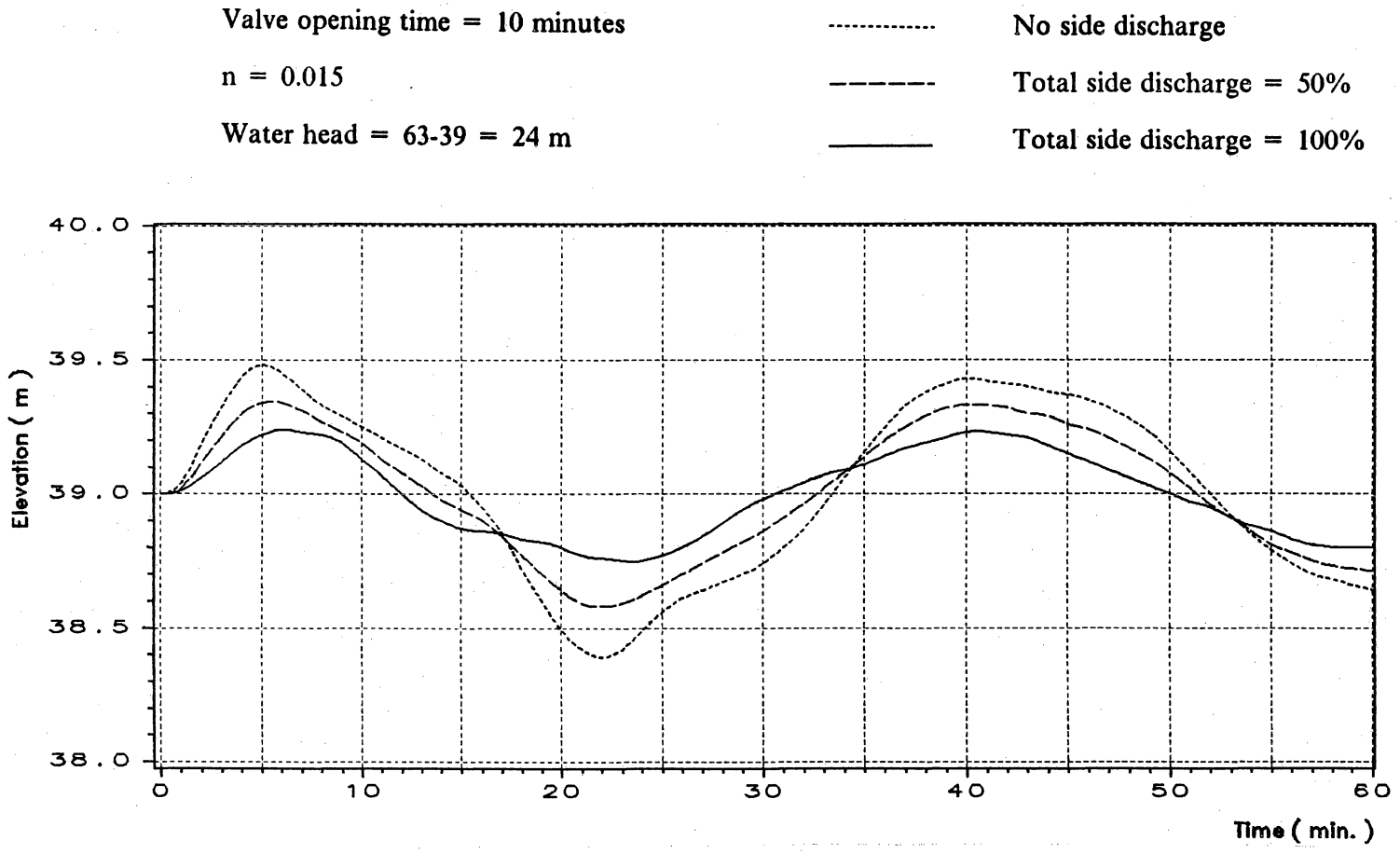

Figure 35. Comparison of water surface elevation variation by uniform side discharges

(at cross-section *No.*2)

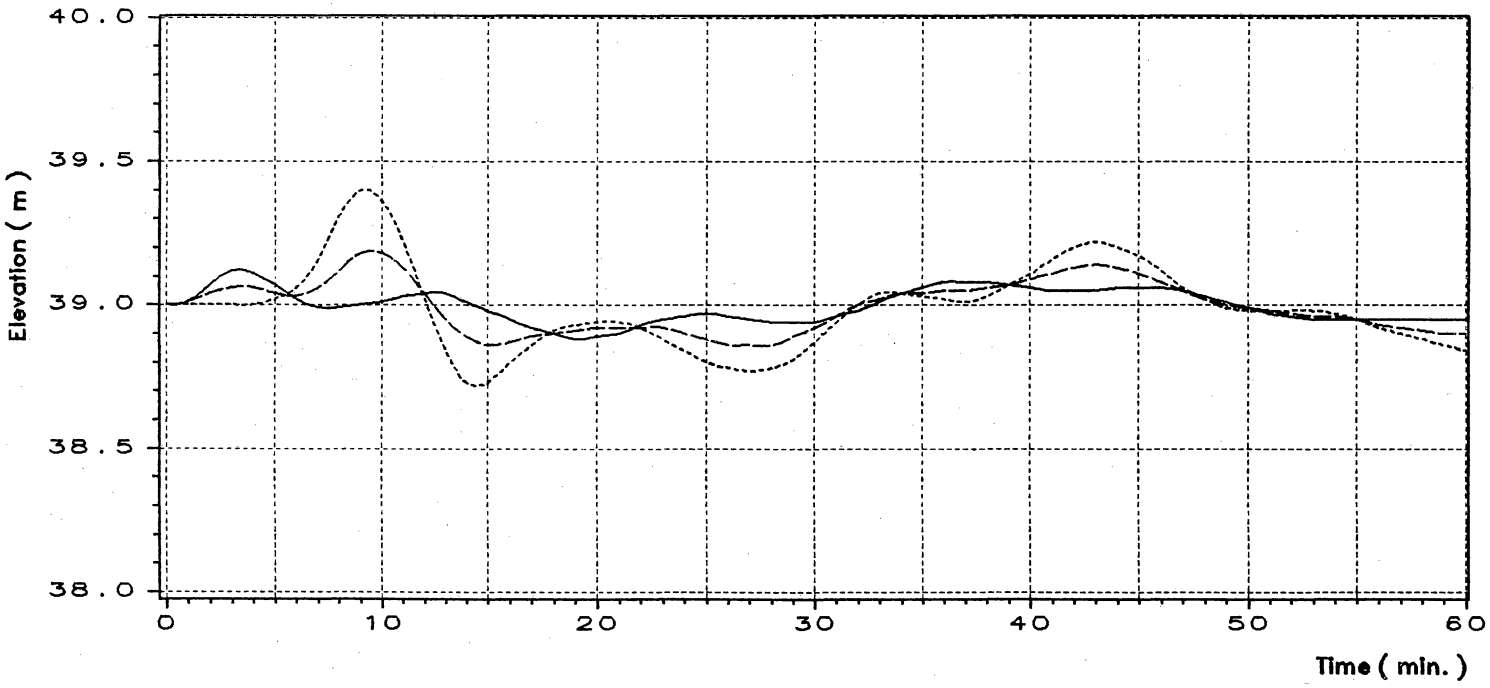

Figure 36. Comparison of water surface elevation variation by uniform side discharges

(at cross-section *No.*11)

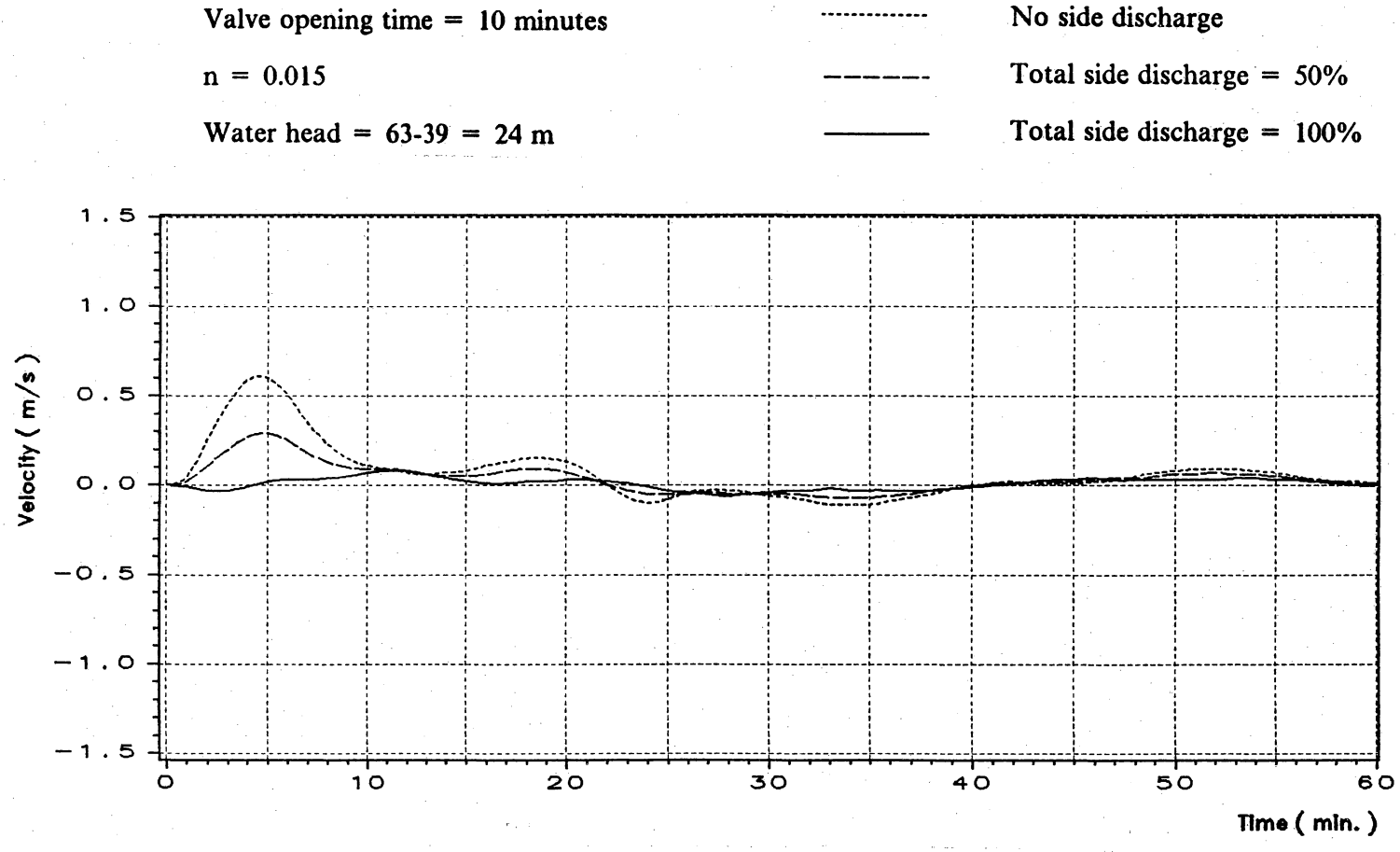

Figure 37. Comparison of velocity variation by uniform side discharges

(at cross-section *No.*2)

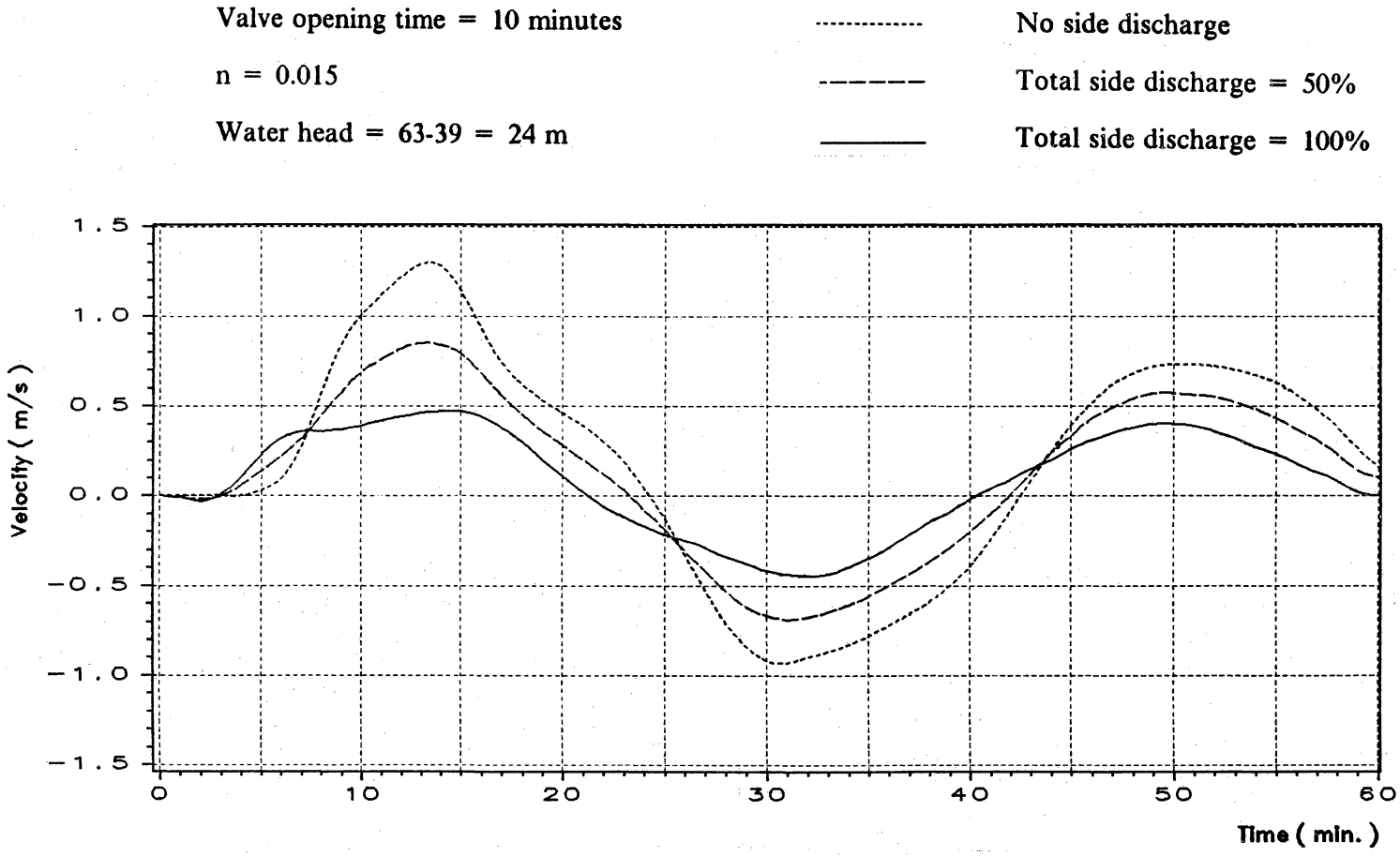

Figure 38. Comparison of velocity variation by uniform side discharges

(at cross-section *No.*11)

Total side discharge = 25% of discharge released from lock chamber

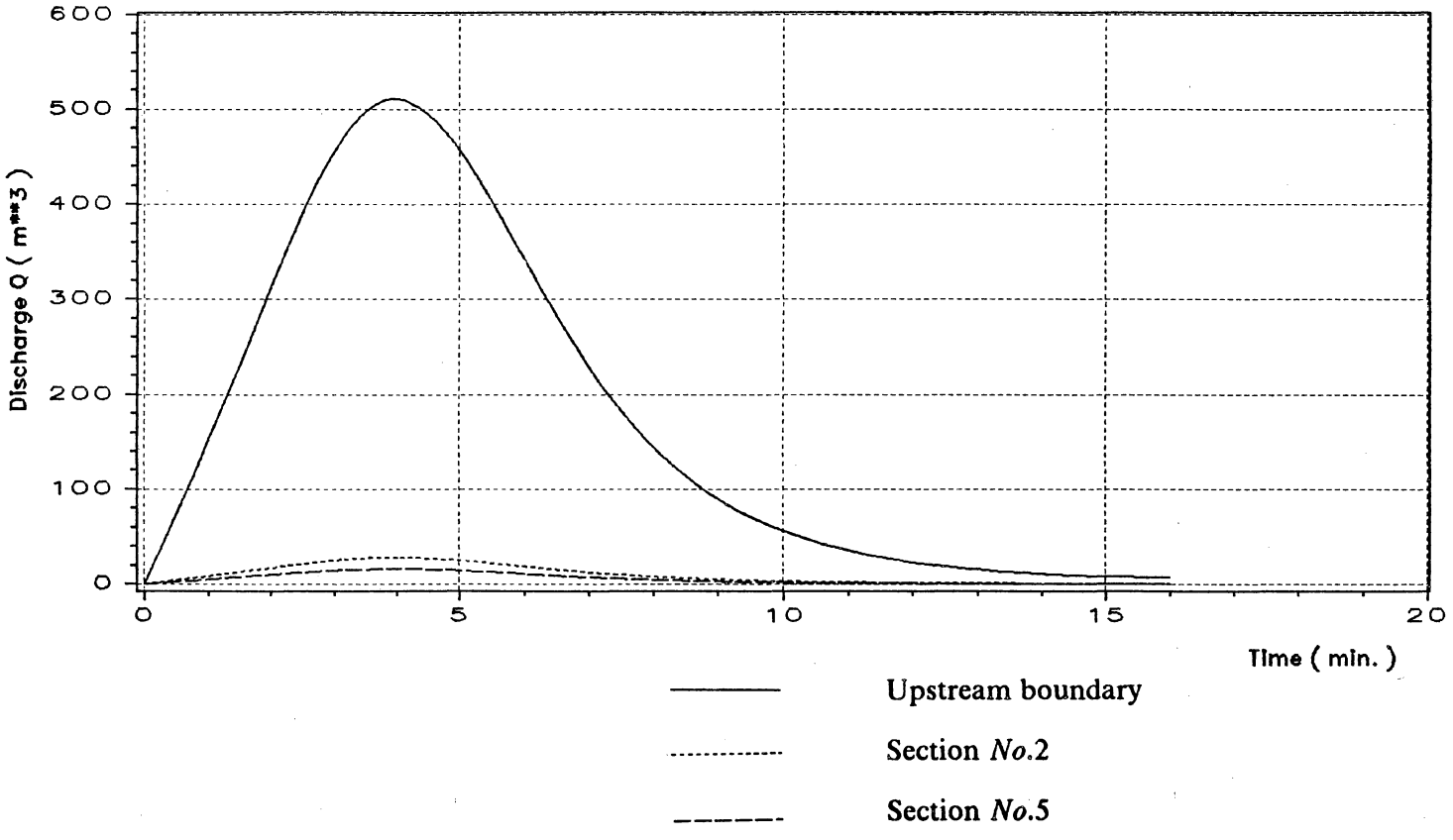

Figure 39. Nonuniform side discharge hydrographs at different sections
(total side discharge = 25% of the discharge)

Total side discharge = 50% of discharge released from lock chamber

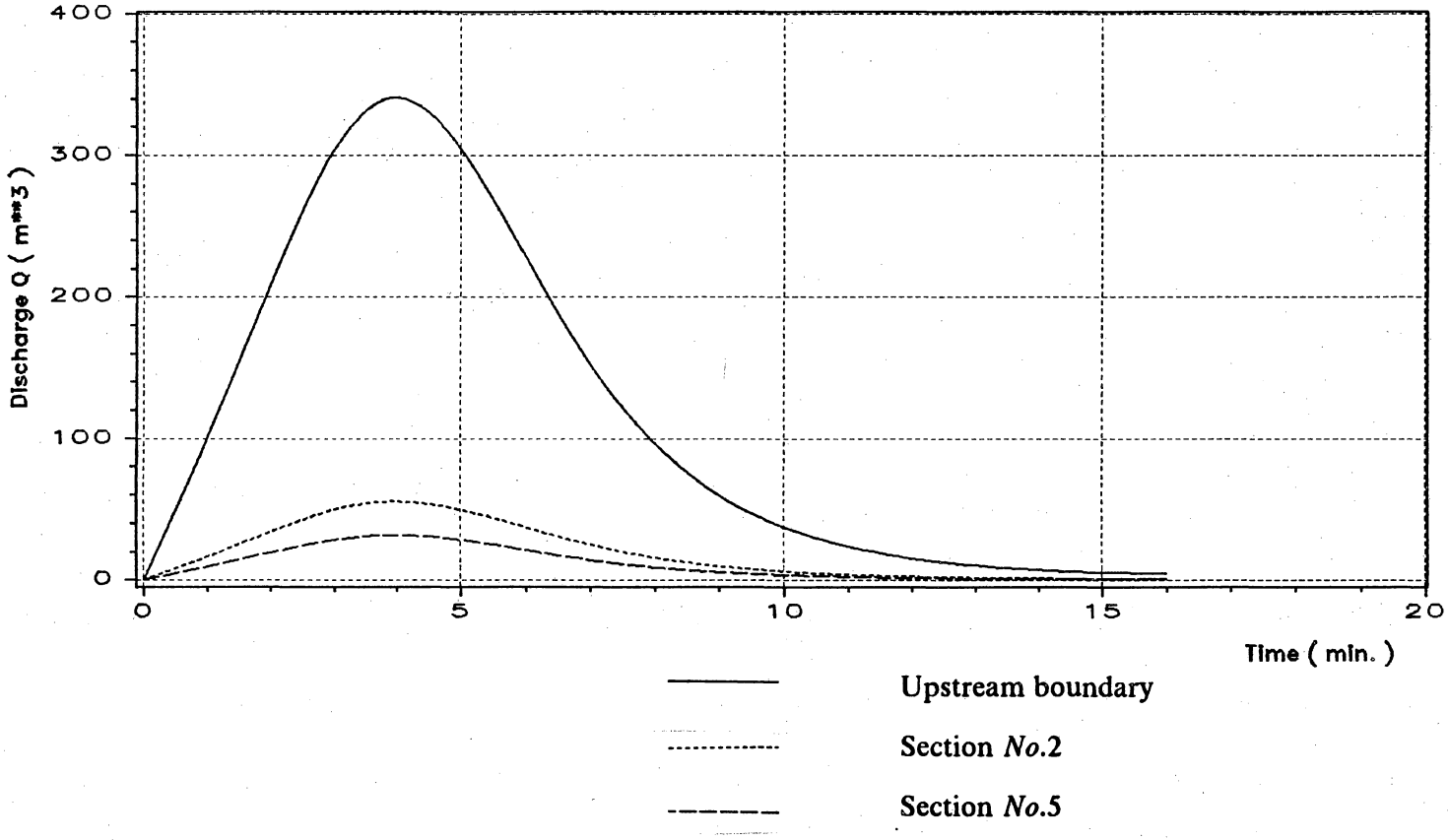

Figure 40. Nonuniform side discharge hydrographs at different sections
(total side discharge = 50% of the discharge)

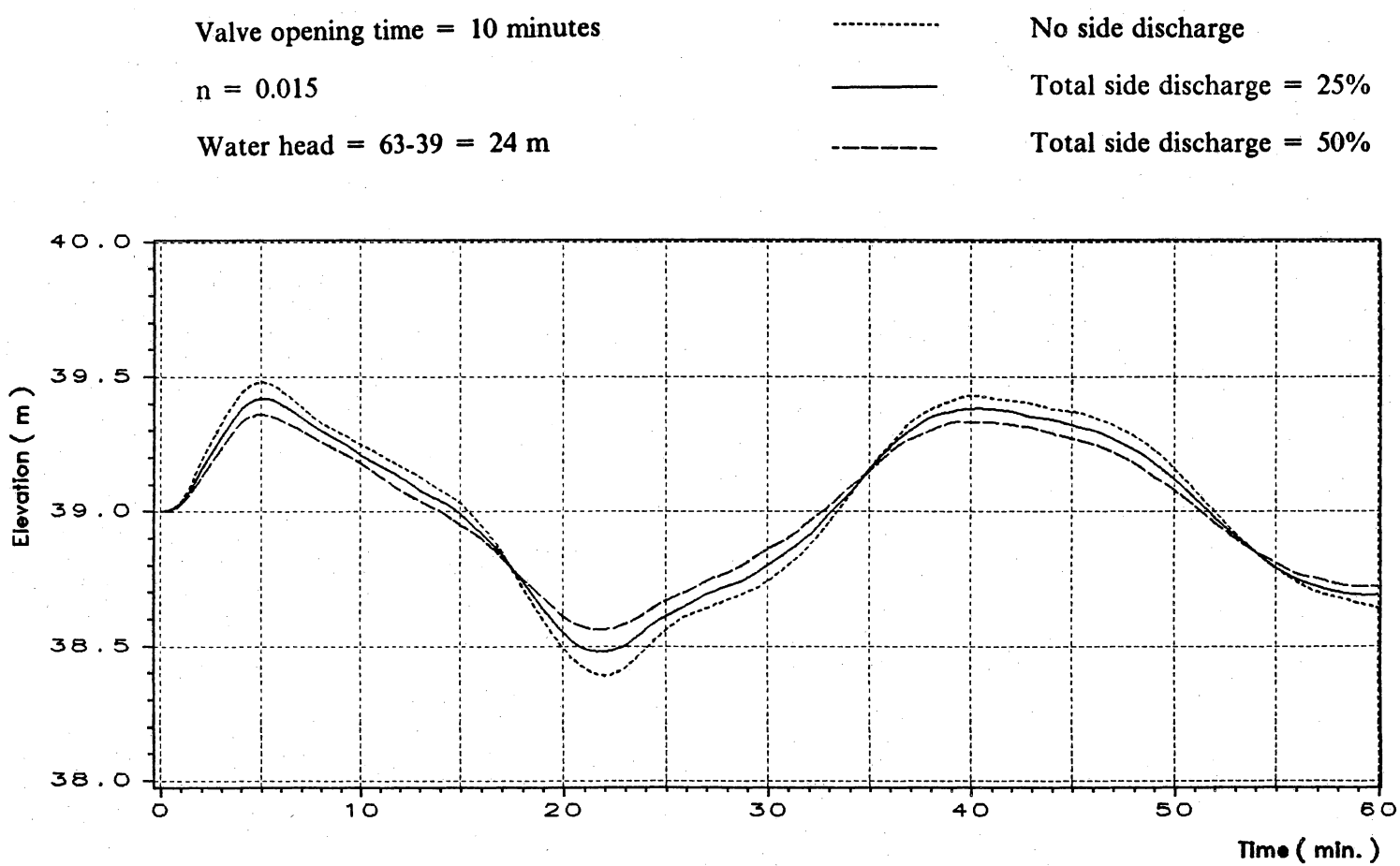

Figure 41. Comparison of water surface elevation variation by nonuniform side discharges

(at At cross-section *No.*2)

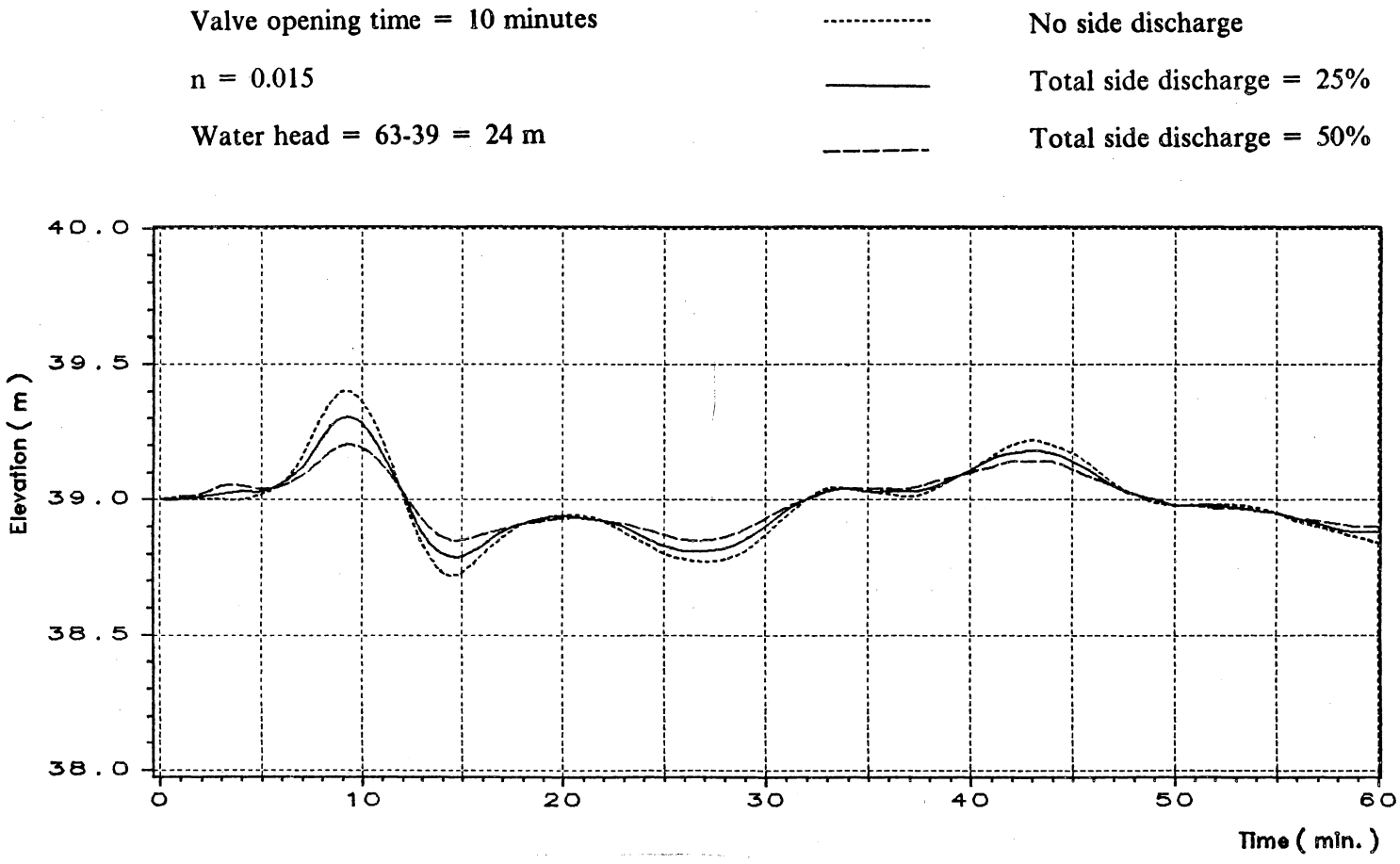

Figure 42. Comparison of water surface elevation variation by nonuniform side discharges

(at cross-section *No.*11)

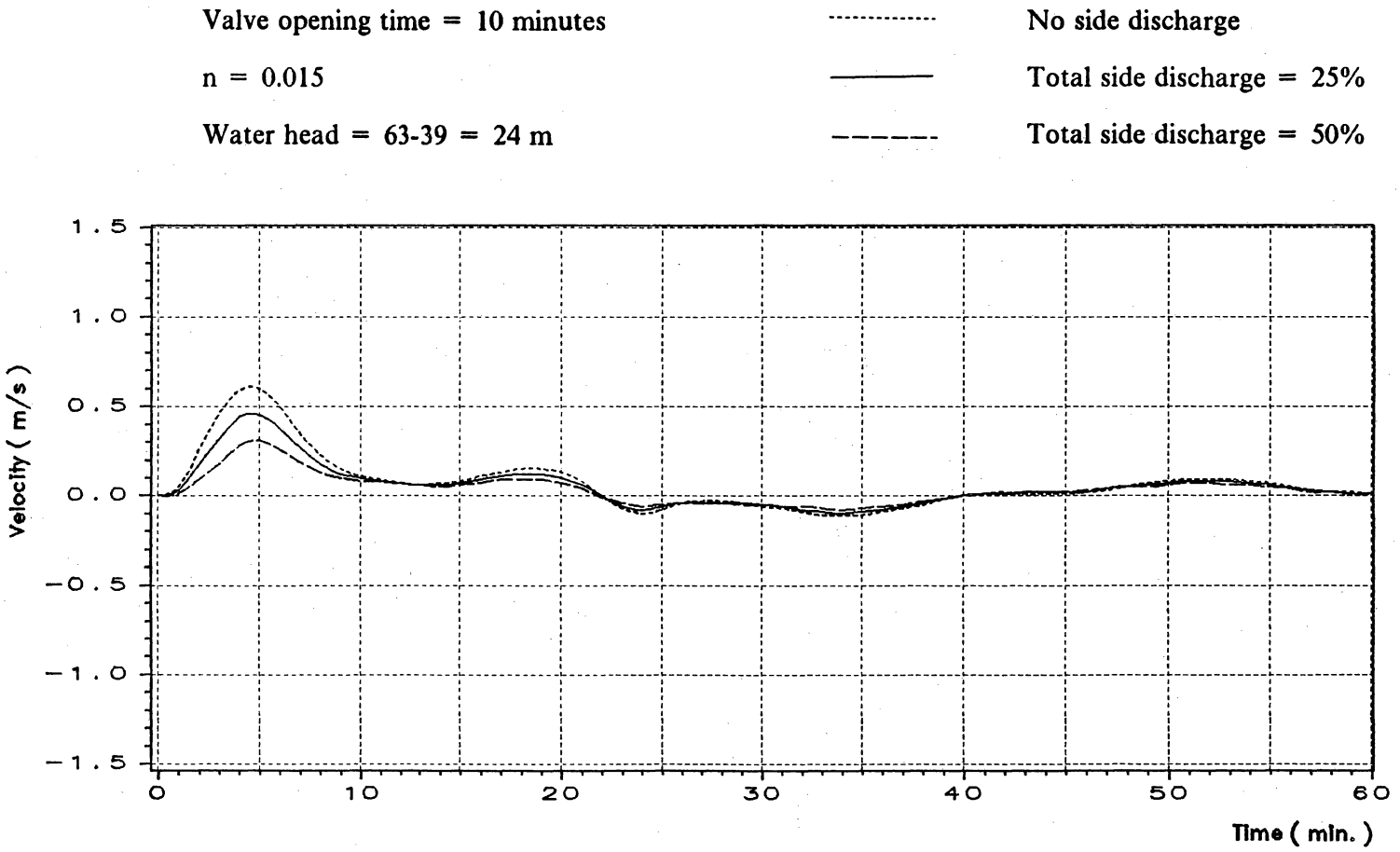

Figure 43. Comparison of velocity variation by nonuniform side discharges

(at cross-section *No.*2)

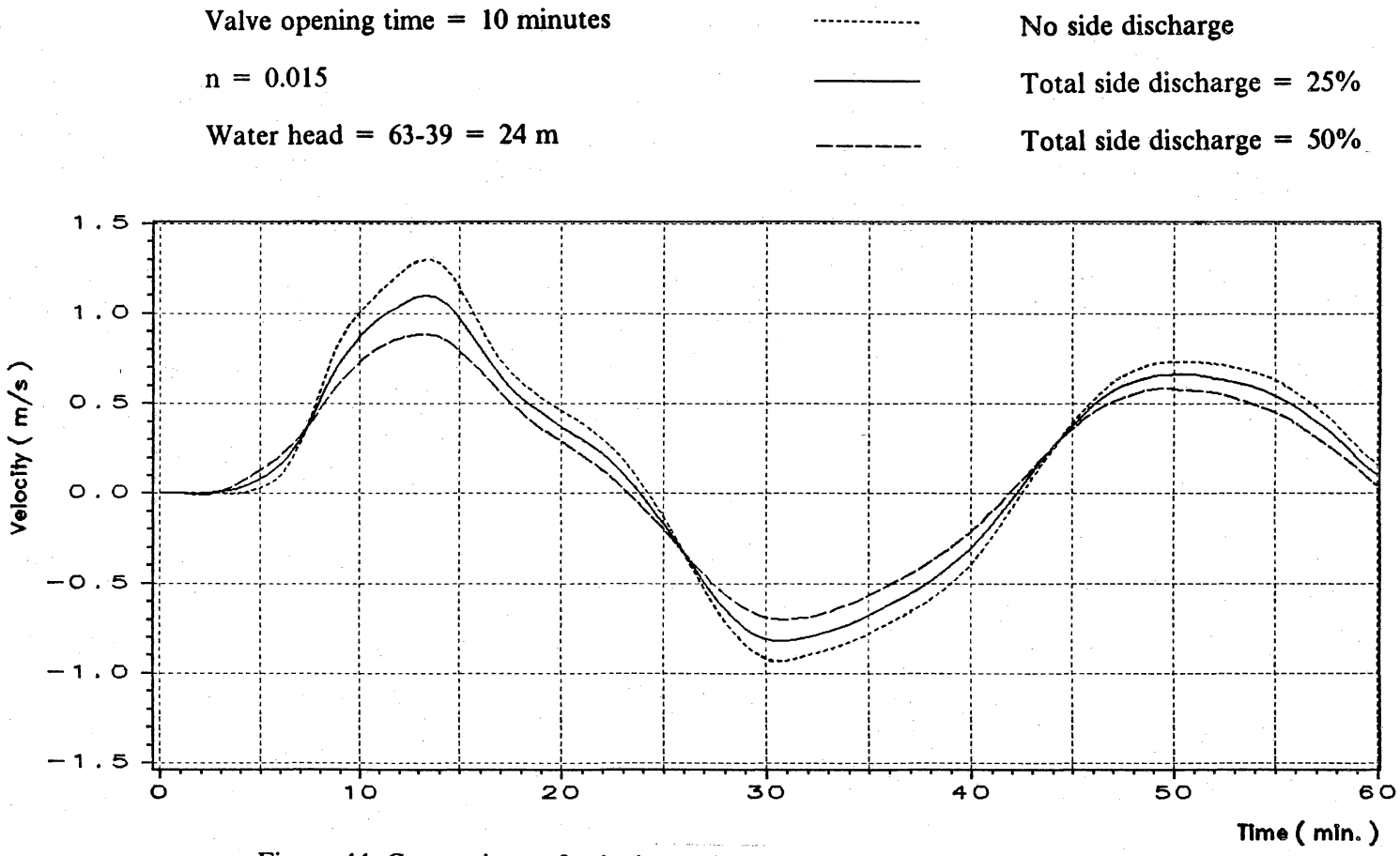

Figure 44. Comparison of velocity variation by nonuniform side discharges

(at cross-section *No.*11)

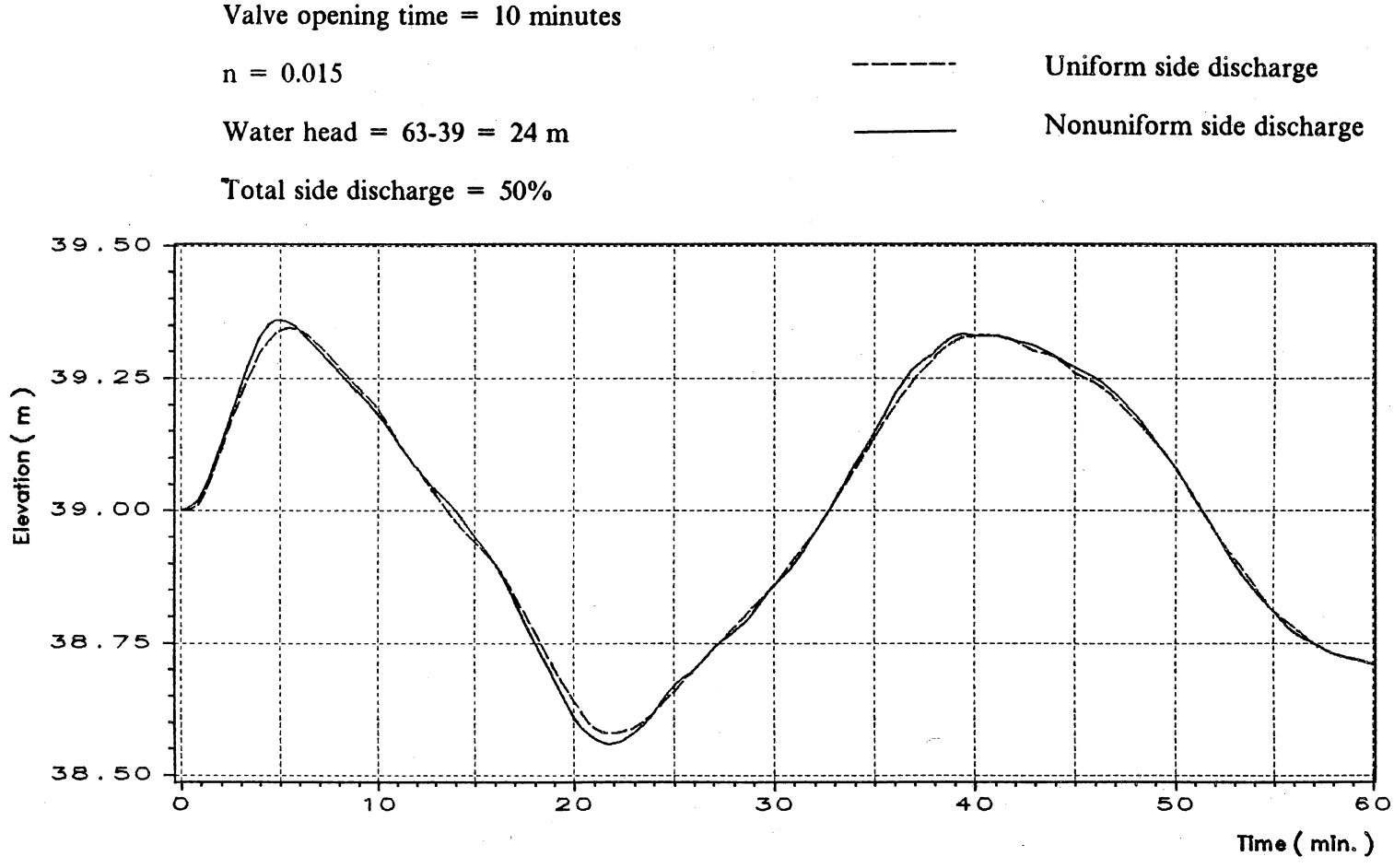

Figure 45. Comparison of water surface elevation variation by uniform and nonuniform side discharges (at cross-section *No.2*)

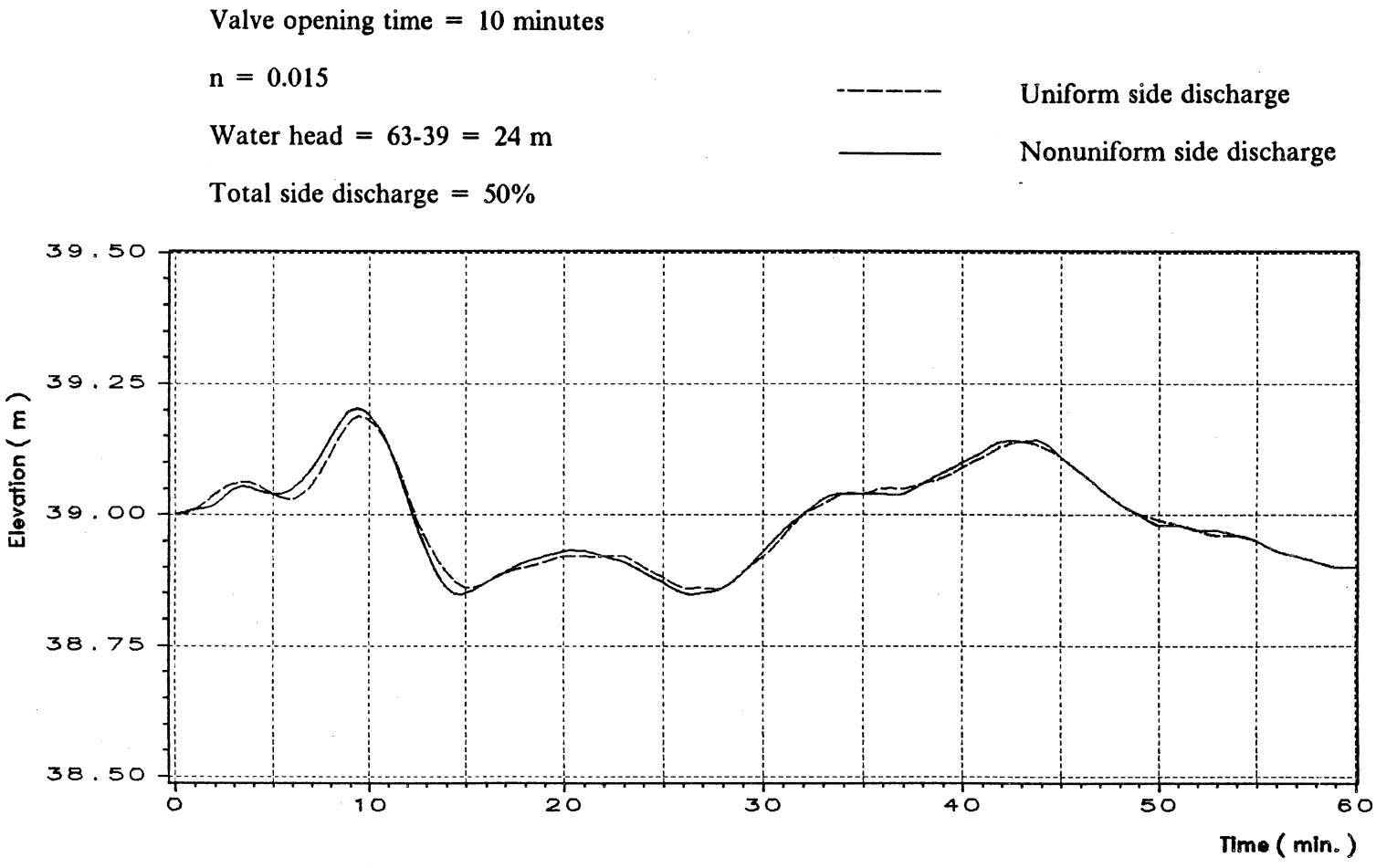

Figure 46. Comparison of water surface elevation variation by uniform and nonuniform side discharges (at cross-section *No.*11)

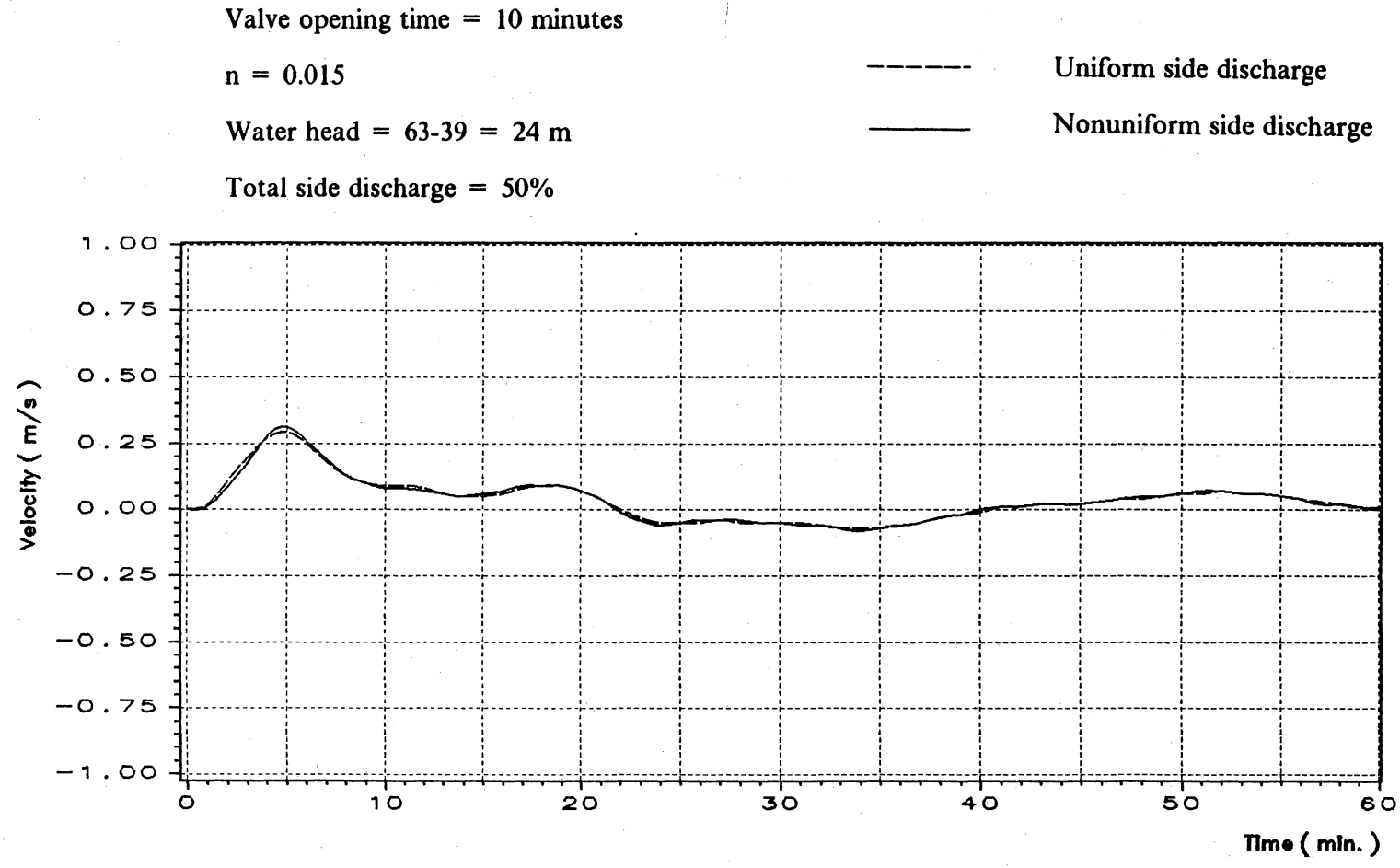

Figure 47. Comparison of velocity variation by uniform and nonuniform side discharges (at cross-section *No.*2)

Valve opening time = 10 minutes

n = 0.015

Water head = 63-39 = 24 m

Total side discharge = 50%

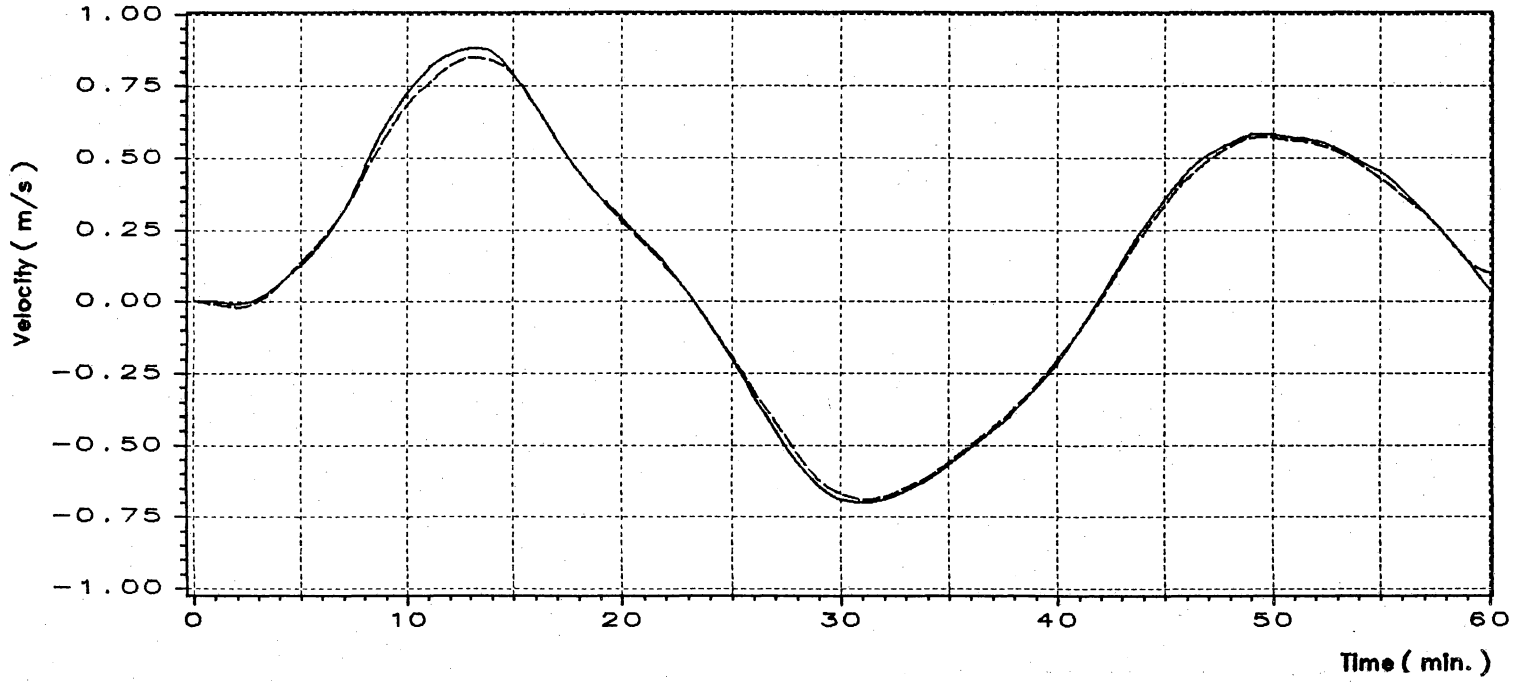

Figure 48. Comparison of velocity variation by uniform and nonuniform side discharges

(at cross-section *No.*11)

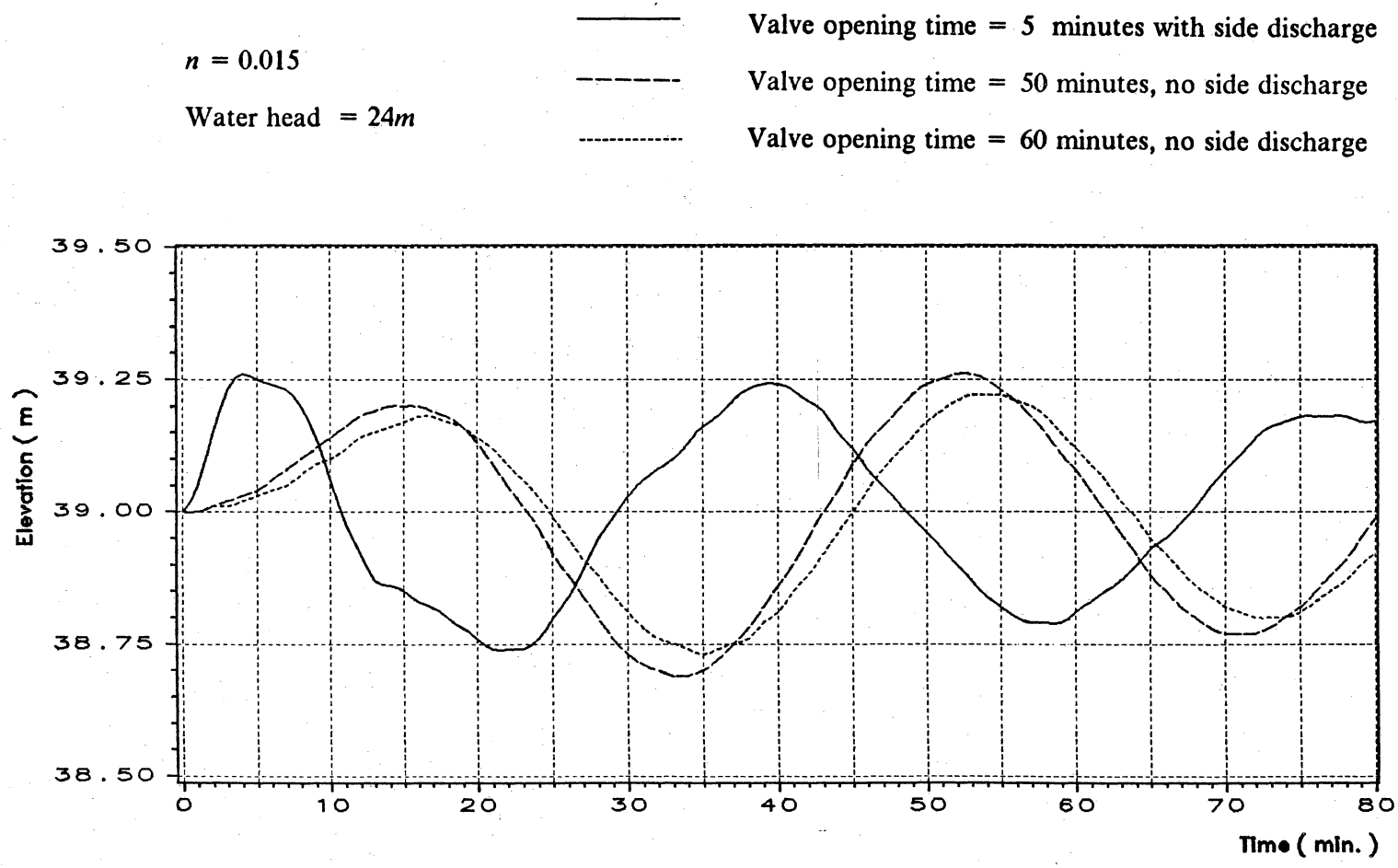

Figure 49. Comparison of water surface elevation variation between side discharge and no side discharge (at cross-section *No.*2)

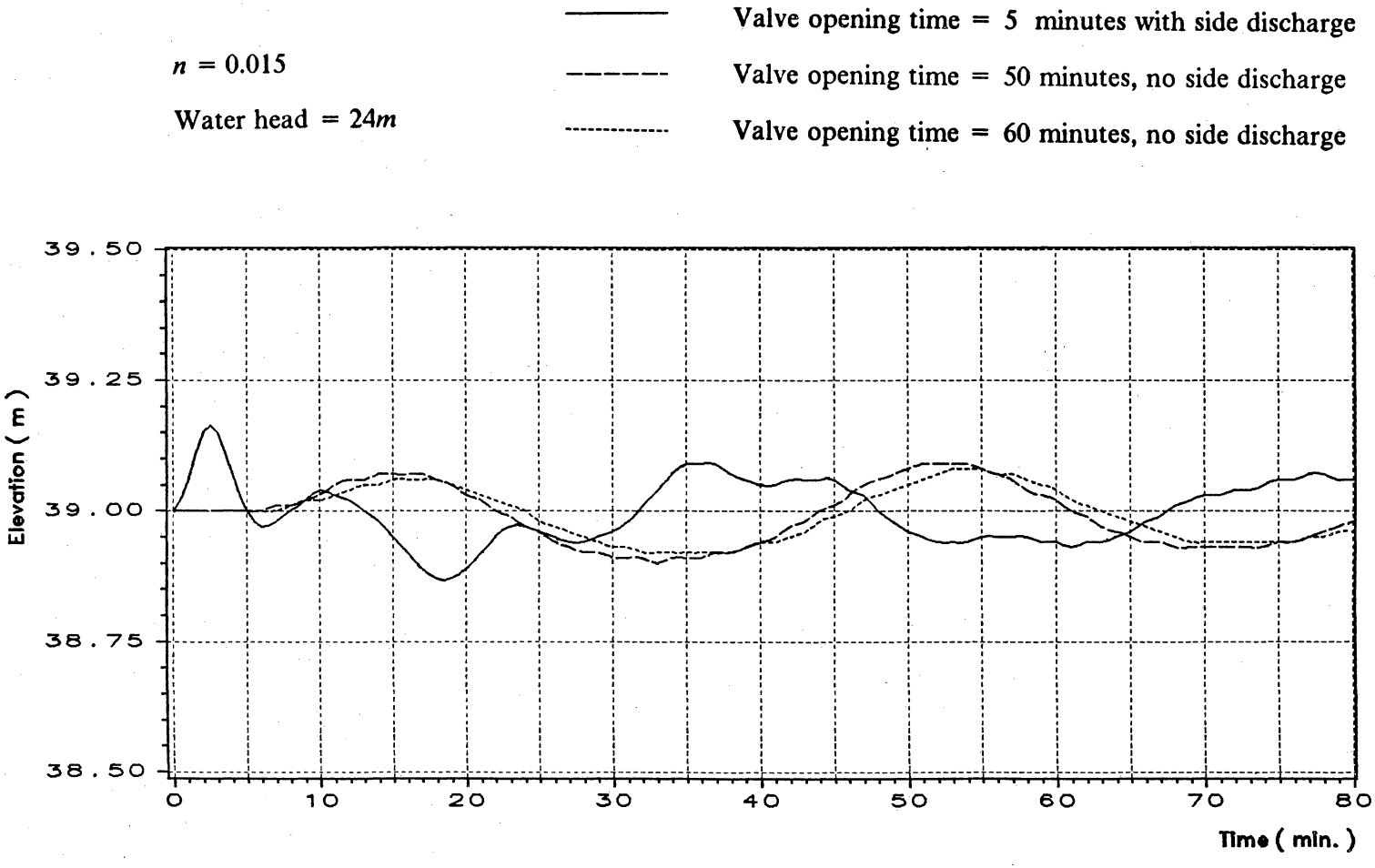

Figure 50. Comparison of water surface elevation variation between side discharge and no side discharge (at cross-section *No.*11)

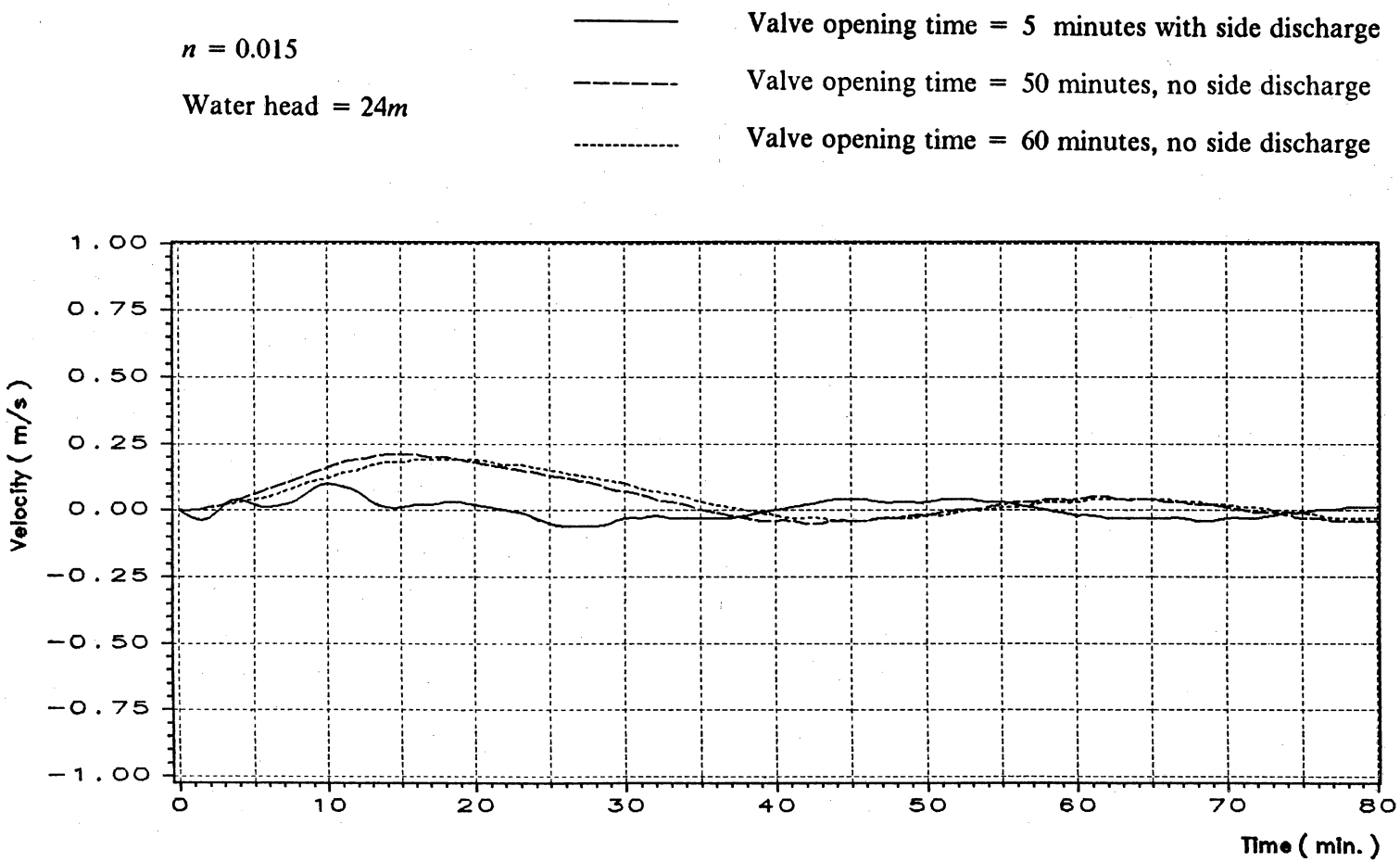

Figure 51. Comparison of velocity variation between side discharge and no side discharge (at cross-section *No.*2)

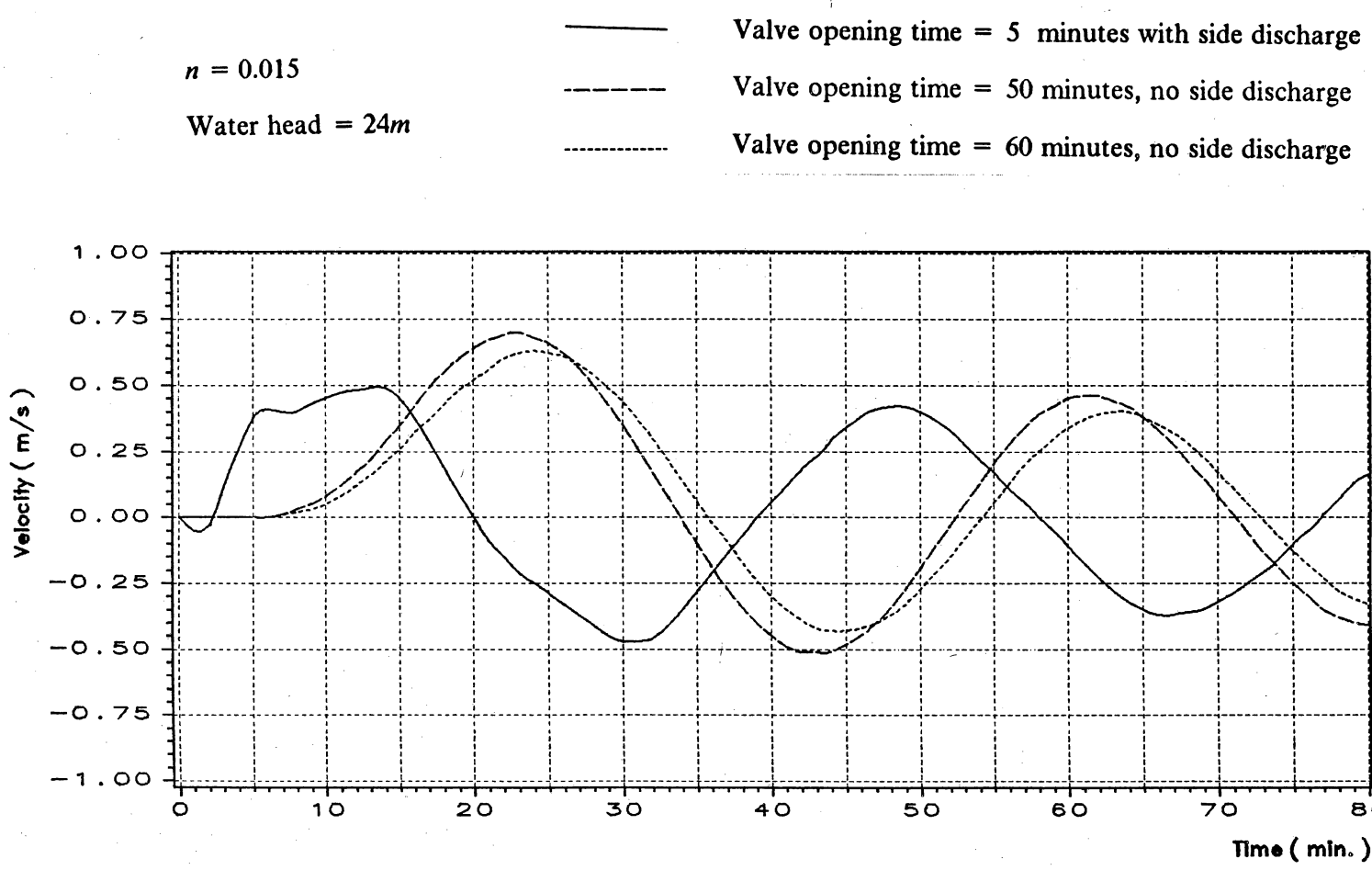

Figure 52. Comparison of velocity variation between side discharge and no side discharge

(at cross-section *No.*11)

Valve opening time = 10 minutes

Water head = 63-39 = 24 m

——— n = 0.012

---------- n = 0.015

– – – – – n = 0.020

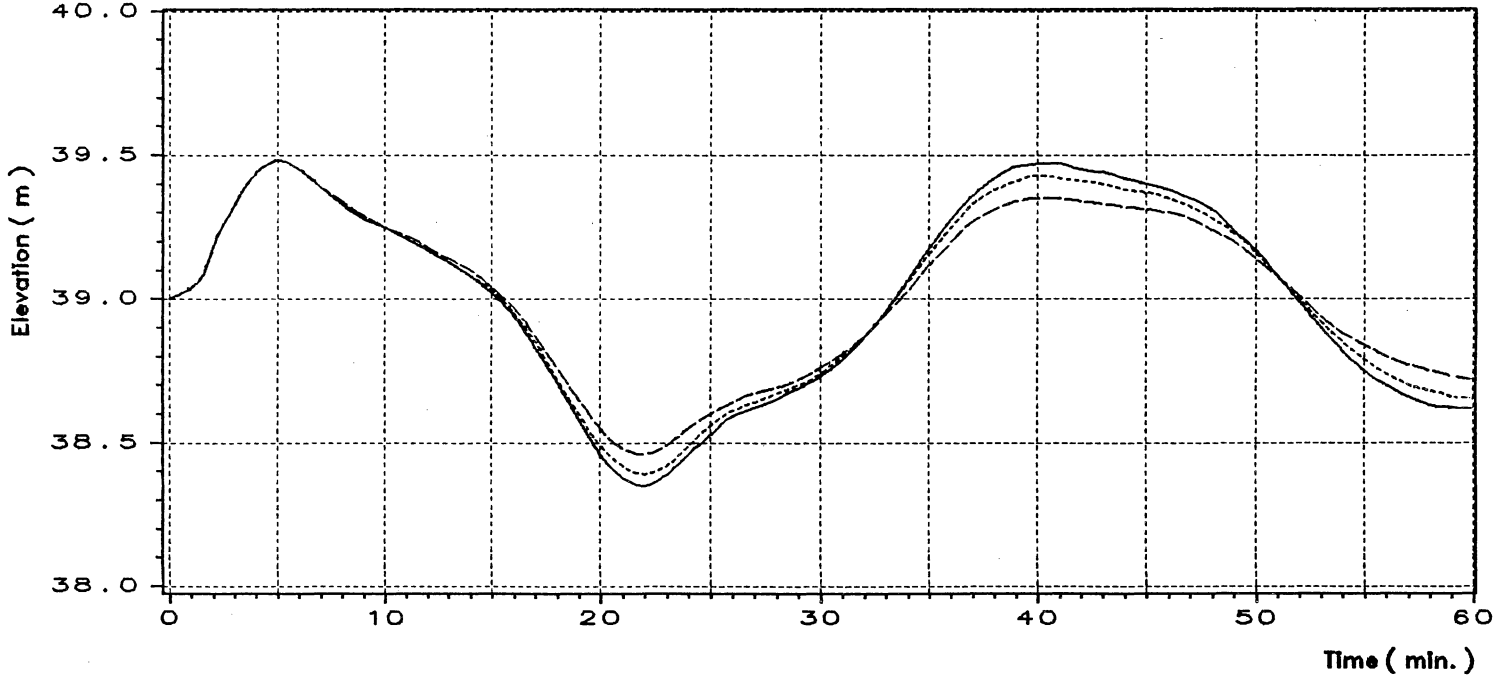

Figure 53. Comparison of water surface elevation variation by different roughness

(at cross-section *No.*2)

Valve opening time = 10 minutes

Water head = 63-39 = 24 m

——— n = 0.012

---------- n = 0.015

– – – – – n = 0.020

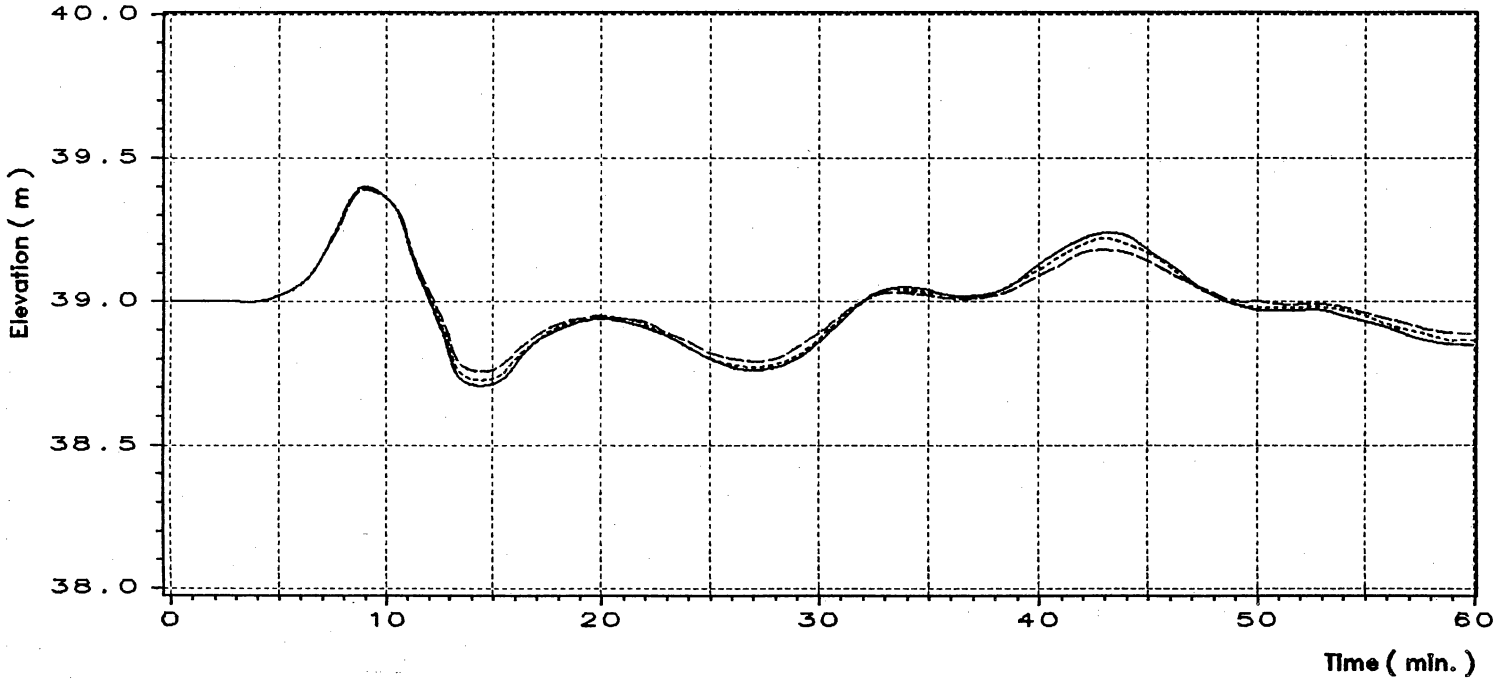

Figure 54. Comparison of water surface elevation variation by different roughness

(at cross-section *No.*11)

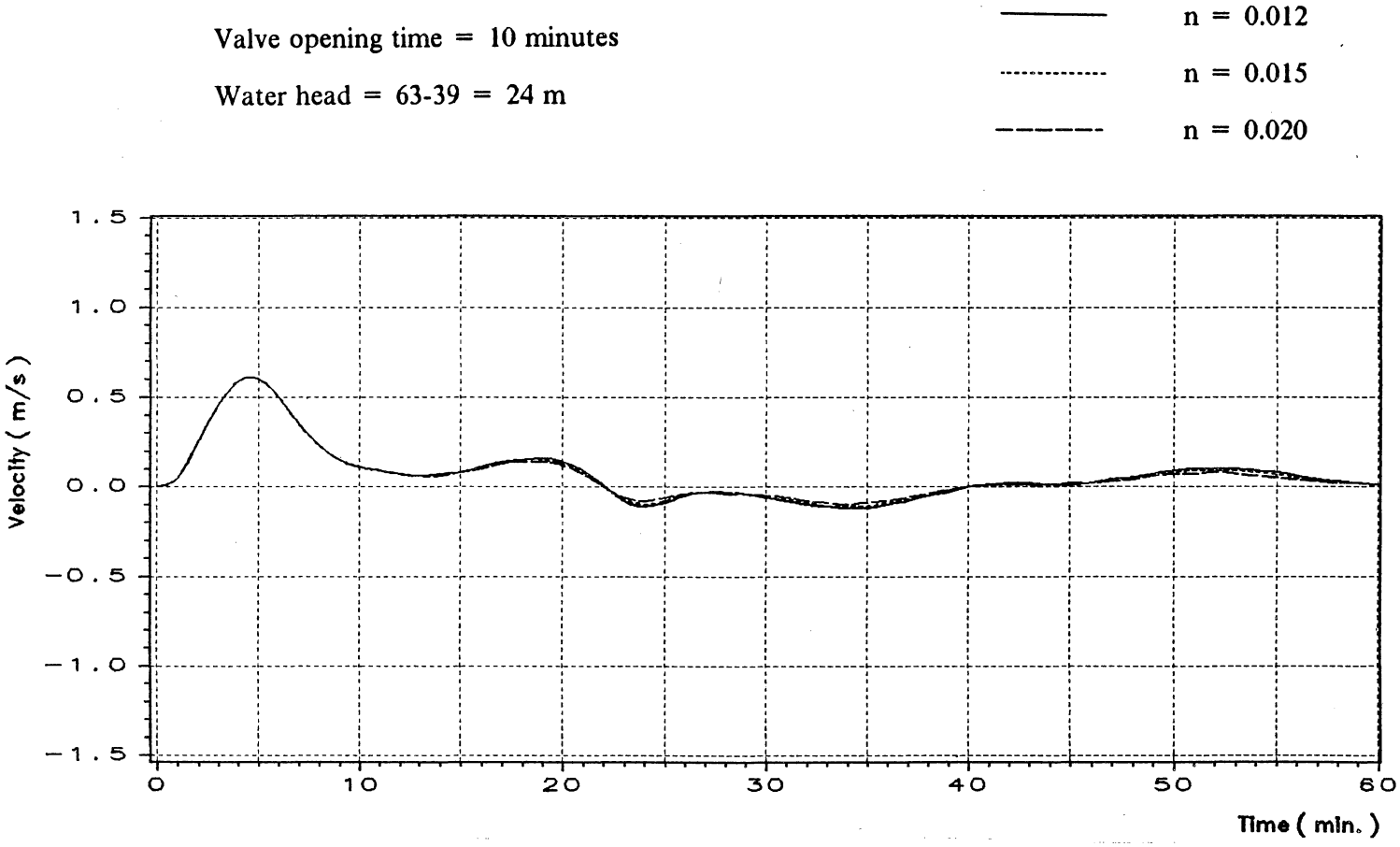

Figure 55. Comparison of velocity variation by different roughness

(at cross-section *No.*2)

Valve opening time = 10 minutes

Water head = 63-39 = 24 m

——— n = 0.012

---------- n = 0.015

– – – – – n = 0.020

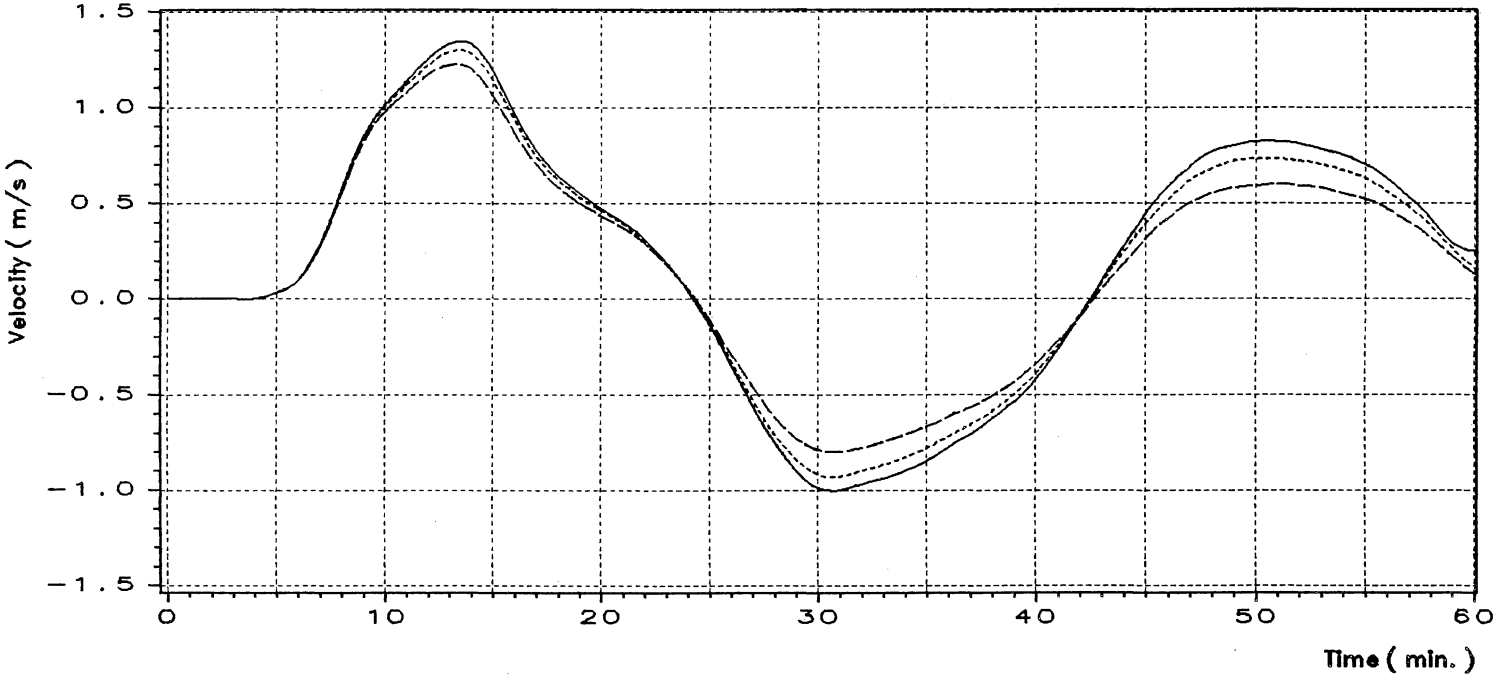

Figure 56. Comparison of velocity variation by different roughness

(at cross-section *No.*11)

Valve opening time = 10 minutes

n = 0.015

Water head = 63-39 = 24 m

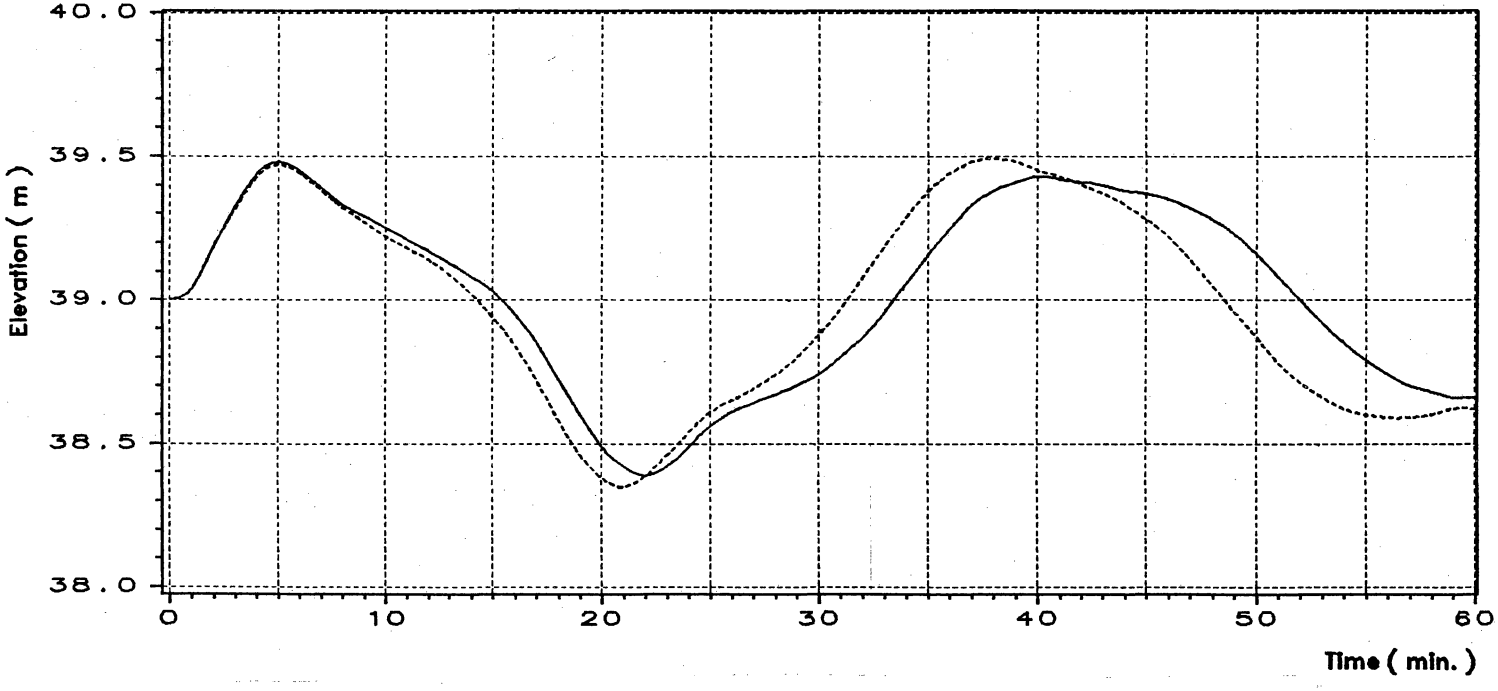

Figure 57. Comparison of water surface elevation variation by modifying channel bed

(at cross-section *No.*2)

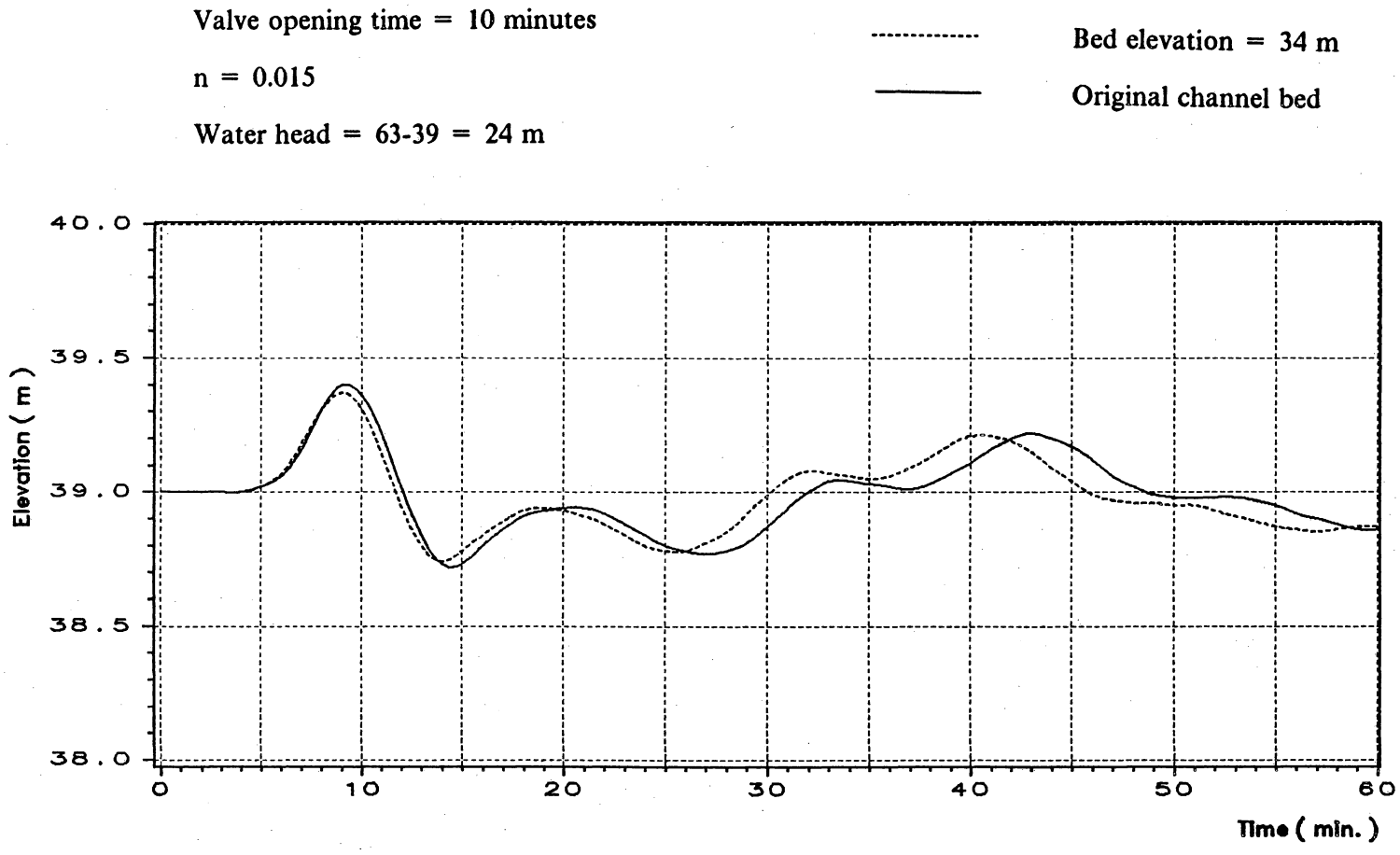

Figure 58. Comparison of water surface elevation variation by modifying channel bed

(at cross-section *No.*11)

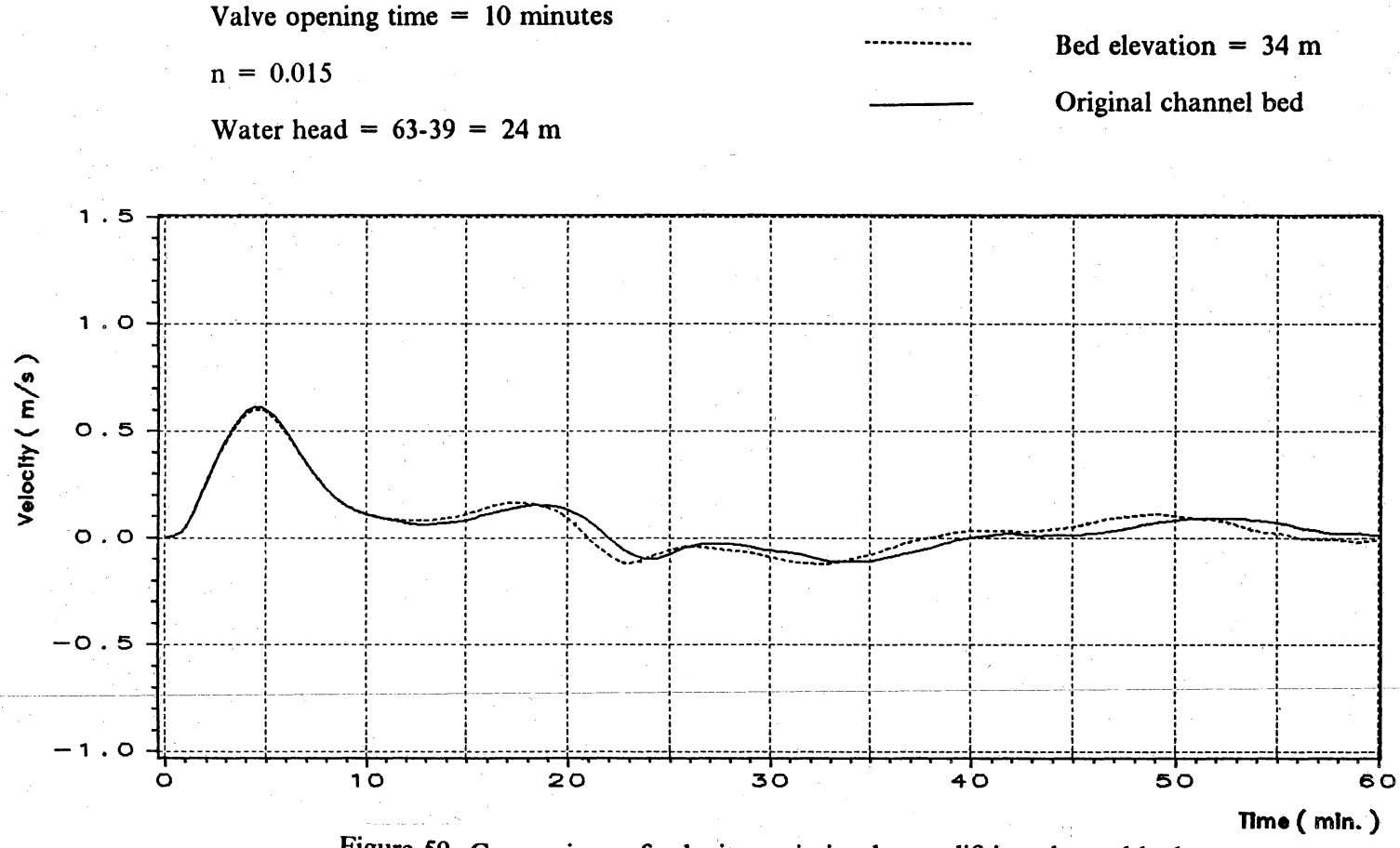

Figure 59. Comparison of velocity variation by modifying channel bed

(at cross-section *No.2*)

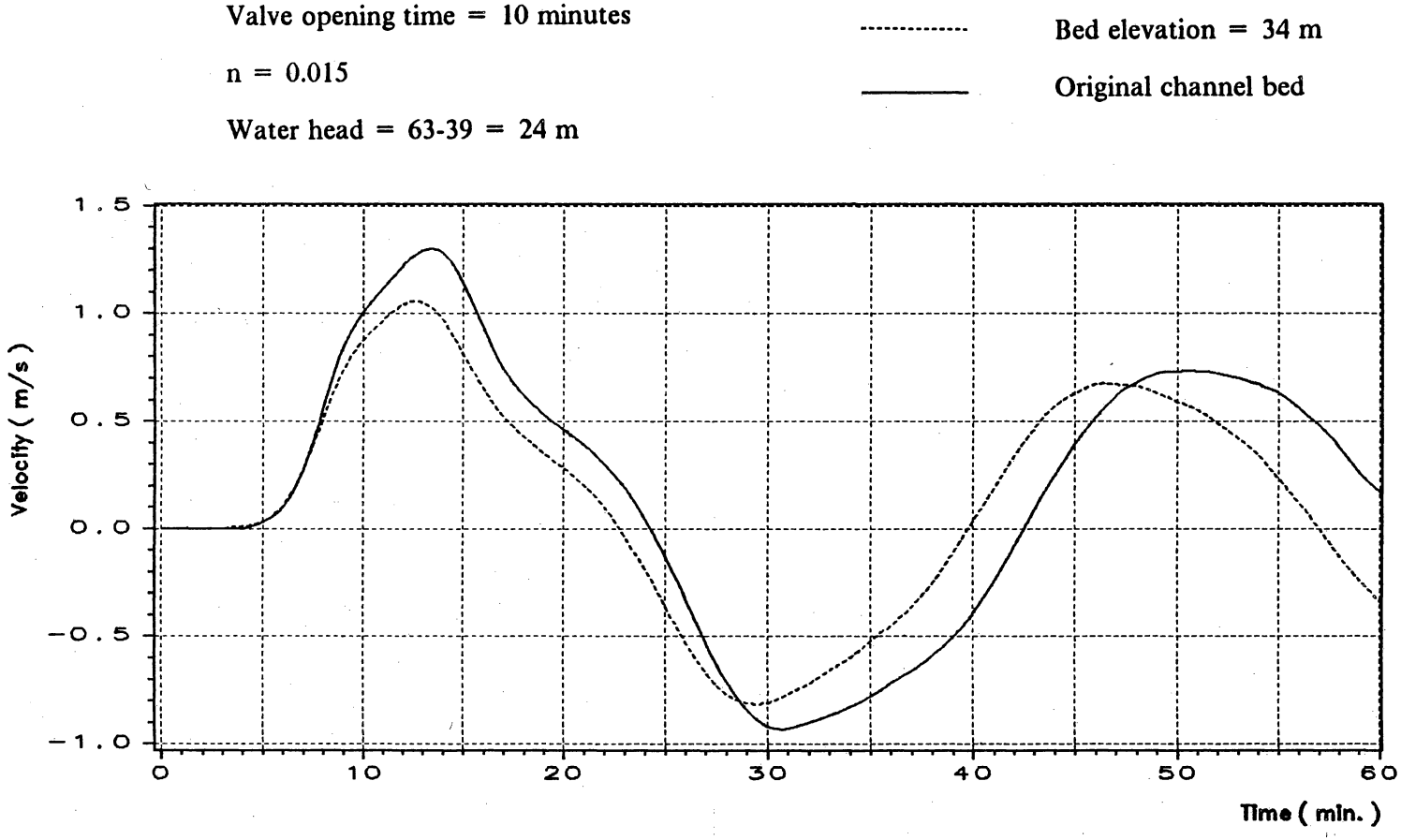

Figure 60. Comparison of velocity variation by modifying channel bed

(at cross-section *No.*11)

Bibliography

[1] Abbott, M. B., *Computational Hydraulics* , Pitman Publishing Limited, London, 1979.

[2] Bender, C., Orszag, S., *Advanced Mathematical Methods for Scientists and Engineers,* McGraw-Hill, New York, N.Y., 1978.

[3] Chevereau, G. and Gauthier, M., *Use of mathematical models as an approach to flow control problems, Proceedings of the Int. Symp. on Unsteady Flow in Open Channels,* BHRA Fluid Engineering, Newcastle-upon-Tyne, 1976.

[4] Chow, V. T., *Open Channel Hydraulics,* McGraw-Hill, New York, 1959.

[5] Cunge, J. A., *Applied Mathematical Modelling of Open Channel Flow,* Chapter 10 of Unsteady Flow in Open Channels, edited by Mahmood, K., Yevjevich, V., Water Resources Publications, P.O.Box 303, Fort Collins, Colorado, USA, 1975.

[6] Cunge, J. A., Holly, F. M. Jr, Verway, A., *Practical Aspects of Computational River Hydraulics* , Pitman Advanced Publishing Program, 1980.

[7] Hydraulic Laboratory, Yangtze River Planning Commission, *The Prototype Test and Analysis of Unsteady Flow in the Third Navigation Channel, Gezhouba Water Control Project* , Journal of People's Yangtze, Wuhan, China, No.6, 1984.

[8] Joliffe, I. B., *Free Surface and Pressurised Pipe Flow Computations, Analysis and Design of Stormwater Systems, Vol. 1, Proceedings of the Third Int. Conf. on Urban Storm Drainage,* Goteborg, Sweden, June 4-8, 1984.

[9] Katapodes, N. D., *A Dissipative Galerkin Scheme for Open Channel Flow* Journal of Hydraulics Division, ASCE Vol. 110, Apr., 1984.

[10] Katapotes, N. D., Wu, C. T., *Explicit Computation of Discontinuous Channel Flow,* Journal of Hydraulic Division, ASCE June, 1986, p456-475.

[11] Keuning, D. H. *Application of Finite Element Method to Open Channel Flow* , Journal of Hydraulic Division, ASCE Vol. 102, April, 1976.

[12] King, I. P., *Finite Element Models for Unsteady Flow Routing through Irregular Channels, Finite Elements in Water Resources,* edited by Gray, W. G., Pinder, G. F., Brebbia, C. A., Pentech Press, London: Plymouth, 1976.

[13] Liggett, J. A., *Basic Equations of Unsteady Flow* , Chapter 2 of Unsteady Flow in Open Channels, edited by Mahmood, K., Yevjevich, V., Water Resources Publications, P.O.Box 303, Fort Collins, Colorado, USA, 1975.

[14] Liggett, J. A., Cunge, J. A., *Numerical Method of Solution of the Unsteady Flow Equations,* Chapter 4 of Unsteady Flow in Open Channels, edited by Mahmood, K., Yevjevich, V., Water Resources Publications, P.O.Box 303, Fort Collins, Colorado, USA, 1975.

[15] Lyn, D. A., Goodwin, P., *Stability of a General Preissmann Scheme* , Journal of Hydraulic Engineering, ASCE, Vol. 113, No. 1, Jan. 1987, pp. 16-28.

[16] Morris, H. M., Wiggert, J. M., *Applied Hydraulics in Engineering* , John Wiley & Sons, New York, 1972.

[17] National Research Council, *An Evaluation of Flood-Level Predictions Using Alluvial River Models,* National Academy Press, Washington, D. C., 1983.

[18] Schmitz, G., Edenhofer, J., Czirwitzky, H. J., *An Analytical and Numerical Solution of Saint-Venant Equations, Refined Modelling of Flows, Vol. 2, Proceedings of the Symposium,* Paris, September 7-10, 1982.

[19] Strelkoff, T., *Numerical Solutions for Saint-Venant Equations* , Journal of the hydraulics Division, ASCE Vol. 96, No. HY1, Proc. paper 7043, Jan., 1970. pp.223-253.

[20] Vasiliev, O. F., *Numerical Solution of the Non-linear Problems of Unsteady Flow in Open Channels, Proceedings of the 2nd Int. Conf. on Numerical Methods in Fluid Dynamics,* Berkeley, pp.410-421, 1970.

[21] Yangtze River Planning Commission, *An Introduction to the Gezhouba Water Control Project* , Brochure, Wuhan, China, 1980.

[22] Yapa, P. D., Shen, H. T., *Unsteady Flow Simulation for an Ice-Covered River* , Journal of Hydraulic Division, ASCE Nov. 1986, p1036-1049.

[23] Yu, W. D., Zhao, X. X., Huang, J., *The Numerical Solution for One-dimensional Unsteady Flow in Open Channels* , Journal of Hydraulic Engineering, Beijing, China, No.4, 1986.

The vita has been removed from the scanned document